

**EFFECTS OF MOLYBDENUM NANOPARTICLES ON LEAD-
FREE TIN-BASED SOLDER**

MD. ARAFAT MAHMOOD

**FACULTY OF ENGINEERING
UNIVERSITY OF MALAYA
KUALA LUMPUR**

2012

**EFFECTS OF MOLYBDENUM NANOPARTICLES ON LEAD-
FREE TIN-BASED SOLDER**

MD. ARAFAT MAHMOOD

**DISSERTATION SUBMITTED IN FULLFILLMENT OF THE
REQUIREMENTS FOR THE DEGREE OF MASTER OF
ENGINEERING SCIENCE**

**FACULTY OF ENGINEERING
UNIVERSITY OF MALAYA
KUALA LUMPUR**

2012

University of Malaya

ORIGINAL LITERARY WORK DECLARATION

Name of Candidate: **Md. Arafat Mahmood** (Passport No:

Registration/Matric No: **KGA080033**

Name of Degree: **Master of Engineering Science**

Title of Dissertation (“this Work”):

Effects of Molybdenum Nanoparticles on Lead-Free Tin-Based Solder

Field of Study: **Materials Engineering**

I do solemnly and sincerely declare that:

- (1) I am the sole author/writer of this Work;
- (2) This Work is original;
- (3) Any use of any work in which copyright exists was done by way of fair dealing and for permitted purposes and any excerpt or extract from, or reference to or reproduction of any copyright work has been disclosed expressly and sufficiently and the title of the Work and its authorship have been acknowledged in this Work;
- (4) I do not have any actual knowledge nor do I ought reasonably to know that the making of this work constitutes an infringement of any copyright work;
- (5) I hereby assign all and every rights in the copyright to this Work to the University of Malaya (“UM”), who henceforth shall be owner of the copyright in this Work and that any reproduction or use in any form or by any means whatsoever is prohibited without the written consent of UM having been first had and obtained;
- (6) I am fully aware that if in the course of making this Work I have infringed any copyright whether intentionally or otherwise, I may be subject to legal action or any other action as may be determined by UM.

Candidate’s Signature

Date:

Subscribed and solemnly declared before,

Witness’s Signature

Date:

Name: Dr. Md. Abul Kalam

Designation: Senior Lecturer,

Department of Mechanical Engineering,

University of Malaya.

ABSTRACT

Recent environmental concern led to worldwide legislation banning the use of lead (Pb) containing solders in microelectronic devices. Near eutectic Sn-Ag-Cu solders are considered as replacement for traditional Pb-Sn solders. But Sn-Ag-Cu solder alloys can not guarantee the required performance in wide ranging semiconductor products. The aim of this work is to develop tin-based nanocomposite solder with improved high temperature stability with respect to microstructure and properties.

In this study, Mo nanoparticles were used as a reinforcing material into the Sn-3.8Ag-0.7Cu (SAC) solder. The Mo nanoparticles were characterized by transmission electron microscopy (TEM) and X-ray diffractometer (XRD). The composite solder paste was prepared by manually mixing of Mo nanoparticles into the SAC solder paste. The melting behavior of the solder paste was determined by differential scanning calorimetry (DSC). The as-prepared solder paste was placed on polycrystalline Cu substrate and reflowed at 250°C for 45 seconds. After reflow, elemental compositions of the nanocomposite solders were analyzed by inductively coupled plasma-optical emission spectrometer (ICP-OES). The microstructural investigations, spreading rate and wetting angle measurement were carried out on the solders after first reflow. After that one set of samples subjected to multiple reflow up to six times and another set of samples were put for high temperature aging up to 1008h at 100°-175°C. Microstructural investigations were performed at the solder/substrate interface using conventional scanning electron microscopy (SEM), high resolution field emission scanning electron microscopy (FESEM) and energy dispersive X-ray (EDX). To evaluate the solder/substrate interaction in the liquid state in presence of Mo nanoparticles, Cu wire (250 μm in diameter) was dipped into the liquid composite

solder at 250°C up to 15 min. After that, the solder-substrate reaction couple was taken out from the molten solder and examined thoroughly by optical microscopy, SEM, FESEM, and EDX.

Results reveal that after reflow only a fraction of Mo nanoparticles retain inside the solder matrix. The spreading rate decreased and wetting angle is increased with the addition of Mo nanoparticles to the SAC solder. It is found that Mo nanoparticles are effective in suppressing the growth of total IMC layer thickness and scallop diameter during reflow and high temperature aging. With the addition of Mo nanoparticles, the diffusion coefficient is decreased but the activation energy of the IMC scallop growth remains unchanged. The dissolution of Cu substrate and IMC formation are decreased in presence of Mo nanoparticles.

From this present research, it was found that Mo nanoparticles do not dissolve or react with the solder during reflow and high temperature aging. The retardation of IMC thickness and scallop diameter is due to the discrete particle effect of Mo nanoparticles. The intact, discrete nanoparticles, by absorbing preferentially at the interface, hinder the diffusion flux of the substrate and thereby suppress the IMC growth. The retardation of total IMC layer with the addition of Mo nanoparticles improves the reliability of the solder joint.

ABSTRAK

Kebimbangan alam sekitar baru-baru ini menyebabkan kepada undang-undang di seluruh dunia melarang penggunaan lead (Pb) yang mengandungi solders dalam peranti mikroelektronik. Eutectic Sn-Ag-Cu solder berhampiran dianggap sebagai pengganti Pb-Sn solder tradisional. Tetapi Sn-Ag-Cu solder aloi tidak dapat menjamin prestasi yang diperlukan dalam produk semikonduktor luas. Tujuan kerja ini adalah untuk membangunkan nanocomposite solder berasaskan timah dengan kestabilan suhu meningkat tinggi berkenaan dengan mikrostruktur dan hartanah.

Dalam kajian ini, nanopartikel Mo telah digunakan sebagai bahan pengukuhan ke dalam pateri Sn-3.8Ag-0.7Cu (SAC). Nanopartikel Mo telah ditandai oleh mikroskop elektron penghantaran (TEM) dan X-ray diffractometer (XRD). Pes solder komposit telah disediakan oleh pencampuran manual nanopartikel Mo ke dalam pes SAC solder. Perilaku lebur paste solder telah ditentukan oleh calorimetry pembezaan pengimbasan (DSC). Pes solder yang disediakan diletakkan pada substrat polycrystalline Cu dan dialirkan kembali pada suhu 250°C selama 45 detik. Selepas reflow, komposisi unsur daripada solders nanocomposite dianalisis oleh induktif serta plasma optik pelepasan spektrometer (ICP-OES). Siasatan mikrostruktur, tingkat penyebaran dan pengukuran sudut pembasahan telah dijalankan pada solder selepas reflow pertama. Selepas itu satu set sampel tertakluk kepada reflow berulang sehingga enam kali dan satu lagi set sampel diletakkan pada suhu tinggi penuaan sehingga 1008h pada suhu 100°-175°C. Mikrostruktur siasatan telah dijalankan di antara muka pateri/substrat menggunakan mikroskop elektron imbasan konvensional (SEM), resolusi tinggi bidang pengeluaran mikroskop elektron pengimbasan (FESEM) dan tenaga serakan sinar-X (EDX). Untuk

menilai interaksi pateri / substrat dalam keadaan cecair dalam kehadiran nanopartikel Mo, dawai Cu (250 μm diameter) telah dicelup ke dalam pateri komposit cair pada suhu 250°C sehingga 15 min. Selepas itu, pasangan solder-substrat dibawa keluar dari solder yang lebur dan diperiksa dengan teliti oleh mikroskop optik, SEM, FESEM, dan EDX.

Keputusan menunjukkan bahawa selepas reflow hanya sebahagian kecil daripada nanopartikel Mo yang kekal di dalam matriks solder. Kadar penyebaran menurun dan sudut basah bertambah dengan penambahan nanopartikel Mo untuk SAC solder. Ia didapati bahawa nanopartikel Mo berkesan untuk menekan pertumbuhan jumlah ketebalan lapisan IMC dan diameter scallop semasa reflow dan penuaan suhu tinggi. Dengan tambahan nanopartikel Mo, pekali resapan dikurangkan tetapi tenaga pengaktifan pertumbuhan scallop IMC kekal tidak berubah. Pembubaran substrat Cu dan pembentukan IMC berkurang dalam kehadiran nanopartikel Mo.

Daripada penyelidikan sekarang ini, didapati bahawa nanopartikel Mo tidak membubarkan atau bertindak balas dengan solder semasa reflow dan penuaan suhu tinggi. Perlambatan ketebalan IMC dan scallop diameter adalah disebabkan oleh kesan partikel diskret daripada nanopartikel Mo. Yang utuh, nanopartikel diskret, dengan menyerap preferentially pada antara muka, menghalang fluks penyebaran substrat dan dengan itu menekan pertumbuhan IMC. Perlambatan lapisan jumlah IMC dengan tambahan nanopartikel Mo meningkatkan kehandalan sendi solder.

ACKNOWLEDGEMENT

First and foremost, I would like to thank almighty Allah SWT to be most gracious and merciful. I would also like to express my deepest appreciation, sincere thanks and gratitude to my honorable supervisors, Prof. Dr. A.S.M.A. Haseeb and Dr. Mohd Rafie Johan. I greatly appreciate their contributions, precious time to monitor and guidance during my period of study. Specially, I deeply appreciate Prof. Dr. A. S. M. A. Haseeb for his valuable academic guidance, encouragement, advice and support throughout my graduate study at UM.

I deeply appreciate the Ministry of Science and Technology (MOSTI, Project No. 13-02-03-3072) and University Malaya (Project no. PS072-2009B) for providing a full financial support to carry out my present research study.

Special thanks to Mr. Nazarul Zaman bin Mohd Nazir for SEM, FESEM and EDX analysis. Without his efforts and patience it would not be possible to finish my large number of samples in time.

Finally, I gratefully acknowledge to my all friends for their input and cooperation during my period of study. Last but not least, I would like to thank my beloved family members specially my parents for their kind support, encouragement and love.

TABLE OF CONTENTS

ORIGINAL LITERARY WORK DECLARATION.....	ii
ABSTRACT	iii
ABSTRAK	v
ACKNOWLEDGEMENT	vii
TABLE OF CONTENTS.....	viii
LIST OF FIGURES	xii
LIST OF TABLES.....	xviii
LIST OF NOTATIONS	xix
LIST OF ABBRIVIATION	xx
CHAPTER 1 INTRODUCTION.....	1
1.1 Background	1
1.2 Research Objectives	3
1.3 Scope of Research	3
1.4 Organization of the Dissertation	4
CHAPTER 2 LITERATURE REVIEW	5
2.1 Electronic Packaging and Soldering Technology	5
2.2 Adverse Health Effect of Lead and Legislation.....	7
2.3 Lead Free Solder Candidates	7
2.3.1 Sn-Au	8
2.3.2 Sn-Bi	8
2.3.3 Sn-Zn	9

2.3.4	Sn-In	9
2.3.5	Sn-Ag	10
2.3.6	Sn-Cu	10
2.3.7	Sn-Ag-Cu	10
2.4	Thermodynamics of Sn-Ag-Cu Solder Alloy Selection.....	10
2.5	Phase Diagram of Mo with Sn, Ag and Cu	13
2.6	Interfacial Reactions of Sn-Ag-Cu Solder alloys with Cu Substrate	14
2.6.1	Reactions in Liquid State	15
2.6.1.1	Initial Formation Mechanism of Interfacial IMCs in Liquid Solder ..	15
2.6.1.2	Growth Kinetics of Interfacial IMCs in the Molten State.....	17
2.6.1.2.a	Dybkov's Analysis.....	17
2.6.1.2.b	Flux Driven Ripening.....	19
2.6.1.3	Dissolution Behavior of the Cu Substrate.....	24
2.6.2	Reaction in the Solid State.....	25
2.6.2.1	Morphology of the Intermetallic Compounds.....	26
2.6.2.2	Kinetic Analysis of the Intermetallic Compounds	27
2.7	Effects of Alloying Elements on the Interfacial IMCs.....	30
2.8	Effects of Nanoparticles on Interfacial IMC.....	32
2.9	Summery and Conclusions	34
CHAPTER 3 METHODOLOGY.....		36
3.1	Raw Materials and Characterization	36
3.2	Sample Preparation and Treatment	36
3.2.1	Preparation of Composite Solder Paste and Nanoparticles Distribution....	36
3.2.2	Preparation of Reflowed Samples	37
3.2.3	Multiple Reflow	37

3.2.4	Solid State Aging.....	38
3.3	Characterization of Samples	39
3.3.1	Differential Scanning Calorimetry Measurement of Solder Paste	39
3.3.2	Inductively coupled-Optical Emission Spectrometer	39
3.3.3	Spreading Rate and Wetting Angle	39
3.4	Reactions in the Liquid State and Dissolution Behavior.....	40
CHAPTER 4 RESULTS AND DISCUSSION		42
4.1	Characterization of As-Received Materials	42
4.1.1	Morphology and Particle Sizes of Solder Paste	42
4.1.2	Transmission Electron Microscopy of Mo nanoparticles	42
4.1.3	X-Ray Diffraction of Mo Nanoparticles	43
4.2	Distribution of Nanoparticles with the SAC Solder Paste.....	44
4.3	Chemical Analysis of the Reflowed Samples	45
4.4	Melting Behavior of Composite Solder Paste.....	47
4.5	Spreading Rate and Wetting Angle.....	49
4.6	Effect of Mo Nanoparticles on IMC during Reflow	50
4.6.1	IMC Morphology and Thickness in Cross-Sectional View	50
4.6.2	IMC Morphology and Scallop Diameter in Plan View	52
4.6.3	Distribution of Mo Nanoparticles in the Solder	55
4.7	Effect of Mo Nanoparticles on Interfacial IMC.....	58
4.7.1	State of Mo Nanoparticles during Reflow	58
4.7.2	Suggested Mechanism for Retardation of IMC Growth by Mo Nanoparticles	59
4.8	High Temperature Aging	62
4.8.1	Morphology of Interfacial IMC during High Temperature Aging.....	62

4.8.2	Growth Kinetics	71
4.8.2.1	Mechanism of IMC Growth during Solid State Aging.....	71
4.8.2.2	Calculation of Diffusion Coefficient	72
4.8.2.3	Calculation of Activation Energy for the Growth of Scallop Diameter	76
4.9	Effect of Mo Nanoparticles on Interfacial Reaction between Liquid SAC and Cu	81
4.9.1	Effect on Dissolution Behavior of Cu Substrate	82
4.9.2	Interfacial IMC Formation and Growth in Liquid Solder.....	84
4.9.3	Mechanism for Suppression of Copper Dissolution.....	87
CHAPTER 5 CONCLUSIONS AND RECOMMENDATIONS.....		89
5.1	Conclusions.....	89
5.2	Recommendation for the Future Works	91
APPENDIX A PUBLICATIONS		92
REFERENCES		94

LIST OF FIGURES

Figure 2. 1: Cross section of a (a) ball grid array (BGA) and (b) flip chip microelectronics connection (Abtew and Selvaduray, 2000).....	6
Figure 2. 2: Phase diagram of the (a) Sn-Ag, (b) Sn-Cu and (c) Ag-Cu system (Ohnuma et al., 2000).....	11
Figure 2. 3: Calculated liquidus surface of the Sn rich region of Sn-Ag-Cu alloy system (Moon et al., 2000).	12
Figure 2. 4: Phase diagram of the (a) Mo-Sn (Brewer and Lamoreaux, 1980), (b) Mo-Ag (Baren, 1990) and (c) Mo-Cu (Subramanian and Laughlin, 1990) system.	14
Figure 2. 5: A Schematic diagram of creation-dissolution mechanism of Cu_6Sn_5 IMC growth on Cu substrate in presence of molten Sn based solder (Lord and Umantsev, 2005).	16
Figure 2. 6: Schematic diagram of the formation mechanism of A_pB_q IMC layer under the condition of simultaneous dissolution into molten solder (Dybkov, 1998).	17
Figure 2. 7: The top surface view of the Cu_6Sn_5 scallops formed at the interface between 50Sn50Pb solder and Cu substrate at 183.5°C for 3 min reaction (Suh et al., 2008).	20

Figure 2. 8: Schematic diagram of Cu_6Sn_5 scallops on Cu substrate in presence of molten Sn-based solder (Gusak and Tu, 2002).	21
Figure 2. 9: Cross-sectional optical microscope of SnPb solder on Cu substrate (a) after two reflow without solid state aging (b) after two reflow followed by solid state again at 170°C for 500 h (Tu and Zeng, 2001).....	26
Figure 2. 10: Morphology of Cu_6Sn_5 IMC between Sn-3.5Ag and polycrystalline Cu substrate (a) scallop type Cu_6Sn_5 after reflow for 60 s at 240°C , (b) planner type Cu_6Sn_5 IMC after aging for 16 days at 150°C (Yang et al., 2011).....	27
Figure 2. 11: Schematic diagram of Cu and Sn diffusion in the Cu- Cu_3Sn - Cu_6Sn_5 -Sn structure (Laurila et al., 2010).	28
Figure 4. 1: SEM image of SAC solder powder (Flux has been removed).	42
Figure 4. 2: (a) TEM micrograph of the Mo nano particles, (b) Histogram of particle size.	43
Figure 4. 3: X-Ray diffraction (XRD) patterns of Mo nanoparticles.	44
Figure 4. 4: FESEM images of solder paste after blending, nominally containing 2 wt% of Mo nanoparticles (a) distribution of Mo nanoparticles into the solder paste, (b) elemental mapping of the composite paste showing Mo (red), Sn (cyan), Ag (blue), and Cu (yellow), (c) high resolution image focused on the solder ball surface and (d) high resolution image focused on the flux.	45

Figure 4. 5: (a) DSC curve of the composite solders, (b) Effect of Mo content on the onset temperature of the solders.	48
Figure 4. 6: (a) Spread rate and (b) wetting angle as a function of wt % of Mo nanoparticles.....	49
Figure 4. 7: Backscattered electron micrographs of the cross sectional view (a) SAC after first reflow, (b) (SAC + 0.10 n-Mo) after first reflow, (c) SAC after six times reflow and (d) (SAC + 0.10 n-Mo) after six times reflow.	51
Figure 4. 8: Effect of Mo nanoparticles on the reflow behavior.	52
Figure 4. 9: SEM micrograph of (SAC + 0.10 n-Mo) sample showing the extent of etching [2x reflow].	53
Figure 4. 10: Top view of the interfacial IMC (a) SAC after first reflow, (b) (SAC + 0.04 n-Mo) after first reflow, (c) (SAC + 0.10 n-Mo) after first reflow, (d) SAC after four times reflow, (e) (SAC + 0.04 n-Mo) after four times reflow, (f) (SAC + 0.10 n-Mo) after four times reflow, (g) SAC after six times reflow, (h) (SAC + 0.04 n-Mo) after six times reflow, and (i) (SAC + 0.10 n-Mo) after six times reflow.	54
Figure 4. 11: Scallop diameter as a function of number of reflows.	54
Figure 4. 12: (a) FE-SEM image of (SAC + 0.04 n-Mo) solder after four times reflow (b) EDX spectrum taken on particle 'X' and (c) EDX spectrum on 'Y'.	56

Figure 4. 13: (a) FESEM micrograph of (SAC + 0.10 n-Mo) solder after six times reflow, and elemental distribution of (b) Mo, (c) Sn and (d) overlapping of the elemental distribution of Sn, Ag, Cu, Mo. 57

Figure 4. 14: Schematic diagram of scallop growth in (a) SAC solder, (b) Mo nanoparticles added SAC solder preferentially absorbed at the IMC scallops (Figures are not in scale)..... 61

Figure 4. 15: Cross sectional backscattered electron micrographs of solder samples aged at 150°C (a) SAC, 48h; (b) (SAC + 0.04 n-Mo), 48h; (c) (SAC + 0.10 n-Mo), 48h; (d) SAC, 168h; (e) (SAC + 0.04 n-Mo), 168h; (f) (SAC + 0.10 n-Mo), 168h; (g) SAC, 504h; (h) (SAC + 0.04 n-Mo), 504h; (i) (SAC + 0.10 n-Mo), 504h; (j) SAC, 1008h; (k) (SAC + 0.04 n-Mo), 1008h; (l) (SAC + 0.10 n-Mo), 1008h..... 63

Figure 4. 16: (a) Total IMC thickness, (b) Cu_3Sn layer thickness of the SAC and nanocomposite solder as a function of aging time. 64

Figure 4. 17: SEM images of the top surface of interfacial IMC of (a) SAC, aged for 504 h, (b) (SAC + 0.10 n-Mo), aged for 504 h, (c) SAC, aged for 840 h, (d) (SAC + 0.10 n-Mo), aged for 840 h at 100°C. 65

Figure 4. 18: SEM images of the top surface of interfacial IMC of (a) SAC, aged for 504 h, (b) (SAC + 0.10 n-Mo), aged for 504 h, (c) SAC, aged for 840 h, (d) (SAC + 0.10 n-Mo), aged for 840 h at 125°C. 66

Figure 4. 19: SEM images of the top surface of interfacial IMC of (a) SAC, aged for 504 h, (b) (SAC + 0.10 n-Mo), aged for 504 h, (c) SAC, aged for 840 h, (d) (SAC + 0.10 n-Mo), aged for 840 h at 150°C. 67

Figure 4. 20: SEM images of the top surface of interfacial IMC of (a) SAC, aged for 504 h, (b) (SAC + 0.10 n-Mo), aged for 504 h, (c) SAC, aged for 840 h, (d) (SAC + 0.10 n-Mo), aged for 840 h at 175°C. 68

Figure 4. 21: Average IMC diameter of the SAC and nanocomposite solder as a function of aging time at (a) 100°C, (b) 125°C, (c) 150°C and (d) 175°C. 69

Figure 4. 22: A typical EDX elemental mapping showing the distribution of Sn, Ag, Mo and Cu on the top of Cu_6Sn_5 layer of the (SAC + 0.10 n-Mo) solder age at 150°C for 840h. 70

Figure 4. 23: Mechanism of IMC growth during solid state aging (a) SAC solder, (b) Mo nanoparticles added nanocomposite solder (The figure is not in scale). 71

Figure 4. 24: The growth of total IMC layer in logarithmic scale during solid state aging at 150°C of (a) SAC, (b) (SAC + 0.04 n-Mo) and (c) (SAC + 0.10 n-Mo) solder. 73

Figure 4. 25: Calculation of diffusion coefficient of SAC and nanocomposite solders. 75

Figure 4. 26: Scallop diameter as a function of aging time for (a) SAC, (b) (SAC + 0.04 n-Mo) and (c) (SAC + 0.10 n-Mo) solder. 76

Figure 4. 27: Relationship between logarithm of (dD_t/dt) vs. logarithm of D for (a) SAC, (b) (SAC + 0.04 n-Mo) and (c) (SAC + 0.10 n-Mo) solder.	78
Figure 4. 28: Plot of $(D_t^n - D_o^n)$ vs. aging time for (a) SAC, (b) (SAC + 0.04 n-Mo) and (c) (SAC + 0.10 n-Mo) solder.	79
Figure 4. 29: Plot of $\ln(k)$ against $1/T$ for SAC and nanocomposites.....	80
Figure 4. 30: Optical micrographs showing cross-section of copper wire after dipping in molten solder for two different time periods (a) SAC for 5 min, (b) SAC for 15 min, (c) (SAC + 0.30 n-Mo) for 5 min, (d) (SAC + 0.30 n-Mo) for 15 min.....	83
Figure 4. 31: (a) Thickness of consumed Cu in the molten solder and (b) Dissolution rate of Cu substrate at 250°C.....	83
Figure 4. 32: Cross sectional SEM micrographs of solder/Cu interface for samples immersed in liquid solder at 250°C (a) SAC for 5 min, (b) SAC for 15 min, (c) (SAC + 0.30 n-Mo) for 5 min, (d) (SAC + 0.30 n-Mo) for 15 min.	85
Figure 4. 33: Graphical representation of the total IMC thickness with time in the liquid state reaction.....	86
Figure 4. 34: (a) High resolution FESEM image of the top surface of Cu_6Sn_5 IMC for (SAC + 0.30 n-Mo) solder for 5 minute reflow (b) EDX spectrum on Mo particles.	87

LIST OF TABLES

Table 2. 1: Dissolution rate and Values of C_s , C and (C_s-C) for different solders with Cu substrate at different temperatures (Yen et al., 2008).	25
Table 2. 2: Effective inter-diffusion coefficient of Cu_3Sn and Cu_6Sn_5 IMC layers.	29
Table 2. 3: Activation energy of the different IMC layers in Sn-based solders.....	30
Table 3. 1: Aging test conditions for different solder samples.	38
Table 4. 1: Molybdenum content of solders analyzed by ICP-OES after reflow.....	46
Table 4. 2: Diffusion Coefficient and n values of SAC and nanocomposite solders.	75
Table 4. 3: Scallop growth exponent, n and scallop growth constant k , activation energy E_a of the SAC and nanocomposite solders.....	81

LIST OF NOTATIONS

SAC	=	Sn-3.8Ag-0.7Cu
Sn	=	Tin
Ag	=	Silver
Cu	=	Copper
Pb	=	Lead
Mo	=	Molybdenum
Co	=	Cobalt
Ni	=	Nickel
Au	=	Gold
Bi	=	Bismuth
Zn	=	Zinc
In	=	Indium
IMC	=	Intermetallic compound
H ₂ SO ₄	=	Sulphuric acid
HNO ₃	=	Nitric acid
HCl	=	Hydrochloric acid
CNT	=	Carbon nanotube
TiO ₂	=	Titanium dioxide
Al ₂ O ₃	=	Alumina
nm	=	Nanometer
μm	=	Micrometer

LIST OF ABBRIVIA TION

TEM	=	Transmission Electron Microscopy
SEM	=	Scanning Electron Microscopy
FESEM	=	Field Emission Scanning Electron Microscopy
EDX	=	Energy Dispersive X-Ray
XRD	=	X-ray Diffraction
DSC	=	Differential Scanning Calorimeter
ICP-OES	=	Inductive Couple Plasma- Optical Emission Spectrometer
ITRS	=	International Technology Roadmap for Semiconductor
EPA-US	=	Environmental Protective Agency-United States
NCMS	=	National Center for Manufacturing Science
EU	=	European Union
WEEE	=	Waste Electrical and Electronic Equipment
IC	=	Integrated Circuit
PCB	=	Printed Circuit Board
BGA	=	ball Grid Array
FC	=	Flip Chip
SMT	=	Surface Mount Technology
PIH	=	Pin in Hole
PTH	=	Pin through Hole
OSP	=	Organic Solderability Preservative

CHAPTER 1

INTRODUCTION

1.1 Background

Regulations restricting the use of lead in electronics have resulted in the recent upsurge in research activities on the development of lead free solders. Research done so far had lead to the emergence of tin based alloys as alternatives to lead based solder alloys. Among the tin based alloys, tin-silver-copper (Sn-Ag-Cu, SAC) alloys have been found to be popular because of their advantages such as good wetting characteristics with substrate, good fatigue resistance, good joint strength etc.

One of the major challenges in the development of a reliable lead-free solder is to improve the mechanical and interfacial properties, and reliability of the solder joints (Koo and Jung, 2005). The microstructure of SAC alloys has been found to coarsen to a greater extent during use and during high temperature exposure as compared with that of their lead containing counterparts (Cheng et al., 2009). Moreover, tin based solders form thicker intermetallic compound (IMC) layer at the solder/substrate interface compared with the lead based solders (Wu et al., 2004). The interfacial IMCs in lead free solder also grow at a rate faster than that in lead based solders. Coarsening of microstructure and rapid growth of brittle interfacial IMC are known to degrade the properties of lead free solder joints resulting in lower long term reliability. Research efforts are therefore underway to improve the quality of tin based solder alloys.

One of the approaches towards improving the properties of tin based solder is through appropriate additions. Both alloy additions (Wang et al., 2009, Laurila et al., 2010) and

particle additions (Das et al., 2009a, Shen and Chan, 2009) are being studied currently. Particles additions to tin based solder leads to the development of composite solders with superior properties. Addition of different types and sizes of particles are under investigations. Particles types investigated so far include metallic (Lin et al., 2002, Amagai, 2008), ceramics (Shen et al., 2006, Lin et al., 2003b) and carbon nanotubes (Kumar et al., 2008). Both micrometer (Das et al., 2009a) and nanometer (Shi et al., 2008) sized particles are currently being considered.

The rationale behind particle addition is that when appropriate types of particles are added to the solder, they should lead to dispersion strengthening. They are also expected to stabilize the microstructure by restricting the growth of different phases in the solder during use. Nanosized particles addition to tin based solders are attracting a great deal of attention in recent years (Shen and Chan, 2009, Amagai, 2008). With the decrease of solder pitch size in electronic packages, the additions of nanoparticles are becoming more relevant.

Improvement in bulk mechanical properties like strength (Shen et al., 2006), hardness (Gain et al., 2011), creep resistance (Shi et al., 2008) etc. have been observed in lead free solders reinforced by nanoparticles additions. In particular, the addition of Mo nanoparticles has resulted in considerable improvement in the bulk mechanical properties of solder (Kumar et al., 2006b, Kumar and Tay, 2004, Rao et al., 2009). However, the performance of a solder joint not only depend on its bulk properties, they also depend on the properties of the solder/substrate interface. It is therefore important to understand the effect of the nanoparticles additions on the interfacial characteristics. There are only a few studies available on the influence of nanoparticles on the interfacial IMC.

1.2 Research Objectives

The objectives of this research are listed as below:

01. To prepare nanocomposite solder based on Sn-3.8Ag-0.7Cu by adding Mo nanoparticles.
02. To study the wetting and reflow characteristics of Sn-3.8Ag-0.7Cu solder on copper substrate with and without the addition of Mo nanoparticles.
03. To investigate the effects of Mo nanoparticles on the morphology and growth of intermetallic compounds during reflow and solid state aging.
04. To study the effects of the presence of Mo nanoparticles in liquid Sn-3.8Ag-0.7Cu on the dissolution rate of copper substrate.

1.3 Scope of Research

The overall aim of this research is to investigate the effect of molybdenum (Mo) nanoparticles on the interfacial reactions between Sn-3.8Ag-0.7Cu solder and Cu substrate during reflow and high temperature aging. For this reason, Mo nanoparticles were manually mixed with the SAC solder paste at various wt% to prepare composite solder paste. Solder joints were prepared on Cu substrate at standard experimental conditions.

The characterizations of nanocomposite solder were carried out using several analytical techniques. SAC solder was used as an experimental reference. Data obtained from this research work also compared and analyzed with other published works.

The characterization of raw materials was carried out by Transmission Electron Microscopy (TEM), Scanning Electron Microscopy (SEM) and X-Ray Diffraction (XRD) analysis. The melting behavior of the nanocomposite solders were investigated

by Differential Scanning Calorimeter (DSC). The Inductively Coupled Plasma-Optical Emission Spectrometry (ICP-OES) was carried out to measure the actual amount of nanoparticles incorporated to the solder. The spreading rate and wetting angle of the solders were measured by following the Japanese Industrial Standard (JIS). The interfacial microstructure of the solder samples were investigated by optical microscopy, conventional SEM, high resolution field emission SEM (FESEM) equipped with Energy Dispersive X-Ray (EDX).

1.4 Organization of the Dissertation

This dissertation consists of five chapters. The first chapter provides a brief introduction of this research work. This chapter states the research background, the current technical problems in this field, research objectives and the scope of this research. The chapter two provides a comprehensive overview of the existing literature background on various topics related with this research. These topics include the electronic packaging and soldering technology, lead-free solder candidates, thermodynamics of alloy selection, interfacial reaction between the solder and substrate during reflow and high temperature aging, effect of alloying elements and effects of nanoparticles on the solder. The experimental procedure is presented in the chapter three which includes the procedures of sample preparations, characterization techniques, the equipments, fixtures and procedure used during characterization. Chapter four of this dissertation reports the results obtained from the experimental work and these results are analyzed and compared with the other published work. A brief summary of this research work is presented in chapter five and the recommendation of the future work is also state.

CHAPTER 2

LITERATURE REVIEW

2.1 Electronic Packaging and Soldering Technology

Soldering technology plays an important role in the electronic packaging industries at various levels such as, wire bonding in surface mount technology, solder ball connection in ball grid arrays (BGA), IC package assembly in printed circuit board (PCB) or flip chip (FC) connections (Kang and Sarkhel, 1994). Solder joint provides the electrical connections among the component in conjunction with thermal, physical and mechanical support in the electronic devices (Abtew and Selvaduray, 2000). When solder joints fail to perform any of these functions, the reliability of the whole electronic system is threatened and may cause shut down of the whole system.

Lead (Pb) based solders are being used in the electronic industries for a quite long time for the purpose of joining electrical components (Tu and Zeng, 2001). Due to the sustained trend of the miniaturization of the electronic devices requires smaller solder joint and fine pitch interconnections (Shen and Chan, 2009). At the same time functional density enhancement and reliability issue are the key concerns in the electronic industries for the market demand. For these reasons ball grid array (BGA) and flip chip (FC) packaging technologies are being used in the electronic industries for having higher input/output connections in a certain area (ITRS, 2001). These ultra-fine solder joints in BGA and FC packaging leads to high localized temperature during service which lead to coarsening the solder microstructure and deteriorate the reliability. This issue has become the main technological issue for electronic packaging and soldering. A typical BGA and FC package is shown in Figure 2.1.

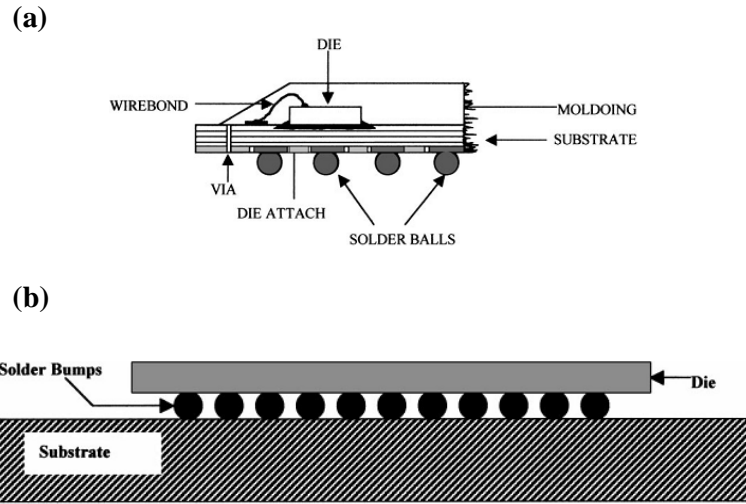


Figure 2. 1: Cross section of a (a) ball grid array (BGA) and (b) flip chip microelectronics connection (Abtew and Selvaduray, 2000).

Reflow and wave soldering processes are being used in the electronic industries for the preparation of solder joints (Robert and Warren, 1993). In reflow soldering process solder is applied as paste by using a stencil mask and then heated to the reflow temperature. This soldering process is quite common in Surface Mount Technology (SMT) process on Printed Circuit Boards (PCBs) (Fujiuchi, 2004). On the other hand, wave soldering is used for pin-in-hole (PIH) or pin-through-hole (PTH) type assemblies where molten solder is applied in the bottom side of PCB and then heated to the soldering temperature. In order to full-fill the technological demand and reliability requirements the choice of proper material is very crucial in both reflow and wave soldering process. For the manufacturing of miniaturized, higher performance and multifunctional electronic device more fundamental challenges need to overcome in the near future specially in the metallurgical aspects.

2.2 Adverse Health Effect of Lead and Legislation

The environmental Protection Agency (EPA) has cited lead and lead-products as one of the top 17 chemicals posing the greatest threat to human life and the environment (Wood and Nimmo, 1994). The exposure of lead (Pb) from the electronic industries is considered as hazardous material for the environment. Again at the end of usual life time of electronic products they are usually disposed to the landfills. At that time Pb is disposed from the electronic materials and contaminates the soil, water, human body and food-chain in ecosystem (Glazer, 1994). As a result “green” electronic products entirely free of toxic materials such as lead are being actively looked into by the researcher worldwide (NCMS, 1997, Harrison and Vincent, 1999, DEIDA, 2000).

Due to the circumstances state above, a bill was introduced in the US court in 1990 to ban lead from all electronic materials, but it was opposed by the industries because of having no alternative solution to replace lead. The EU, on the other hand put their effort to recycle the lead products. At the same time, according to the EU directives on Waste Electrical and Electronic Equipment (WEEE) all products should be lead-free from 2008 (COM, 2000). The RoHS directives strictly restrict the use of lead from all electronic components. But for many applications in electronic products no alternative or “drop-in” solution is found yet for the replacement of Pb from electronic components. All major manufacturers of electronic components planned to eliminate Pb from electronic products and actively looking for an alternative solution.

2.3 Lead Free Solder Candidates

A great deal of effort has been put into the development of Pb-free solder alloys. Certain criteria must be met before a lead-free solder may be put into use. Among these criteria, the most important are physical reliability, temperature requirements,

compatibility with parts and processes, repairs and rework, low cost etc. There are several Pb-free solders, such as, Sn-Au, Sn-Bi, Sn-Zn, Sn-In, Sn-Ag, Sn-Cu, Sn-Ag-Cu etc. which have been investigated in the electronic industry for different applications. The main characteristics of these solder alloy are discussed below.

2.3.1 Sn-Au

Among all the Pb-free solders, Au-based solder has been found as one of the most environmental friendly solder and it is being used in the semiconductor industry for the assembly process (Liu et al., 2008b). Au has been ranked among the least toxic elements by both EPA-US (Environmental Protective Agency-United States) and OSHA (Occupational and Safety Health Administration). The eutectic 80Au-20Sn solder has excellent high-temperature performance, superior resistance to corrosion, high electrical and thermal conductivity and offers fluxless soldering. But, the hardness decreases, creep penetration and creep strain rate of Au-based solder increase with temperature (Liu et al., 2008b, Chidambaram et al., 2010). Beside this, Au-based solder possess satisfactory properties such as suitable melting temperature, good thermal and electrical conductivities, good fluidity and wettability. However, the alloy system has some problems such as low ductility and high cost, which prevent its wide application (Takaku et al., 2008).

2.3.2 Sn-Bi

The eutectic Sn-58Bi solder offer a lower melting point than Sn-Pb alloys of 139° C (Abtew and Selvaduray, 2000). The cost of bismuth is almost similar to that of tin (Abtew and Selvaduray, 2000). But unfortunately, bismuth possesses a potential supply problem since it is a by-product of Pb mining. If a bismuth alloy picks up any Pb, the melting temperature will drop again with the formation of another secondary eutectic

formed at 96°C (Suraski and Seelig, 2001). Beside this, bismuth soldering alloys tends to create embrittlement (Wild, 1971). Bismuth alloys also are prone to failure in peel strength tests due to poor fatigue resistance. Bismuth is also a poor conductor, both thermally and electrically.

2.3.3 Sn-Zn

Zinc is a readily available metal and cheap. The eutectic Sn-9Zn alloy has a low melting point of 198°C which is the closest to eutectic Pb-Sn solder among all other lead-free alternatives (Abtew and Selvaduray, 2000). For this reason, in the recent years the Sn-9Zn alloy received much attention to the electronic industries. But zinc shows a very poor wetting behavior with the substrate including poor corrosion resistance in humid or high temperature environment and forms a stable oxide which keeps its use limited in the electronic packaging industries (Lin et al., 1998, Liu et al., 2008c).

2.3.4 Sn-In

The eutectic Sn-52In alloy has a relatively low temperature of 120°C (Korhonen and Kivilahti, 1998), which makes this solder suitable for low temperature applications. This alloy is a good choice for temperature sensitive equipments which are not exposed to any harsh or high-stress environments. But indium is a scarce metal and too expensive to consider it for board applications (Sharif and Chan, 2005). Beside this, In alloys suffers poor corrosion resistance, forms oxide very rapidly during melting and show strong segregation behavior in the liquid (Korhonen and Kivilahti, 1998).

2.3.5 Sn-Ag

The Sn-4Ag is a fairly good alloy and has a long history in the hybrid circuit industries for electronic packaging applications. But the melting point of this alloy is 221°C which is considered higher for many surface mount technology (SMT) applications.

2.3.6 Sn-Cu

The eutectic Sn-0.7Cu is another promising solder alloy for reflow and wave soldering applications. The melting temperature of this solder is 227°C which is undesirable in many reflow applications. Moreover, the microstructure of this alloy is prone to whisker growth because of high Sn concentration (Boettinger et al., 2005). The cost of this solder is much lower comparing other solders since it does not contain any expensive elements such as, Ag, Bi or In.

2.3.7 Sn-Ag-Cu

This family of lead-free Sn-Ag-Cu alloys has shown high promise in the electronic industries due to having good wetting characteristics with substrate, good fatigue resistance, good joint strength etc. Owing to these advantages, in 2000 the National Electronic Manufacturing Initiative (NEMI) recommended to replace eutectic Sn-Pb solder by near eutectic Sn-Ag-Cu alloys.

2.4 Thermodynamics of Sn-Ag-Cu Solder Alloy Selection

The phase transformation of Sn-Ag-Cu system is evaluated based on the following binary systems: Sn-Ag, Sn-Cu and Ag-Cu (Moon et al., 2000). The calculated binary phase diagrams for the binary system Sn-Ag, Sn-Cu and Ag-Cu are shown in Figure 2.2.

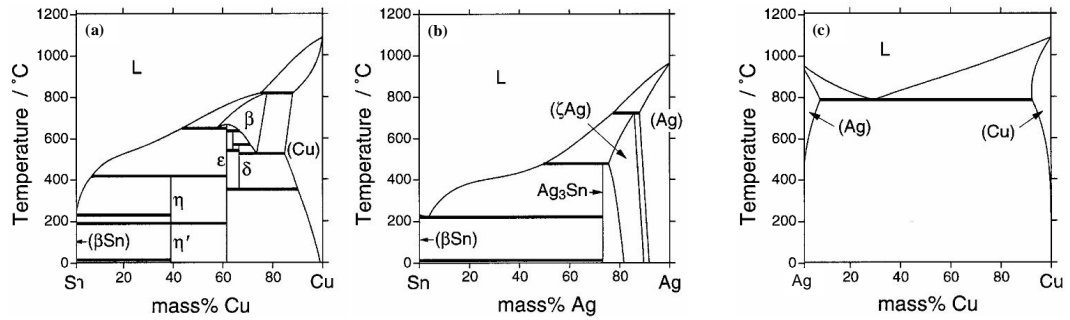


Figure 2. 2: Phase diagram of the (a) Sn-Ag, (b) Sn-Cu and (c) Ag-Cu system (Ohnuma et al., 2000).

The eutectic temperature of the Sn-Cu system is 227°C. The eutectic composition is varied from 0.7 to 0.9 wt% Cu (Moon et al., 2000). The eutectic constituents obtained from the Sn-Cu phase diagram (Figure 2.2a) are β -Sn and Cu_6Sn_5 intermetallics. On the other hand, the eutectic composition of the Sn-Ag system is unanimously taken at 3.5 wt % of Ag and calculated eutectic temperature is 220.1°C (Oh et al., 1996). From the Sn-Ag phase diagram (Figure 2.2b), the eutectic constituents are β -Sn and Ag_3Sn intermetallics. Not all binary or ternary elements form the intermetallic compound in a binary or ternary alloy system. For example, in the Ag-Cu binary system there is no intermetallic compounds as it is seen in the Figure 2.2c.

These binary phase diagrams are used to understand the melting behavior of ternary Sn-Ag-Cu alloy. The alloy design criterion for the Sn-Ag-Cu alloy is as follows (Bath, 2007):

01. The liquidus melting temperature of the alloy should be close to the eutectic Sn-Pb alloy (183°C) to avoid changing the manufacturing process, materials and infrastructure.
02. The gap between the solidus and liquidus temperature should be as low as possible to avoid tombstoning phenomenon and fillet lifting.

03. The solidus temperature of the solder should be significantly higher than the operating temperature of the solder.

The National Center for Manufacturing Sciences (NCMS), Michigan, USA suggested that the solder liquidus temperature should be less than 225°C with a maximum 30°C difference between solidus and liquidus temperature (Bath et al., 2000). Obviously the ternary eutectic or near eutectic Sn-Ag-Cu alloys meet the first two criteria since the melting temperature of the ternary eutectic Sn-Ag-Cu alloy is 217°C (Moon et al., 2000). Depending on particular applications the operating temperature of electronic equipments may be as high as 150°C (Suganuma, 2001). So the ternary eutectic or near eutectic Sn-Ag-Cu alloys are one of the best candidates for lead-free solder alternatives. The calculated eutectic composition of the Sn-Ag-Cu system is 3.66 wt% Ag, 0.91 wt% Cu as it is seen in Figure 2.3 (Moon et al., 2000). But the experimentally determined value of the Sn-Ag-Cu system is 3.5 wt% Ag, 0.9 wt% Cu which differs a little from the calculated value.

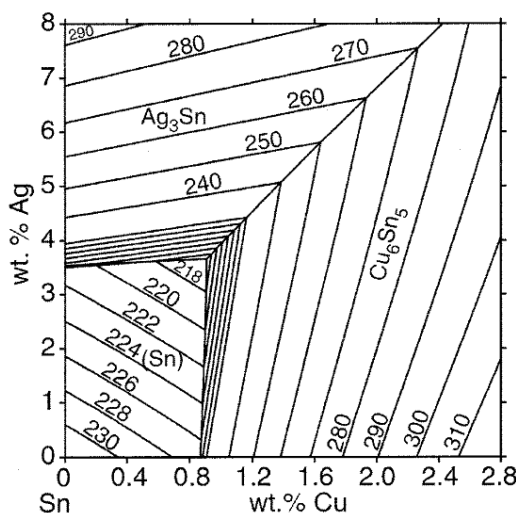


Figure 2. 3: Calculated liquidus surface of the Sn rich region of Sn-Ag-Cu alloy system (Moon et al., 2000).

2.5 Phase Diagram of Mo with Sn, Ag and Cu

The phase diagrams of Mo with Sn, Ag and Cu are shown in the Figure 2.4(a-c) respectively. It is seen in the Mo-Sn phase diagram (Figure 2.4a) (Brewer and Lamoreaux, 1980) that Mo has no solubility in Sn at low temperatures ($<300^{\circ}\text{C}$). The calculated results on solubility of Mo in Sn also show that there is a very negligible solubility of Mo in Sn (Brewer and Lamoreaux, 1980). Three intermetallics e.g. Mo_3Sn , $\text{Mo}_2\text{Sn}_3/\text{Mo}_3\text{Sn}_2$ and MoSn_2 can form in the Mo-Sn system below 300°C (Brewer and Lamoreaux, 1980). On the other hand, the Mo-Ag phase diagram (Figure 2.4b) (Baren, 1990) and Mo-Cu phase diagram (Figure 2.4c) (Subramanian and Laughlin, 1990) show that Mo has no solubility in Ag and Cu respectively. Beside, it is also revealed that Mo does not form any compound with Ag and Cu (Subramanian and Laughlin, 1990, Baren, 1990).

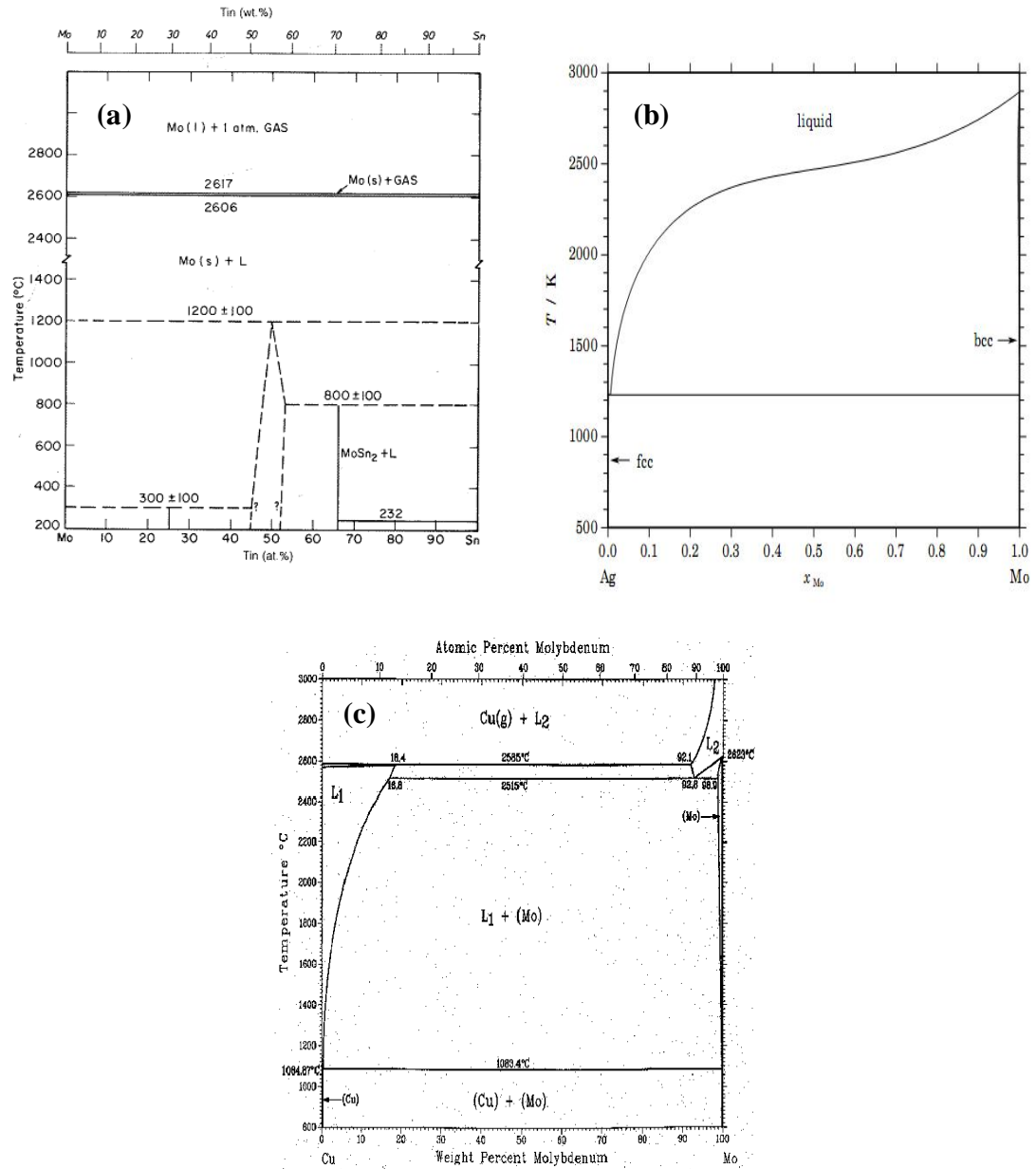


Figure 2. 4: Phase diagram of the (a) Mo-Sn (Brewer and Lamoreaux, 1980), (b) Mo-Ag (Baren, 1990) and (c) Mo-Cu (Subramanian and Laughlin, 1990) system.

2.6 Interfacial Reactions of Sn-Ag-Cu Solder alloys with Cu Substrate

During the soldering process, reactions happen between the solder and substrate and intermetallic compounds (IMCs) form between them. For a good metallurgical bond it is essential to have a uniform IMC layer between the solder and substrate. However, the thickness of IMC strongly affects the reliability and mechanical properties of the solder

joint. A thick IMC hamper the interface integrity because of its brittle nature and creates mismatch in physical properties such as elastic modulus, thermal expansion etc. For this reason, the interfacial reaction should be controlled to ensure the optimized conditions. The interfacial reaction between the solder and substrate can be categorized into two groups, namely:

01. Reactions during reflow process,
02. Reactions during high temperature aging.

The former process is encountered during the reflow and wave soldering processes and the latter happens during service or high temperature aging test.

2.6.1 Reactions in Liquid State

The interfacial reaction between Pb-free solder and metallic substrate during reflow has been studied by many researchers (Su et al., 1997, Alam et al., 2003, Mannan and Clode, 2004, Sharif and Chan, 2004, Yu and Lin, 2005, Sharif and Chan, 2005, Yu et al., 2005b, Yeh et al., 2006), but still the details of the reaction mechanisms are not clear. Typically copper (Cu) is widely used as a substrate in under bump metallurgy due to its good solderability and excellent thermal conductivity performance (Zeng et al., 2010). The growth of scallop type of intermetallic compounds (IMCs) is dominant during soldering between Cu substrate and near eutectic Sn-based solders (Suh et al., 2008).

2.6.1.1 Initial Formation Mechanism of Interfacial IMCs in Liquid Solder

The formation of initial IMC is mainly due to the reason of diffusion of substrate into the molten solder (Yoon et al.). Lord and Umantsev *et al.* (Lord and Umantsev, 2005) has developed one techniques based on fast dipping of Cu coupon into molten Sn solder

2.6.1.2 Growth Kinetics of Interfacial IMCs in the Molten State

2.6.1.2.a Dybkov's Analysis

According to the analysis of Dybkov (Dybkov, 1998), the reaction layer A_pB_q at the interface between the solid substrate (A) and liquid metal (B) forms at the expense of counter-diffusion of components across the bulk when solder is saturated with the substrate as it is illustrated in Figure 2.6. The counter-diffusion of components follows the partial chemical reactions as state below:

$$qB_{diffusing} + pA_{surface} = A_pB_q \quad (2.1)$$

$$pA_{diffusing} + qB_{surface} = A_pB_q \quad (2.2)$$

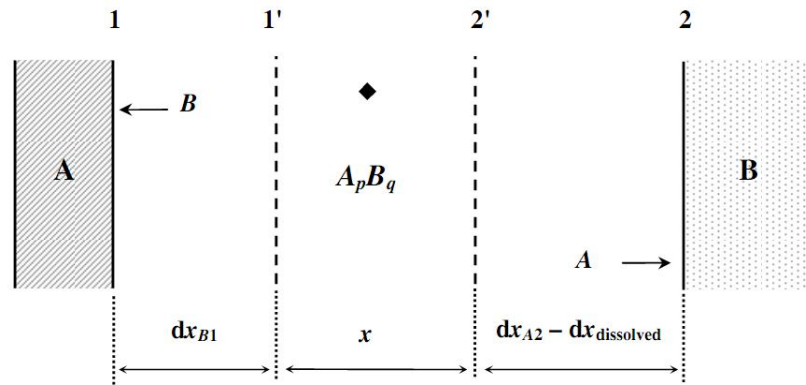


Figure 2. 6: Schematic diagram of the formation mechanism of A_pB_q IMC layer under the condition of simultaneous dissolution into molten solder (Dybkov, 1998).

These reactions yield the increases of layer thickness dx_{B1} and dx_{A2} , during a time, dt , as it is shown in Figure 2.6. It is important to note that the immediate initial stage when substrate (A) react with the molten solder (B) is not considered. The layer growth rate as shown by Dybkov (Dybkov, 1998) is:

$$\left(\frac{dx}{dt} \right)_{growth} = \frac{k_{0B1}}{1 + \frac{k_{0B1}x}{k_{1B1}}} + \frac{k_{0B2}}{1 + \frac{k_{0A2}x}{k_{1A2}}} \quad (2.3)$$

Where k_{0B1} and k_{0A2} are chemical constants, and k_{1B1} and K_{1A2} are diffusional constants.

If the solder is under-saturated with the substrate then the net growth rate of the IMC is the difference between the growth rate at the substrate-IMC interface and IMC-solder interface. In this case, the dissolution rate is described (Dybkov, 1998) as:

$$\left(\frac{dx}{dt} \right)_{dissolution} = b_t = b_0 \exp(-at) \quad (2.4)$$

In this equation, $b_0 = \frac{c_s k}{\rho \varphi}$ and $a = \frac{ks}{v}$

Where, c_s is the saturation concentration of the substrate (A) in the solder (B) at a given temperature, k is the dissolution rate constant, ρ is the density of the $A_p B_q$ compound, φ is the content of substrate (A) in mass fraction in $A_p B_q$, s is the surface area of the solid content with the liquid and v is the volume of the liquid.

So, considering the dissolution and growth of the interfacial IMC, the mathematical equation of the net growth rate of IMC is;

$$\frac{dx}{dt} = \frac{k_{0B1}}{1 + \frac{k_{0B1}x}{k_{1B1}}} + \frac{k_{0B2}}{1 + \frac{k_{0A2}x}{k_{1A2}}} - b_0 \exp(-at) \quad (2.5)$$

From the Equation 2.5, it is seen that the IMC growth is not parabolic. Moreover, if the sum of the rates of chemical reactions at the interface is less than the initial rate of dissolution, i.e., $k_{0B1} + k_{0A2} < b_0$, then no $A_p B_q$ layer would form at the interface. In this case, $k_{0B1} + k_{0A2}$ must be replaced by some other constant k_0 characterized by the rate of direct reaction of the substrate (A) and solder (B). Again the dissolution rate diminishes exponentially from b_0 to b_t in the time range 0 to t . Hence, when $k_{0B1} + k_{0A2} = b_t$, the

A_pB_q layer start to grow at the interface. At large t , $b_t \approx 0$, and layer growth kinetics become parabolic.

If the growth of A_pB_q layer is under constant dissolution rate (b_t) and diffusion control

($k_{0B1} \gg \frac{k_{1B1}}{x}, k_{0A2} \gg \frac{k_{1A2}}{x}$), then Equation 2.5 reduces to;

$$\frac{dx}{dt} = \frac{k_1}{x} - b_t \quad (2.6)$$

The maximum layer thickness can be defined from the condition, $\frac{k_1}{x} - b_t = 0$

$$\text{So, } x_{\max} = \frac{k_1}{b_t} \quad (2.7)$$

2.6.1.2.b Flux Driven Ripening

During the wetting reaction between the molten Sn-based solder and copper substrate, Cu-Sn IMC is formed due to the simultaneous action of growth and ripening (Kim and Tu, 1996). At the solder-substrate interface two types of Cu-Sn compounds are formed: a scallop like Cu_6Sn_5 IMC and a very thin layered Cu_3Sn IMC. Between the Cu_6Sn_5 IMC grains, there are molten solder channels extending all the way to Cu_3Sn /Cu interface. These channels serve as a diffusion and dissolution path for Cu substrates to feed the interfacial reactions. This implies that the ripening process is non-conservative (Suh et al., 2008). A classical theory of conservative ripening was proposed by Lifshitz and Slyozov (Lifshitz and Slyozov, 1961) which is addressed as LSW theory (Suh et al., 2008). This theory is not applicable in the case of molten solder and substrate reaction for the following reasons:

01. When molten solder wets the substrate, the system is considered as an open system. The substrate continuously diffuses through the narrow channels between the IMC scallops to feed the interfacial reaction. On the other hand, in the classic LSW theory, the system is considered as a close system.
02. The LSW theory considers infinitely dilute solution where the distance between the particles are very large compare to their size. But the case of molten solder and substrate reaction, the distance among the particles are not large compare to their size. However, the Cu_6Sn_5 scallops are almost in contact with each other as it is shown in the Figure 2.7.

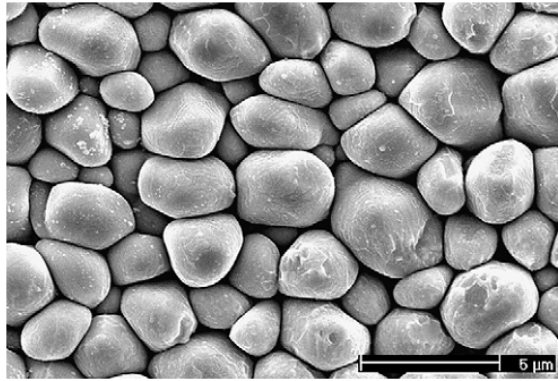


Figure 2. 7: The top surface view of the Cu_6Sn_5 scallops formed at the interface between 50Sn50Pb solder and Cu substrate at 183.5°C for 3 min reaction (Suh et al., 2008).

Since LSW theory can not explain the current situation between the molten solder and substrate, another kinetic theory is proposed by Gusak and Tu (Gusak and Tu, 2002) to have a better understanding on the physical model of the formation and growth of interfacial IMC between molten solder and substrate. This alternative kinetic model is called Flux-driven ripening or FDR theory, where the growth and ripening process is considered as non-conservative. The Figure 2.8 shows a schematic diagram of hemispherical Cu_6Sn_5 scallops grown on Cu substrate to illustrate the FDR theory.

Some assumptions are made in the FDR theory to analyze the kinetics of scallop growth (Kim and Tu, 1996, Gusak and Tu, 2002):

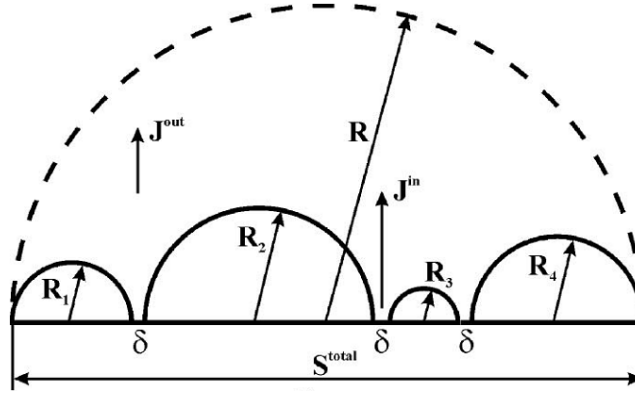


Figure 2. 8: Schematic diagram of Cu₆Sn₅ scallops on Cu substrate in presence of molten Sn-based solder (Gusak and Tu, 2002).

1. The presence of Cu₃Sn is ignored in the analysis.
2. The channel width (δ) is considered small compared with the scallops. In the presence of molten solder, the morphology of channels and scallops are thermodynamically stable. The channels serve as a rapid diffusion path for the Cu substrate to go to molten solder.
3. The scallops are considered hemispherical. For a given surface area between the scallops and Cu substrate (S^{total}), the total surface area between the scallops and molten solder is twice of S^{total} .
4. The in-flux of Cu from the substrate is used for the growth of the scallops. The out-flux of Cu from the ripening zone to the molten solder is considered negligible.

In FDR theory, the average radius of the scallop (r) depends on time (t), obeying following equation:

$$r = 0.913(kt)^{1/3} \quad (2.8)$$

The constant k , in Equation 2.8 depends on several thermodynamics parameters as given below:

$$k = \frac{9}{2} \cdot \frac{n}{n_i} \cdot \frac{D(C^b - C^e)\delta}{C_i} \quad (2.9)$$

Where, C_i is the concentration of Cu in the scallop, C^e is the concentration of Cu at the interface of Cu_6Sn_5 -molten solder in stable equilibrium, C^b is the quasi-equilibrium concentration of Cu in the vicinity of the Cu substrate, n is the atomic density in the molten solder, n_i is the atomic density in the scallop, D is the diffusivity of the Cu in the molten solder, and δ is the width of the channel between scallops.

In the FRD theory, it is considered that there are two kinds of flux responsible for the growth of interfacial IMC: one is ripening flux (J^R) and another is interfacial reaction flux (J^I) (Kim and Tu, 1996). The net growth of the scallops is the result of simultaneous action of these two fluxes.

Ripening Flux

To consider the flux of ripening, it is assumed that the Cu_6Sn_5 IMC is a hemisphere of radius r . Considering the Gibbs-Thomson effect (Yao et al., 1993, Lifshitz and Slyozov, 1961), the ripening flux (J^R) can be written as follows;

$$J^R = \frac{2\gamma\Omega DC_0}{3LRT} \cdot \frac{1}{\bar{r}^2} \quad (2.10)$$

Here, $L = \frac{\bar{\delta}}{\bar{r}}$, C_0 is the equilibrium concentration of Cu, γ is interfacial energy per unit area between Cu_6Sn_5 and molten solder, Ω is molar volume of Cu_6Sn_5 , D is the diffusivity of Cu in the molten solder, δ is the mean separation distance between the scallops, \bar{r} is the mean scallop size, R is the gas constant and T is the temperature.

Interfacial Reaction Flux

As mentioned earlier, there are channels between the IMC scallops extending all the way to $\text{Cu}_3\text{Sn}/\text{Cu}$ interface. These channels serve as a fast diffusion and dissolution path of Cu substrate into the molten solder (Bartels et al., 1994). The interfacial reaction flux (J^I) calculated by Kim and Tu (Kim and Tu, 1996) is:

$$J^I = \frac{\rho N_A A v(t)}{2\pi m N_p(t)} \cdot \frac{1}{\bar{r}^2} \quad (2.11)$$

Here, $v = \frac{dh}{dt}$, ρ is the density of Cu, m is the atomic mass of Cu, N_A is the Avogadro's number, A is the total area of solder-Cu interface, dh is the consumed thickness of Cu, t is the time, $N_p(t)$ is the total number of grains at the interface and $2\pi\bar{r}^2$ is the surface area of a hemispherical Cu_6Sn_5 grain.

Total Flux

The net growth of scallop type Cu_6Sn_5 IMC is a combined kinetic process of ripening and interfacial reaction. Using Gauss' theorem, the growth equation of scallop type Cu_6Sn_5 is:

$$r^3 = \int \left(\frac{\gamma \Omega^2 D C_0}{3 N_A L R T} + \frac{\rho A \Omega v(t)}{4 \pi m N_p(t)} \right) \quad (2.12)$$

From Equation 2.12, it is seen that the kinetics of Cu_6Sn_5 scallops has $t^{1/3}$ dependence with time. This indicates that the kinetics of the growth of Cu_6Sn_5 scallops is not diffusion controlled or interfacial reaction controlled (Kim et al., 1995). Furthermore, this scallop type morphology is stable as long as there is unreacted Cu in the molten state. When all available Cu is consumed due to the reactions into the molten solder, the non-conservative ripening become conservative ripening and leads to spalling of the interfacial IMC (Liu et al., 1996).

2.6.1.3 Dissolution Behavior of the Cu Substrate

In the soldering process, when substrate come in contact with the molten solder, the substrate starts to dissolve. For example, when Cu substrate comes in contact with the molten Sn-based solder, the Cu substrate starts to dissolve and a chemical potential gradient between the elements is generated at the solder-substrate interface. The dissolution behavior of the substrate in the molten solder can be well described by the Nernst-Shchukarev equation (Barmak and Dybkov, 2004);

$$\frac{dc}{dt} = k \cdot \frac{s}{v} \cdot (c_s - c) \quad (2.13)$$

Where k is the dissolution rate constant, s is the surface area of the substrate, V is the volume of the molten solder, C_s is the equilibrium concentration of the substrate and C is the concentration of the substrate at the reaction temperature.

Equation 2.13 indicates that the dissolution of the substrate depends on two parameters: the equilibrium concentration of substrate (C_s) and dissolution rate constant (k). Generally the value of C_s increases with temperature which in turn increases the concentration gradient ($C_s - C$). As a result, the dissolution rate increases with temperature. On the other hand, the concentration of the substrate (C) depends on the

solder composition. Considering the Cu substrate, Table 2.1 presents the values of C_s , C and $(C_s - C)$ for different solders at different immersion temperatures.

Table 2. 1: Dissolution rate and Values of C_s , C and $(C_s - C)$ for different solders with Cu substrate at different temperatures (Yen et al., 2008).

Solder	Immersion Temperature (°C)	C_s wt %	C wt %	$(C_s - C)$ wt %	Dissolution Rate (μm/min)
Sn	300	2.8	0	2.8	7.25
	270	1.9		1.9	4.50
	240	1.2		1.2	2.14
Sn-3.0Ag-0.5Cu	300	2.4	0.5	1.9	4.20
	270	1.9		1.4	2.95
	240	1.3		0.8	0.99
Sn-58Bi	300	1.2	0	1.2	1.15
	270	0.8		0.8	0.95
	240	0.5		0.5	0.57

2.6.2 Reaction in the Solid State

Formation of intermetallic compounds is inevitable during soldering reaction between the molten solder and substrate. An adequate and uniform intermetallic layer is essential for a good metallurgical bond between the solder and substrate. But the inherent brittle nature of interfacial IMCs too thick interfacial layer promotes a brittle failure to the interface (Pang et al., 2004, Lee and Duh*, 1999). For this reason, the thickness of the interfacial IMC should be optimized. During service or high temperature aging the thickness of interfacial IMC increases due to diffusion of Sn from the bulk solder to the substrate (Sivasubramaniam et al., 2008). A number of studies (Zou et al., 2008, Sivasubramaniam et al., 2008) reported the morphology and kinetics of IMC growth in the solid state which is discussed in the next sections.

2.6.2.1 Morphology of the Intermetallic Compounds

Formation of Cu_6Sn_5 IMC during the reaction between molten Sn-based solder and Cu substrate has been reported by a number of studies (Laurila et al., 2005, Gong et al., 2008). Some of the study also reported the formation of a very thin Cu_3Sn layer (a few tens of nanometer) between the Cu_6Sn_5 IMC and Cu substrate (Shang et al., 2009, Gong et al., 2009). But after reflow most of the time this thin Cu_3Sn layer is not visible under SEM in the cross-sectional view. In general, for most of the Sn-based solder this newly form Cu_3Sn IMC layer grows at the side of Cu substrate during solid state aging as it is shown in Figure 2.9 (Tu and Zeng, 2001, Zou et al., 2008). With increasing aging time and temperature, the thickness of both Cu_6Sn_5 and Cu_3Sn layer increases (Zou et al., 2008).

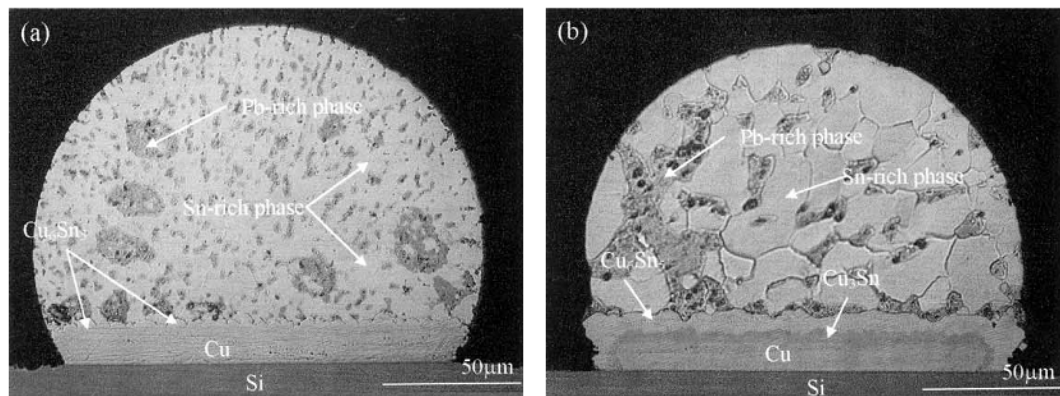


Figure 2. 9: Cross-sectional optical microscope of SnPb solder on Cu substrate (a) after two reflow without solid state aging (b) after two reflow followed by solid state again at 170°C for 500 h (Tu and Zeng, 2001).

Another phenomenon that is observed during solid state aging is that both Cu_6Sn_5 and Cu_3Sn have layer type morphology (Yang et al., 2011). There are no longer any channels between the Cu_6Sn_5 scallops as it is shown in Figure 2.10b. For this reason, it is believed that the growth of interfacial IMC in solid state is diffusion controlled (Sivasubramaniam et al., 2008).

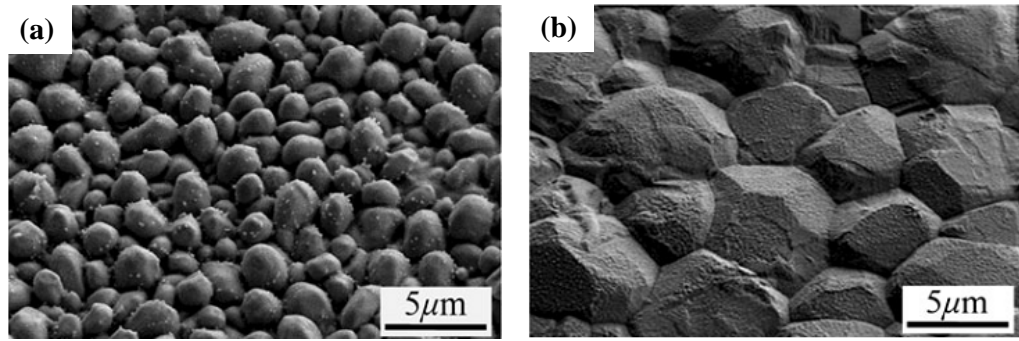


Figure 2. 10: Morphology of Cu_6Sn_5 IMC between Sn-3.5Ag and polycrystalline Cu substrate (a) scallop type Cu_6Sn_5 after reflow for 60 s at 240°C , (b) planner type Cu_6Sn_5 IMC after aging for 16 days at 150°C (Yang et al., 2011).

2.6.2.2 Kinetic Analysis of the Intermetallic Compounds

The kinetics of the reaction during solid state aging can be either diffusion controlled or interfacial reaction controlled (Goesele and Tu, 1982, Kidson, 1961). In the diffusion controlled growth the IMC growth has square root dependence with the aging time. On the other hand, in the interfacial reaction controlled growth the IMC growth has a linear relationship with time. Generally, at any particular temperature the growth kinetics of any reaction layer follow the following empirical power law relationship with time (Alam and Chan, 2005).

$$x_t - x_0 = kt^n \quad (2.14)$$

This equation can also be rewritten in the following logarithmic expression,

$$\log(x - x_0) = \log k + n \log t \quad (2.15)$$

Where x_t is the total IMC thickness at time t , x_0 = thickness of the IMC after reflow, k is the growth rate exponent and n is the time exponent. From the value of n , it is possible to deduce the type of solid state growth kinetic and the growth mechanism of the interfacial IMC at the solder/substrate interface (Frear, 1991). Most of the literatures

agree that the value of n for the growth of total IMC layer in the cross-sectional view is equal to $\frac{1}{2}$ (Zou et al., 2008, Alam and Chan, 2005). So the growth kinetics of interfacial IMC layer follows the parabolic or diffusion controlled process.

Laurila *et al.* (Laurila et al., 2005) has proposed one model to explain the mechanism of Cu and Sn diffusion in the Cu-Cu₃Sn-Cu₆Sn₅-Sn structure as shown in Figure 2.11. Due to the concentration gradient established in the Cu₆Sn₅ phase, Sn is the main diffusion species and diffuses from Sn-Cu₆Sn₅ interface to Cu₃Sn-Cu₆Sn₅ interface. In the case of Cu₃Sn, Cu diffuses from the Cu-Cu₃Sn interface to Cu₃Sn-Cu₆Sn₅ interface. In this growth model it is assumed that all reactions occur at the Cu₃Sn-Cu₆Sn₅ interface. The composition of the IMC formed depends on the ratio of Cu and Sn diffusion at the Cu₃Sn-Cu₆Sn₅ interface.

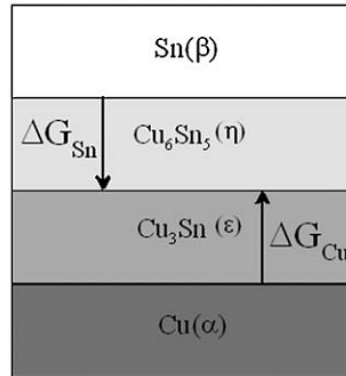


Figure 2. 11: Schematic diagram of Cu and Sn diffusion in the Cu-Cu₃Sn-Cu₆Sn₅-Sn structure (Laurila et al., 2010).

The effective inter-diffusion coefficient (D_{eff}) of the total IMC layer can be determined by the following Fick's law (Zhu et al., 2006);

$$x_t - x_0 = (D_{eff} t)^{\frac{1}{2}} \quad (2.16)$$

The value of inter-diffusion coefficient vary with the composition of solder alloys, substrate orientation, reflow temperature, reflow time, aging temperature etc. From the literature it is found that the value of inter-diffusion coefficient varies in the order of $\sim 10^{-8} \text{ m}^2\text{s}^{-1}$. The values of inter-diffusion coefficient for the Cu_6Sn_5 and Cu_3Sn IMC layer are shown in the Table 2.2.

Table 2. 2: Effective inter-diffusion coefficient of Cu_3Sn and Cu_6Sn_5 IMC layers.

Solder Alloy	Aging Temperature (K)	Effective Inter-Diffusion Coefficient m^2s^{-1}		Reference
		Cu_3Sn	Cu_6Sn_5	
Sn-3.8Ag-0.7Cu	423	3.36×10^{-18}	-	(Peng et al., 2007)
Sn-3.0Ag-0.5Cu	423	1.99×10^{-18}	1.77×10^{-18}	(Yoon et al., 2009)
Sn-3.5Ag	423	9.80×10^{-18}	-	(Nishikawa et al., 2007)
		2.23×10^{-18}	8.31×10^{-19}	(Flanders et al., 1997)
		2.09×10^{-17}	4.96×10^{-17}	(Lee and Chen, 2002)
Sn-58Bi	423	3.90×10^{-18}	-	(Shang et al., 2009)
Sn	423	1.04×10^{-18}	3.15×10^{-17}	(Lee and Chen, 2002)

Activation energy for the IMC growth of different solder-substrate couples are calculated after aging the samples at different temperatures. Activation energy is defined as the minimum energy needed to start a chemical reaction or diffusion to take place. In general, from the published data it is found that the activation energy for the formation of Cu_3Sn IMC is higher than the Cu_6Sn_5 or total IMC in the Sn-based solder (Lee et al., 2003a, Watanabe et al., 2006, Yoon et al., 2009). Higher activation energy reduces the atomic diffusion and inhibits the formation of interfacial IMC (Li and Shi, 2006). Some published results of activation energy for different Sn-based lead-free solders are presented in Table 2.3.

Table 2. 3: Activation energy of the different IMC layers in Sn-based solders.

Solder	Activation energy for IMC layer formation KJ/mol			References
	Cu ₃ Sn	Cu ₆ Sn ₅	Total IMC	
Sn-3.5Ag	89.06	48.54	64.82	(Lee et al., 2003a)
	91.6	-	-	(Lee and Chen, 2002)
	70.8	-	38.9	(Watanabe et al., 2006)
Sn-3.0Ag-0.5Cu	114.7	58.6	75.1	(Yoon et al., 2009)
Sn-3.5Ag-0.5Cu	88.1	-	44.3	(Watanabe et al., 2006)
Sn-3.8Ag-0.7Cu	101.3	-	-	(Lee and Chen, 2002)
Sn-3.0Ag-0.5Ni	-	34.6	47.5	(Yoon et al., 2009)
Sn-3.5Ag-0.5Cu-0.15Ni-0.01Ge	51.4	-	20.3	(Watanabe et al., 2006)
Sn-3.5Ag-0.5Cu-0.25Ni-0.01Ge	62.2	-	18.5	(Watanabe et al., 2006)

2.7 Effects of Alloying Elements on the Interfacial IMCs

A good number of researches have been done on the interfacial IMCs with the addition of alloying elements (Lee et al., 2003b, Li et al., 2009, Yu et al., 2008, Xiao et al., 2009, Wang et al., 2009, Kim et al., 2003). It is concluded from the previous research that addition of alloying elements to the solder attributes their affects on interfacial IMCs in the following three ways (Zeng et al., 2010):

1. Alloying elements can increase or decrease the thickness of interfacial IMCs.
2. The physical and chemical properties of the interfacial IMCs can be altered due to the addition of alloying elements.
3. Additional reaction layer can be formed at the interface between the solder and substrate.

Depending on the solubility, Laurila *et al.* (Laurila et al., 2010) categories the alloying elements into two groups:

1. Elements that show marked solubility on the Sn-Cu intermetallics, such as Ni, Co, Au, Sb, In, etc.
2. Elements that do not show marked solubility on the Sn-Cu intermetallics, such as Al, Bi, P, Ti, S, rare earth elements.

Of all the investigated alloying elements, Ni and Co has a prominent solubility on the interfacial IMCs. It is found that addition of Ni and Co as an alloying element to the solder increases the total IMC thickness but the Cu_3Sn IMC thickness is decreased during reflow and aging compared to the solder with out addition (Wang et al., 2009). Park *et al.* (Park et al., 2003) observed that the addition of Au (less than 0.25 wt %) to the near eutectic SAC solder results scallop type $(\text{Cu,Au})_6\text{Sn}_5$ IMC after reflow. However, if the Au content is more than 0.25 wt% the morphology of the interfacial IMC is changed with the formation of two phase layer $[(\text{Cu,Au})_6\text{Sn}_5)+\text{Sn}]$. Addition of Au reduces the Cu_3Sn IMC, but the effect of Au is weaker than Ni and Co because of having lower solubility in Cu_3Sn IMC (Zakel et al., 1991). On the contrary, though Sb has a strong effect on solid solution strengthening of Sn (Wade et al., 2001, Li et al., 2006), it has virtually no effect on the interfacial IMC (Laurila et al., 2010). Literature results of In addition to the Sn-based solder reports lower dissolution of Cu substrate and suppression of the thickness of Cu_6Sn_5 IMC (Sharif and Chan, 2005). However, the micrographs presented in the literature do not entirely support that In hinders the growth of Cu-Sn IMC (Sharif and Chan, 2005, Laurila et al., 2010). EDX results show that In dissolves into Sn sublattice of the Cu-Sn IMC to form $[\text{Cu}_6(\text{Sn,In})_5]$.

Addition of elements that do not show marked solubility on the interfacial Cu-Sn IMC like Al is found to increase the mechanical properties such as microhardness, strength etc. to the SAC solder (Liu and Lin, 2008, Das et al., 2009b). There is no report on the

effect of Al addition on Cu-Sn IMC. The presence of 0.03 wt% P in Sn-3Ag solder was found to have no effect on the IMC thickness and scallop diameter after one and four time reflow (Takemoto et al., 1987). Addition of rare earth elements (Ce and La) to Sn-3.5Ag and Sn-0.7Cu solder reported not to have a notable effect on the interfacial IMC (Wu and Wong, 2007).

2.8 Effects of Nanoparticles on Interfacial IMC

Recently, nanocomposite solders are being investigated specially for cases where better creep and fatigue resistance are required (Shen and Chan, 2009). Several methods such as ball milling (Lin et al., 2002, Lin et al., 2003a, Lin et al., 2003b), paste mixing (Liu et al., 2008a, Tai et al., 2005), mixing with molten solder alloy (Shen et al., 2006), in-situ method (Lee et al., 2000, Hwang et al., 2002) etc. have been developed for mixing nanoparticles with the solder. Refinement of solder microstructure resulting from nanoparticle addition has been reported in a number of studies (Kumar et al., 2008, Shen et al., 2006, Lin et al., 2003b). Amagai *et al.* (Amagai, 2008) studied the effect of Co, Ni, Pt, Al, P, Cu, Zn, Ge, Ag, In, Sb and Au nanoparticles on the interfacial IMC between Sn-3.0Ag solder and organic solderability preservative (OSP) Cu pads during reflow and aging process. It was also found that nanoparticles of Co, Ni and Pt are effective in influencing the growth of interfacial IMC layer between Sn-based lead-free solder and Cu substrate after reflow (Amagai, 2008). Recent results show that Co and Ni nanoparticles impart their effect on the interfacial IMC through alloying effect (Amagai, 2008, Lin et al., 2009, Haseeb and Leng, 2011). With the addition of Co and Ni nanoparticles to the SAC solder the total thickness of interfacial IMC increases but the thickness of Cu_3Sn IMC decreases (Haseeb and Leng, 2011). Extent of alloying effect of nanoparticles is related to the solubility of that particular element into the solder (Laurila et al., 2010).

Reported results of inert nanoparticles addition to Sn-based solder such as Al_2O_3 (Zhong and Gupta, 2008), ZrO_2 (Shen et al., 2006), SiC (Liu et al., 2008a), TiO_2 (Lin et al., 2003a), carbon nanotubes (Kumar et al., 2006a, Kumar et al., 2008) shows refinement bulk microstructure and improvement of the mechanical properties such as micro hardness. So far, the effect of inert nanoparticles on the interfacial IMC has not been investigated. Some theories have been developed to explain the mechanism through which inert nanoparticles might impart their effect on the interfacial IMC. Inert nanoparticles are considered as a surface active material since they accumulate themselves at the grain boundaries of the solder matrix and do not react with the solder. Hence, surface absorption theory (Zhai et al., 1999, Shen and Chan, 2009) can be applied to explain the controlling mechanism of the suppression of interfacial IMC due to the addition of inert nanoparticles. According to the theory, the surface free energy of a whole crystal is:

$$\sum_k \gamma_{(c)}^k A_k = \sum_k \gamma_{(0)}^k A_k - RT \sum_k A_k \int_0^c \frac{\Gamma^k}{c} dc \quad (2.17)$$

Where, Γ^k is the adsorption of surface-active material at crystal planes k , c is the concentration of the surface-active material, R is the ideal gas constant, T is the absolute temperature, $\gamma_{(c)}^k$ is the surface tension of crystal planes k with adsorption of the active material, $\gamma_{(0)}^k$ is the surface tension of the initial crystal planes k without adsorption, and A_k is the area of the crystal planes k .

The net value of the right hand side becomes lower with increasing the value Γ^k . This implies that the surface free energy of the whole crystal plane would decrease with the maximum amount of adsorption, Γ^k . Thus, an increase in the amount of elements adsorbed decreases its surface energy and, therefore, decreases the growth velocity of this crystal plane (Shen and Chan, 2009). Generally, crystal planes having higher

surface energy grows rapidly. But the surface energy is decreased when surface active materials are absorbed at the crystal plane. As the amount of absorption of surface active material is increased, the growth velocity of the crystal plane is decreased.

Since the explanation in surface absorption theory is qualitative, this theory is not universally accepted to explain the effect of inert nanoparticles on the interfacial IMC. There are several factors that affect the growth process of interfacial IMCs, such as substrate dissolution, grain boundary diffusion, grain coarsening, grain boundary grooving etc, into the molten solder (Schaefer et al., 1998). So this is particularly important to investigate the distribution, locations, reactions of the nanoparticles into the solder during reflow (Shen and Chan, 2009). So a deep and qualitative analysis of the state and distribution of inert nanoparticles into the molten solder is needed.

2.9 Summery and Conclusions

There are several challenges to be met before the lead-based solders are completely replaced by the lead-free solders in the electronic industries. Among them the sustain trend of miniaturization and functional density enhancement requires much smaller solder joints with a fine pitch interconnections. These ultra-fine solder joints lead to high homologous temperature during services which may lead to coarsening of the microstructure at the solder/substrate interface. To ensure a fine and uniform solder joint microstructure, the key issue is to slow down the interfacial reactions between the solder and substrate.

So far, numerous solders have been studied by researchers world wide. Most of the researches focus on the bulk microstructure and mechanical properties with and without the addition of additives. Some researches focus the addition of alloying elements as

well as nanoparticles to the lead-free solder. It was found from the previous research that addition of Fe, Co, Ni as an alloying element to the solder increases the intermetallic compound formation at the solder/substrate interface. Beside, nanoparticles of Co and Ni also show a similar trend of increasing the intermetallic compound thickness. Addition of inert nanoparticles such as TiO_2 , Al_2O_3 , CNTs focus only the bulk microstructure and mechanical properties of the solder. No research has been done on the interfacial IMC with the addition of inert metallic nanoparticles.

Clearly, at present, there is a serious lack of scientific data about the interfacial IMC between solder and substrate in presence of inert metallic nanoparticles such as Mo nanoparticles. Interaction between the solder and inert as well as active nanoparticles are far from being studied. Systematic laboratory work should be carried out under wide spectrum of experimental conditions that is likely to be encountered in practical conditions.

CHAPTER 3

METHODOLOGY

3.1 Raw Materials and Characterization

In this research work commercial molybdenum (Mo) nanoparticle (99.8% trace metal basis) was used as a reinforcing material with the Sn-3.8Ag-0.7Cu (SAC) solder paste (Indium Corporation of America). The particle size of the SAC solder paste was determined from SEM (Philips XL-40) image. For this purpose, flux from the solder paste was removed by using propanol. Then a small amount of solder sample was taken in a sample holder and dried at 100°C for one hour in an oven. After that the dried solder was analyzed under SEM.

The morphology and size of the Mo nanoparticles were investigated by using a Philips CM200 transmission electron microscopy (TEM). For this purpose, a small amount of Mo nanoparticles were dispersed into distilled water onto a carbon film supported by copper grids. The grain size measurement and phase analysis of Mo nanoparticles was conducted by X-Ray diffractometer (XRD). The nanoparticles were exposed to $\text{CuK}\alpha$ ($\lambda=0.15406$ nm) radiation with a scanning speed of 2°/min in the 10-80° diffraction range with a step size of 0.05°.

3.2 Sample Preparation and Treatment

3.2.1 Preparation of Composite Solder Paste and Nanoparticles Distribution

Mo nanoparticles were manually mixed with Sn-3.8Ag-0.7Cu (SAC) solder paste for a nominal composition up to 5 wt%. The mixing time was at least 30 min to obtain a homogeneous paste composition. To find out the distribution of Mo nanoparticles into

the SAC solder paste, small amount composite paste was taken to a SEM sample holder. Then the sample holder along with the composite paste were placed in an oven and heated at 100°C for one hour to dry the paste composition. After that, the dry composite paste was analyzed by high resolution field emission SEM (Zeiss Ultra-60 FESEM) and energy-dispersive X-ray spectroscopy (EDX, EDAX-Genesis Utilities) to check the distribution of Mo nanoparticles into the SAC solder.

3.2.2 Preparation of Reflowed Samples

The solder samples were prepared on commercial polycrystalline copper sheets (30 mm x 30 mm x 0.3 mm). Prior to soldering, the sheets were cleaned and dipped in 10 vol% H₂SO₄ to remove oxide and then rinsed thoroughly in distilled water followed by cleaning with acetone. After the surface preparation the composite solder paste was placed on the copper substrate through a mask having an opening diameter of 6.5 mm and 1.24 mm thickness (JIS Z3198-3, 2003). Then the composite solder paste was reflowed on a hot plate at 250°C for 45 s.

3.2.3 Multiple Reflow

After first reflow one set of samples were reflowed again in a reflow oven (Forced convection, FT02) for two, four and six times at 250°C for 45 s. After reflow, the solders were cleaned with acetone to remove the flux residue. The multiple reflowed samples were also cross sectioned, mounted in epoxy and polished by employing the standard metallographic techniques. The cross-sectional view of the interfacial IMC was observed by backscattered electron detector under a scanning electron microscope (SEM). The elemental analysis was carried out by using energy dispersive X-ray spectroscopy (EDX). To expose the top surface of the intermetallic compound, the solders were chemically etched for 24h as it is mentioned previously. In this case also

the microstructure was observed by SEM and high resolution field emission SEM (Zeiss Ultra-60 FESEM). The elemental analysis was carried out by energy-dispersive X-ray spectroscopy (EDX, EDAX-Genesis Utilities).

3.2.4 Solid State Aging

After first reflow another set of solder samples were subjected to aging at a temperature 100°C, 125°C, 150°C and 175°C up to 1008 h. The aging time and temperatures for different solders are shown in the Table 3.1. After the aging tests, the samples were also cross sectioned and polished to a 0.02 µm finish employing the standard metallographic techniques. To expose the top surface of the intermetallic compound, the solders were chemically etched for 24 h with (93% CH₃OH + 5% HNO₃ + 2% HCl) (Yen et al., 2008). The microstructure was examined by an optical microscope, a scanning electron microscope (SEM) and a high resolution field emission SEM (Zeiss Ultra-60 FESEM). The elemental analysis of the phases was carried out using energy-dispersive X-ray spectroscopy (EDX, EDAX-Genesis Utilities) and elemental mapping.

Table 3. 1: Aging test conditions for different solder samples.

Solder Alloy	Aging Time (h)						
	24	96	168	336	504	840	1008
SAC	100°C	100°C	100°C	100°C	100°C	100°C	-
	125°C	125°C	125°C	125°C	125°C	125°C	-
	150°C	150°C	150°C	150°C	150°C	150°C	150°C
	175°C	175°C	175°C	175°C	175°C	175°C	-
SAC + 0.04 n-Mo	100°C	100°C	100°C	100°C	100°C	100°C	-
	125°C	125°C	125°C	125°C	125°C	125°C	-
	150°C	150°C	150°C	150°C	150°C	150°C	150°C
	175°C	175°C	175°C	175°C	175°C	175°C	-
SAC + 0.10 n-Mo	100°C	100°C	100°C	100°C	100°C	100°C	-
	125°C	125°C	125°C	125°C	125°C	125°C	-
	150°C	150°C	150°C	150°C	150°C	150°C	150°C
	175°C	175°C	175°C	175°C	175°C	175°C	-

3.3 Characterization of Samples

3.3.1 Differential Scanning Calorimetry Measurement of Solder Paste

Differential scanning calorimetry (DSC, Mettler DSC 820, Switzerland) measurements were conducted to find out the melting temperatures of the composite solder pastes. Samples were weighted by a microbalance (~10-15 mg). Then the samples were placed on a 70 μ l platinum crucible inside the DSC furnace and heated to 250°C at a heating rate of 10°C/min. The onset temperature in the DSC curve was taken as the melting point of the solders.

3.3.2 Inductively coupled-Optical Emission Spectrometer

The solder samples were chemically analyzed by inductively coupled-Optical Emission Spectrometer (ICP-OES, Perkin Elmer Optima 2000 DV) to find out the actual amount of molybdenum content in the solder. After reflow, the flux residue on top of the solder matrix was removed by hexane. The solders were scratched out using tweezers. After that 0.5g of flux residue and solders were digested in 5 ml concentrated hydrochloric acid (HCl) separately and then diluted to 100 ml deionized water. The calibration standard solution of Mo (Cat No. 1.70227.0500, Merck) were prepared from the 1000 ppm stock solution. Each calibration curve was created using three standard concentration curves (2, 4 and 6 ppm). The concentration of Mo inside the solder and flux was indicated by the intensity of the emission.

3.3.3 Spreading Rate and Wetting Angle

The ability of the molten solder to spread over the substrate is used to measure the wetting behavior. After first reflow, at least twelve samples were utilized to calculate the spread rate according to the Japanese Industrial Standard (JIS Z3198-3, 2003).

According to the Japanese Industrial Standard, the spread rate was calculated by the following equation (3.1).

$$S_R = \frac{D - H}{D} \times 100 \quad (3.1)$$

$$\text{And, } D = 1.24V^{1/3} \quad (3.2)$$

Where, S_R = Spread rate (%), H = Height of the spread solder (mm), D = Diameter when the solder used for a test is considered as a ball (mm) and V = Mass/density of the solder sample used for the test = 7.5 gm/cm^3 .

After calculating the spreading rate, the solder samples were cross sectioned, mounted in epoxy and polished up to $0.02 \text{ }\mu\text{m}$ finish by employing standard metallographic technique for measuring the wetting angle by optical microscope.

3.4 Reactions in the Liquid State and Dissolution Behavior

To study the reactions in the liquid state and dissolution behavior, polycrystalline Cu wire having a diameter $250 \text{ }\mu\text{m}$ was used as the substrate. Prior to soldering, the wire was cleaned and dipped in 10 vol. % H_2SO_4 to remove any oxide contamination. After that the wire was thoroughly rinsed in distilled water followed by cleaning with acetone. Weighed solder paste with masses of 20.0 g were then placed in a crucible in the furnace. The paste was heated to 250°C and held at that temperature for at least 5 minutes to homogenize the composition. Then the substrates were dipped vertically into the solders. The reaction time was 5 to 15 minute. The copper wire-solder reaction couples were mounted in epoxy resin to prepare the cross-sectional samples for metallographic preparation. The diameter of the Cu wire after reaction with the liquid solder was measured under a low magnification optical microscope. Diameter measurement was done on least three different samples at eight different angles and the

average value is reported here. The interfacial microstructure between the solder and substrate was examined by backscattered electron detector under a scanning electron microscope (SEM). The elemental analysis of the phases was carried out using energy-dispersive X-ray spectroscopy (EDX).

To find out the distribution of Mo nanoparticles, solders were also prepared on commercial polycrystalline copper sheets (30 mm x 30 mm x 0.3 mm) as it is mentioned in the section 3.2.3. In this case, the composite solder paste was reflowed on the hot plate at 250°C for 5 min with a nominal 5 wt% Mo concentration. To expose the top surface of the interfacial IMC the solder samples were chemically etched for 24 h with (93% CH₃OH + 5% HNO₃ + 2% HCl) (Yen et al., 2008). The microstructure and elemental analysis was carried out with conventional SEM, field emission SEM (Zeiss Ultra-60 FESEM) and EDX (EDAX-Genesis Utilities). For observing and analyzing the nanoparticles, In-Lens detector was used in FESEM with EHT voltage of 10kV. The working distance was 7.2mm. Using these parameters the samples were magnified up to 50K for microstructural investigations.

CHAPTER 4

RESULTS AND DISCUSSION

4.1 Characterization of As-Received Materials

4.1.1 Morphology and Particle Sizes of Solder Paste

Figure 4.1 shows the morphology of Sn-3.8Ag-0.7Cu (SAC) solder powder in the solder paste. Flux was removed from the solder paste by dissolving it in propanol. The shape of the SAC solder particles is spherical with a small variation in diameter. The average diameter calculated from Figure 4.1 is $34 \pm 6 \mu\text{m}$.

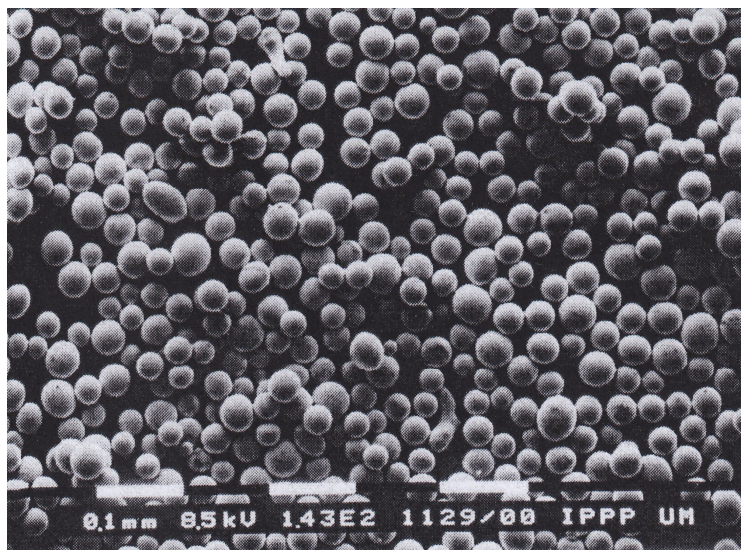


Figure 4. 1: SEM image of SAC solder powder (Flux has been removed).

4.1.2 Transmission Electron Microscopy of Mo nanoparticles

Figure 4.2 shows a transmission electron microscopy (TEM) micrograph and the particle size distribution of Mo nanoparticles. More than 250 particles were used for calculating particle size distribution. It is found from the distribution that the size of the most particles is in between 20-100 nm, although some particles are as big as 200 nm.

But the frequency of the particles having size more than 200 nm is quite low. The weighted average of the size distribution shows that the average size of Mo nanoparticles is 70 nm.

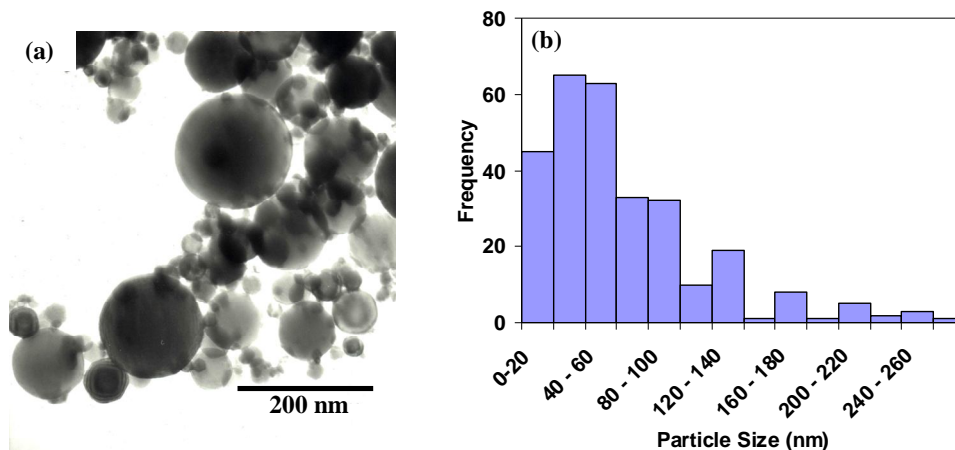


Figure 4. 2: (a) TEM micrograph of the Mo nano particles, (b) Histogram of particle size.

4.1.3 X-Ray Diffraction of Mo Nanoparticles

The XRD pattern of the Mo nanoparticles is shown in Figure 4.3. Three strong peaks at 40.509° , 58.599° and 73.660° clearly indicates the presence of (110), (200) and (211) crystal plane in Mo nanoparticles respectively. It may be noted that no oxide peak was observed from the XRD pattern. The grain size of Mo nanoparticles was calculated by using the Scherrer's equation. The parameter β in the Scherrer's equation was corrected by assuming it as a Gaussian function for the diffraction peaks and instrumental broadening. The average grain size of Mo nanoparticle was found around 40 nm.

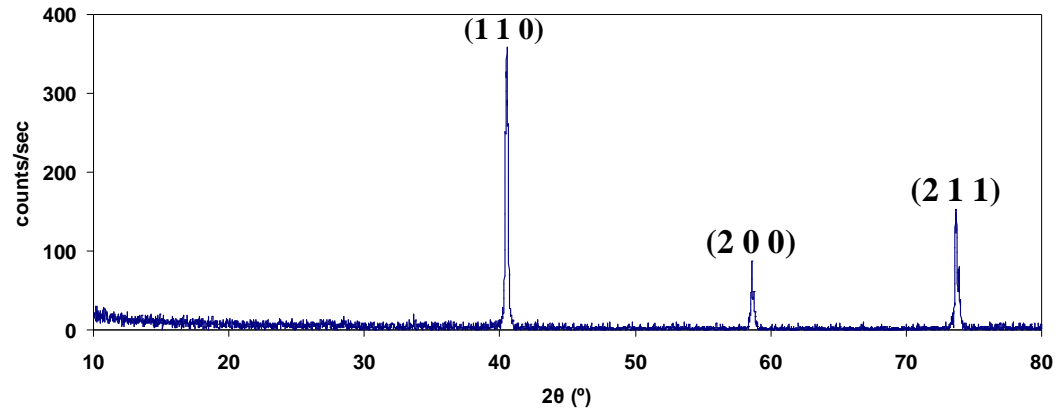


Figure 4. 3: X-Ray diffraction (XRD) patterns of Mo nanoparticles.

4.2 Distribution of Nanoparticles with the SAC Solder Paste

The spatial distribution and elemental map of Mo nanoparticles in the solder paste nominally containing 2 wt% Mo after 30 min mixing are shown in Figure 4.4. Figure 4.4a shows an overall view of the paste at a lower magnification. It is seen in Figure 4.4a that tiny Mo nanoparticles adhere to the surface of large SAC balls. Mo nanoparticles are also seen in the flux situated at the crevices between SAC balls. High magnification images provide clean views of both SAC ball surface (Figure 4.4c) and flux (Figure 4.4d). It is observed that Mo nanoparticles are fairly well distributed in the paste.

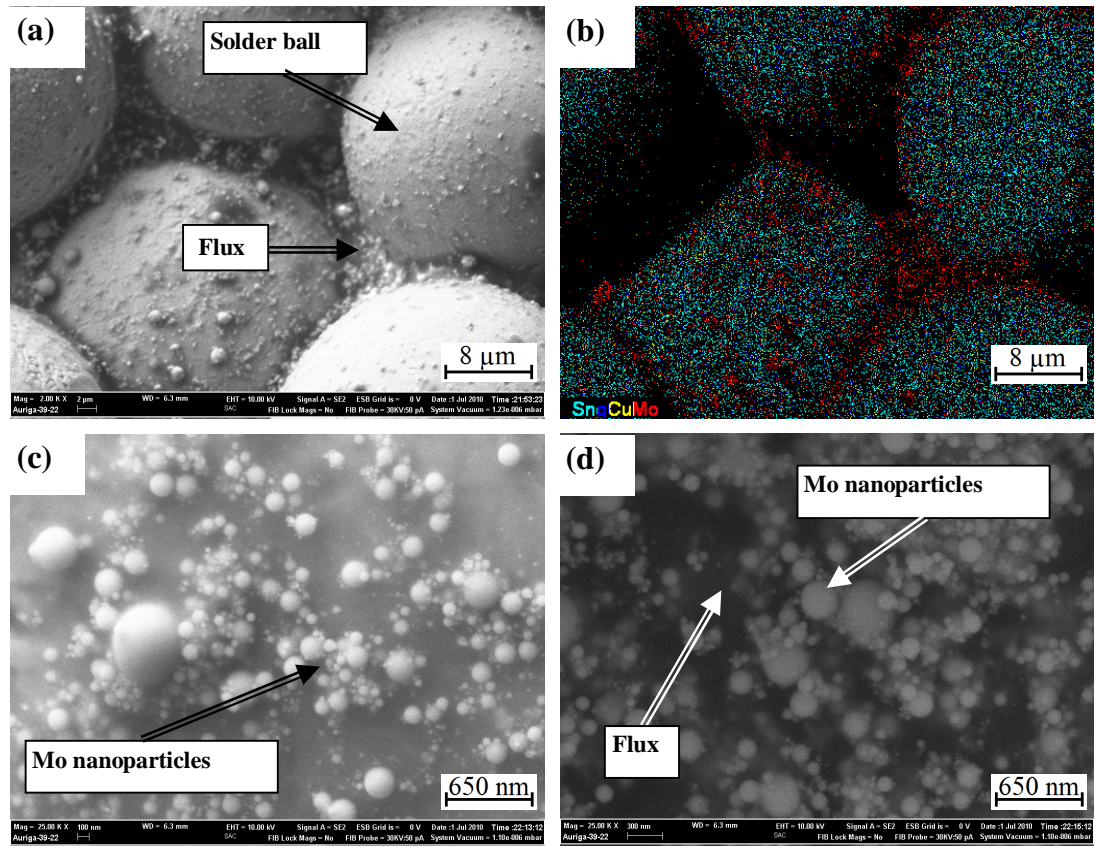


Figure 4. 4: FESEM images of solder paste after blending, nominally containing 2 wt% of Mo nanoparticles (a) distribution of Mo nanoparticles into the solder paste, (b) elemental mapping of the composite paste showing Mo (red), Sn (cyan), Ag (blue), and Cu (yellow), (c) high resolution image focused on the solder ball surface and (d) high resolution image focused on the flux.

4.3 Chemical Analysis of the Reflowed Samples

Upon reflow, the solder balls melted, coalesced and formed the solder joint. The flux residue stays on the surface of the solder joint. In order to find out how much Mo nanoparticles is retained in the solidified solder, the latter was chemically analyzed by ICP-OES. The actual Mo content of the solder is shown in the Table 4.1. For the nominal addition of 1, 2, 3 and 5 wt% of Mo nanoparticles into the solder paste, the actual content in the solder is found to be only 0.04, 0.10, 0.14 and 0.30 wt% of Mo respectively. The rest of the Mo enters in the flux residue (Arafat et al., 2011). Hereafter, solders actually containing 0.04, 0.10, 0.14 and 0.30 wt % Mo will be

designated as (SAC + 0.04 n-Mo), (SAC + 0.10 n-Mo), (SAC + 0.14 n-Mo) and (SAC + 0.30 n-Mo) respectively with n referring to nanoparticles.

Table 4. 1: Molybdenum content of solders analyzed by ICP-OES after reflow.

Nominal Mo Content, wt %	Actual Mo content in the solder, wt %	Actual Mo content in the flux, wt %
1.0	0.04	5.40
2.0	0.10	6.85
3.0	0.14	-
5.0	0.30	-

It may be noted that the solder paste consists of a flux in which SAC solder balls were dispersed. After the addition and mixing of nanoparticles, the Mo nanoparticles also dispersed within in the flux remaining in between the SAC balls (Figure 4.4). During reflow process, a fraction of the nanoparticles enters the molten pool of solder and eventually got trapped inside the solidified solder mass. The rest stays with the flux residue. Similar result was obtained for Co nanoparticles (Arafat et al., 2011). However, in the case of Co nanoparticles, the fraction of nanoparticles retained in the solder was higher. The incorporation of nanoparticles into solder will mainly depend on the interactions between nanoparticles and the solder. It has been suggested that a reinforcing particle can be pushed (rejected), engulfed or entrapped at the particle-liquid metal interface depending upon the interaction mechanisms (Wilde and Perepezko, 2000, Dhindaw, 1999). The incorporation of a lower amount of Mo in SAC suggests that Mo nanoparticles experiences rejection by the liquid SAC interface to a greater extent. Poor wetting of Mo and SAC could be a reason for higher rejection. Notwithstanding the rejection, the amount of Mo nanoparticles still retained in the solder has definite influence on interfacial IMC growth characteristics as will be discussed later.

This simple paste mixing method to incorporate nanoparticles into the solder is gaining increasing attention by the researchers nowadays (Tai et al., 2005, Shen et al., 2006). Reported results on sample prepared by paste mixing method also show that enough nanoparticles can be incorporated to the solder to enhance its properties (Tai et al., 2005, Shen et al., 2006). On the other hand this method can be used in the conventional reflow process using the existing industrial infrastructure (Zerrer et al., 2008, Chen et al., 2009).

4.4 Melting Behavior of Composite Solder Paste

Figure 4.5a shows the DSC curves for SAC and nanocomposite solders. On heating the samples show a clear endothermic peak for SAC and nanocomposites. Addition of Mo nanoparticles is found to broaden the peaks and lead to the occurrence of a shoulder at the higher temperature side of the melting peak. The melting temperature of the solders was measured from the onset of endothermic peaks. It was found from the onset endothermic peaks of SAC solder that the melting temperature of SAC is 217.1°C. This result is consistent with other reported results (Kumar et al., 2008, Gao et al., 2009). The addition of Mo nanoparticles is seen to cause a slight decrease in the onset melting temperature (Figure 4.5b). With the addition of 0.30 wt% Mo into the SAC solder the onset melting point drops from 217.1°C to 215.5°C.

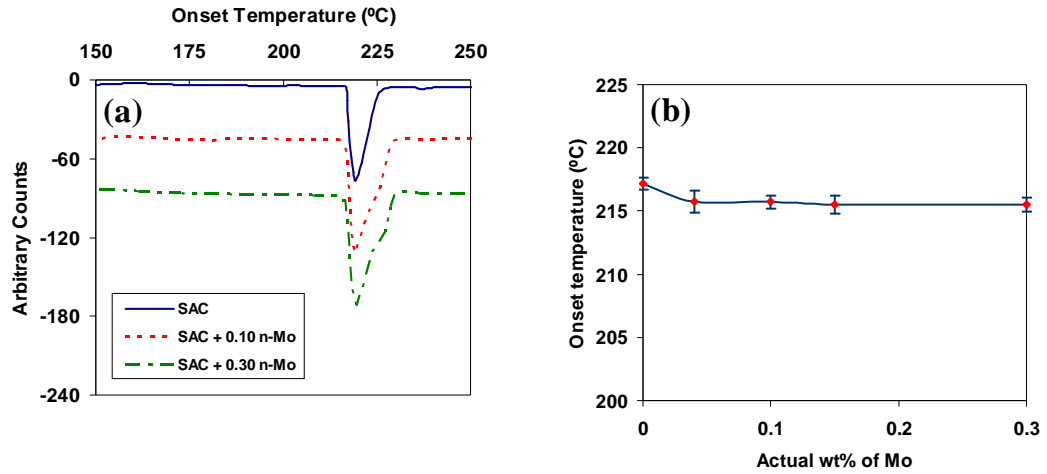


Figure 4. 5: (a) DSC curve of the composite solders, (b) Effect of Mo content on the onset temperature of the solders.

A number of researchers studied the melting behavior of nanocomposite solders (Liu et al., 2008a, Kumar et al., 2008, Shen et al., 2006). The addition of SiC (Liu et al., 2008a), carbon nanotubes (Kumar et al., 2008) was found to lower the onset temperature by a couple of degree. Moreover the onset temperature decreased to a greater extent as more nanoparticles were added to the solder. These observations are similar to what has been observed in the present study. It may be mentioned that in the above reported studies, nanoparticles such as SiC, carbon nanotubes used were inert and are unlikely to dissolve in the solder. Thus the depression in onset temperature can not be attributed to a dissolution or alloying effect. No mechanism for such depression in onset temperature has been confirmed. However, some sort of increased surface instability caused by higher surface energy of nanoparticles has been suggested as a possible reason (Liu et al., 2008a, Kumar et al., 2008). It is possible that higher interfacial energy could cause an early melting at the solder/nanoparticle interface which led to lower onset temperature. It was also observed that the addition of Mo nanoparticles led to the occurrence of a shoulder at the higher temperature side of the melting paste. It may be noted that for the DSC heating rate used in the present study,

10° C/min, no shoulder was obtained for SAC by others (Nishikawa et al., 2009). The DSC curve obtained for SAC in the present study is consistent with the earlier results. The occurrence of shoulders and the broadening in the DSC curve of melting paste brought about by Mo nanoparticle indicate that the presence of these particles change, to some extent, the melting behavior of the solder.

4.5 Spreading Rate and Wetting Angle

Figure 4.6 shows the spreading rate and wetting angle of the Mo added nanocomposite solder as a function of nanoparticles content. The spread rate drops from 79.8 to 76.8% to the (SAC + 0.10 n-Mo) solder with a maximum standard deviation ~ 2 (Figure 4.6 a). On the other hand the wetting angle increases from 17.8° to 28.8° to the (SAC + 0.10 n-Mo) solder with a maximum standard deviation ~ 5 (Figure 4.6.b).

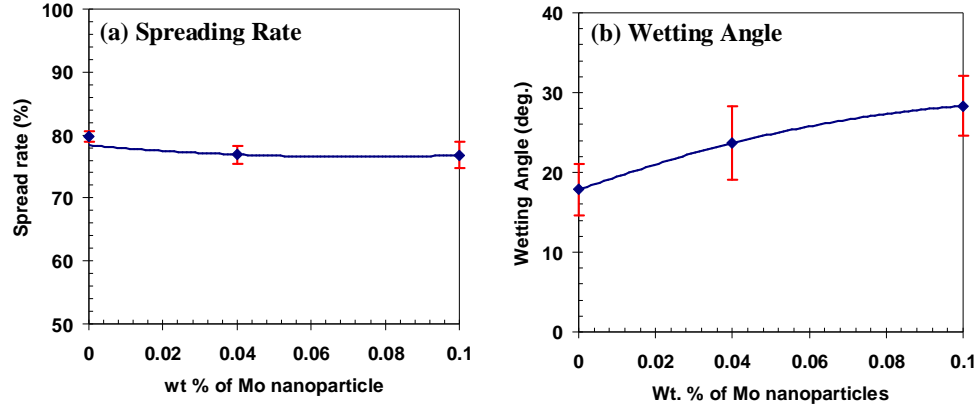


Figure 4. 6: (a) Spread rate and (b) wetting angle as a function of wt % of Mo nanoparticles.

Actually, spreading rate and wetting angle are used to measure the solderability of the composite paste. For good metallurgical bond between solder and substrate, the spreadability and wettability should be in acceptable range. It is generally agreed that

higher spreading rate with a lower wetting angle is desired during reflow. With increasing Mo nanoparticles up to 0.1 wt % into the SAC solder paste the spreading rate decreases from 79.8 to 76.8% but the wetting angle increases from 17.8° to 28.8°. However Mo nanoparticles-added SAC solder shows a considerable solderability comparing the SAC and Sn-Pb solder (Wang et al., 2008). Reported results of wetting angle by wetting balance technique for Sn-Pb solder on Cu substrate was found 20° (Wang et al., 2008). The possible reason for decreasing spreading rate could be due to the increase of melt viscosity for addition of nanoparticles into solder paste. Increased amount of nanoparticles inhibits the molten composite solder to flow on the substrate (Nai et al., 2006). Inhibition to flow of the composite melt on the substrate is believed to lead higher wetting angle compare with SAC solder.

4.6 Effect of Mo Nanoparticles on IMC during Reflow

4.6.1 IMC Morphology and Thickness in Cross-Sectional View

Figure 4.7 (a, b) shows the cross sectional backscattered electron micrographs of SAC and (SAC + 0.10 n-Mo) after first and six reflow. Formation of IMC between the solder and Cu substrate is clearly visible. On all samples, Cu_6Sn_5 with a typical scallop type morphology formed. The composition of Cu_6Sn_5 was confirmed by EDX. Below the Cu_6Sn_5 layer, a thin flat layer of Cu_3Sn having a darker contrast is visible in all samples. Evidence of the formation of a very thin Cu_3Sn IMC layer during reflow is available in the literature between Sn-based solder and Cu substrate (Shang et al., 2009, Gong et al., 2009). A comparison between Figure 4.7a and 4.7b shows that the addition of Mo nanoparticles results in a decrease in overall IMC thickness after first reflow. The effect of Mo nanoparticles is evident after six times reflow as well (Figure 4.7c and 4.7b). No molybdenum could be detected inside the Cu_6Sn_5 IMC by EDX analysis for both first time and six times reflow.

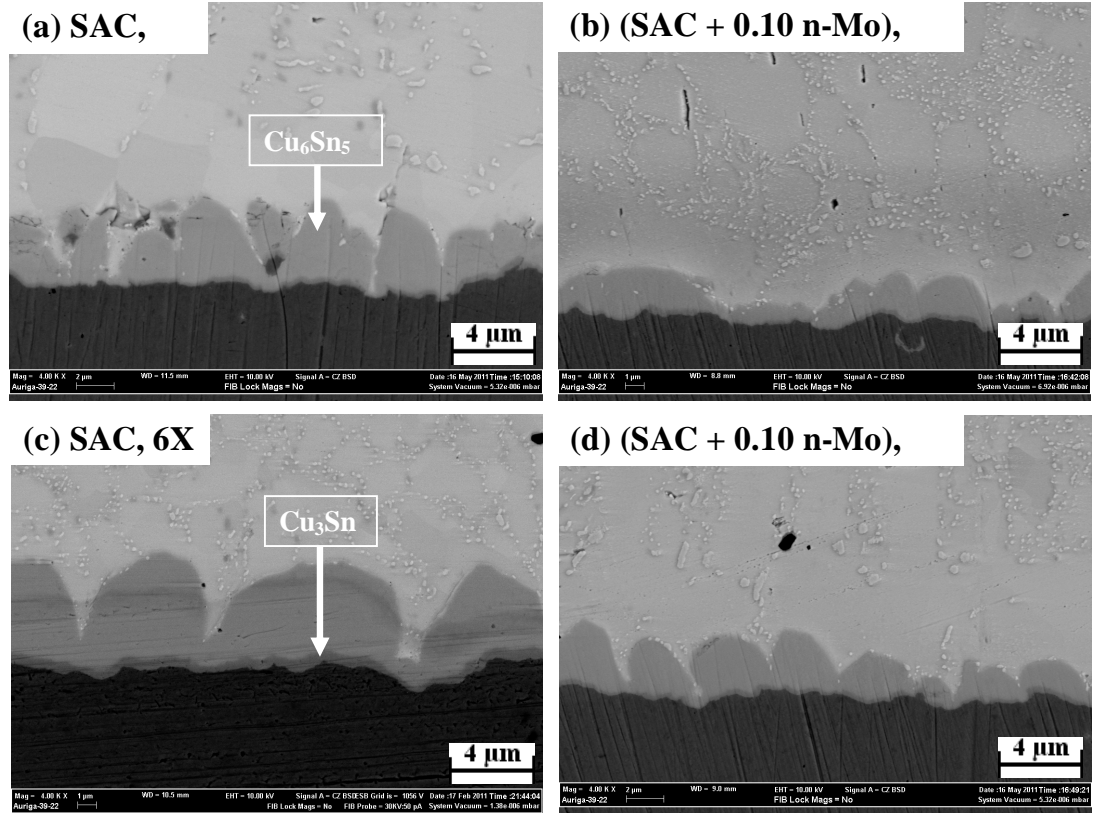


Figure 4. 7: Backscattered electron micrographs of the cross sectional view (a) SAC after first reflow, (b) (SAC + 0.10 n-Mo) after first reflow, (c) SAC after six times reflow and (d) (SAC + 0.10 n-Mo) after six times reflow.

The thickness of the interfacial IMC increases with an increase in the number of reflow for both SAC and Mo nanoparticle added SAC solder. But the thickness of the interfacial IMC is lower in all cases for the Mo nanoparticles-added solder compared with the SAC solder. In Figure 4.8, the variation of IMC thickness is shown with respect to the number of reflow for both SAC and Mo nanoparticles-added solders. Lower IMC thickness is observed for all Mo nanoparticles-added samples.

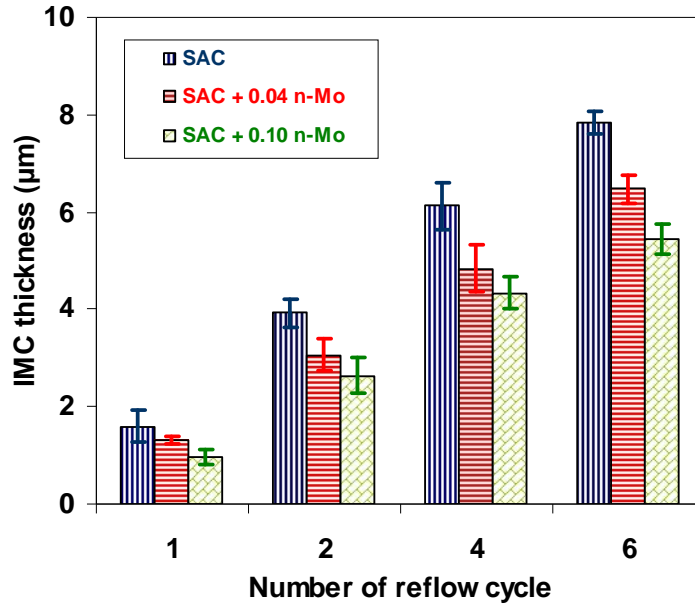


Figure 4. 8: Effect of Mo nanoparticles on the reflow behavior.

4.6.2 IMC Morphology and Scallop Diameter in Plan View

Deep etching was employed to reveal the top view of the interfacial IMC of the solder sample. Figure 4.9 shows a typical low magnification micrograph of the (SAC + 0.10 n-Mo) solder sample after deep etching. It is seen from the figure that the visibility of interfacial IMC in top view depends on the extent of etching. Places where etching is complete, a clear view of IMC can be seen as it is indicated by white outline in the Figure 4.9. To compare top morphology of the top view of interfacial IMC on different samples, places of complete etching was observed under SEM. To find out the distribution of Mo nanoparticles particularly places where the etching was incomplete was observed.

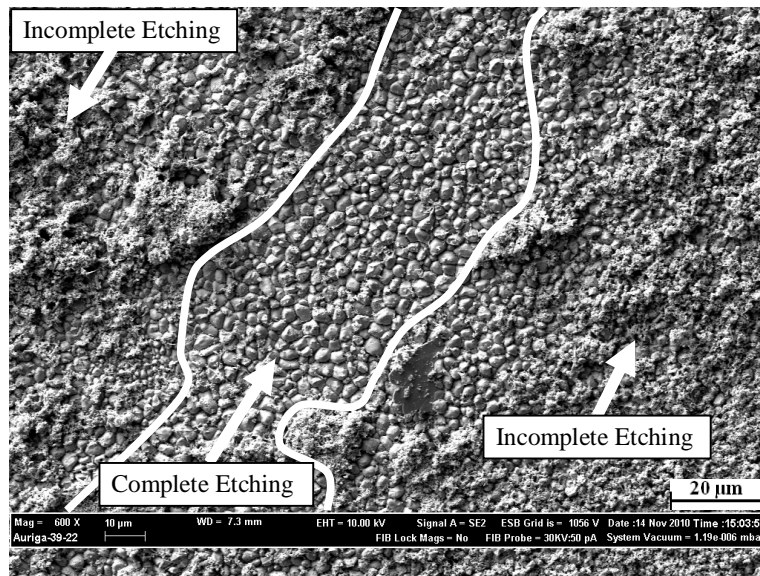


Figure 4. 9: SEM micrograph of (SAC + 0.10 n-Mo) sample showing the extent of etching [2x reflow].

Figure 4.10 shows the top view of the interfacial IMC for the SAC and Mo nanoparticles-added solder samples after first and six times reflow. Places undergoing complete etching were utilized to observe the morphology of the top view of interfacial IMC as mentioned earlier. In all cases, it is found that the morphology of the interfacial IMC is scallop type. EDX analysis on these scallops confirmed that these are Cu_6Sn_5 IMC. From Figure 4.10 it is seen that as the number of reflows is increased, the diameter of the scallop is increased for both SAC and Mo nanoparticles-added solders. It is also seen that the diameter of the scallops is smaller for Mo nanoparticles-added solder compared with that of SAC in all reflow conditions. In Figure 4.11 the average scallop diameter is represented with respect to reflows number for different samples.

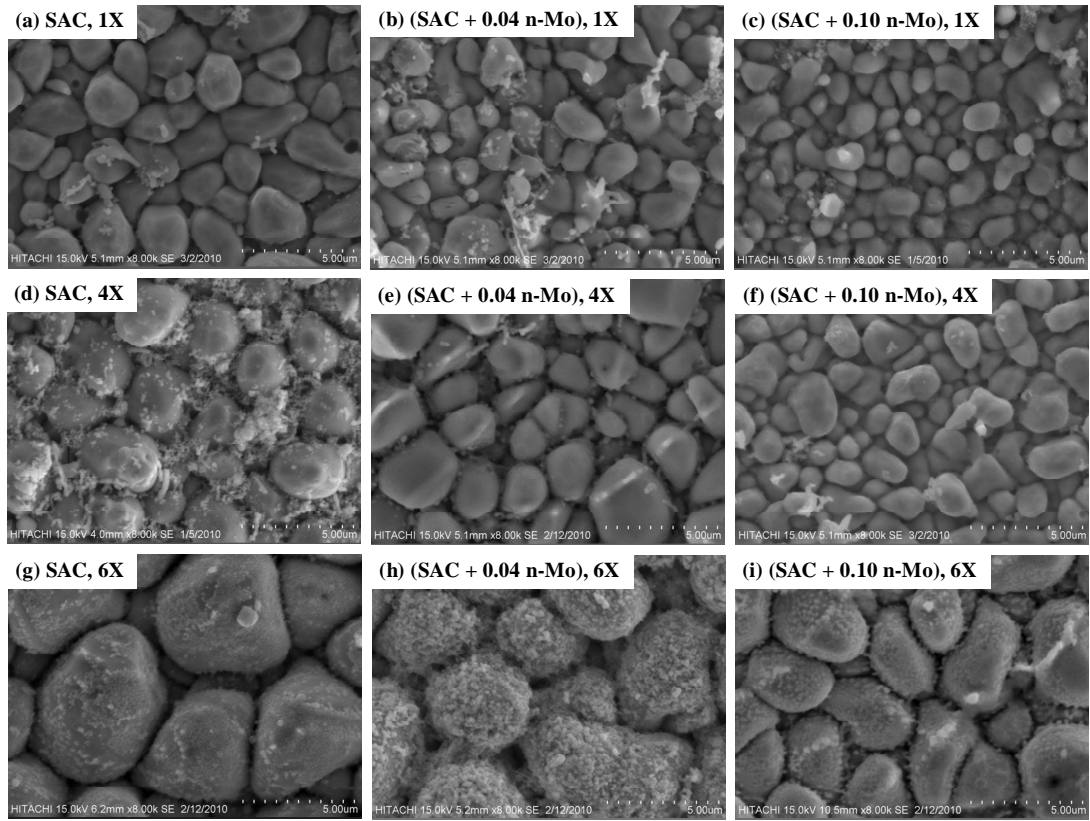


Figure 4. 10: Top view of the interfacial IMC (a) SAC after first reflow, (b) (SAC + 0.04 n-Mo) after first reflow, (c) (SAC + 0.10 n-Mo) after first reflow, (d) SAC after four times reflow, (e) (SAC + 0.04 n-Mo) after four times reflow, (f) (SAC + 0.10 n-Mo) after four times reflow, (g) SAC after six times reflow, (h) (SAC + 0.04 n-Mo) after six times reflow, and (i) (SAC + 0.10 n-Mo) after six times reflow.

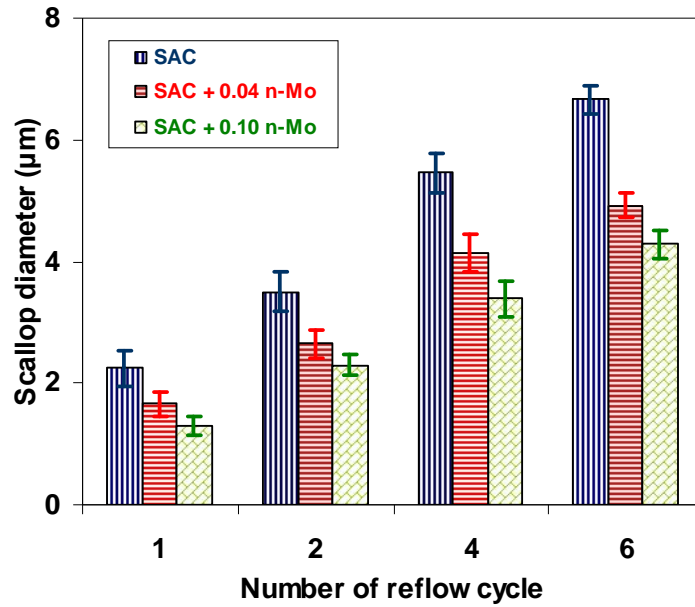


Figure 4. 11: Scallop diameter as a function of number of reflows.

4.6.3 Distribution of Mo Nanoparticles in the Solder

EDX elemental mapping was carried out to find the distribution of Mo nanoparticles on the top surface of the interfacial Cu_6Sn_5 IMC at randomly selected positions. For this purpose places undergoing incomplete etching was examined. Figure 4.12 shows a typical micrograph of the top view of Cu_6Sn_5 IMC of the (SAC + 0.04 n-Mo) solder after four times reflow. Area presented in Figure 4.12 underwent incomplete etching. Two types of white particles can be seen in the micrograph. One type of particles has a bright appearance with an irregular shape (Marked 'X'). These types of irregular shaped particles were found in both SAC and Mo nanoparticles-added SAC solders. EDX spot analysis confirmed that these irregular shaped particles are Ag_3Sn . The formation of Ag_3Sn on Cu_6Sn_5 after reflow has been observed by other researchers for Sn-based solder prepared on Cu or Ni substrate (Yu et al., 2005a). The second type of bright particles have almost perfectly spherical shape (marked 'Y') and were found only in Mo nanoparticles-added solders. EDX spot analysis revealed the occurrence of predominately Mo in these particles. This suggests that these particles are Mo nanoparticles. It may be noted that the microscopic investigation and elemental spot analysis on the Mo nanoparticles were done in an ultra high resolution field emission SEM (Zeiss Ultra-60 FESEM) equipped with EDX (EDAX-Genesis Utilities) which provides good imaging and analytical resolution.

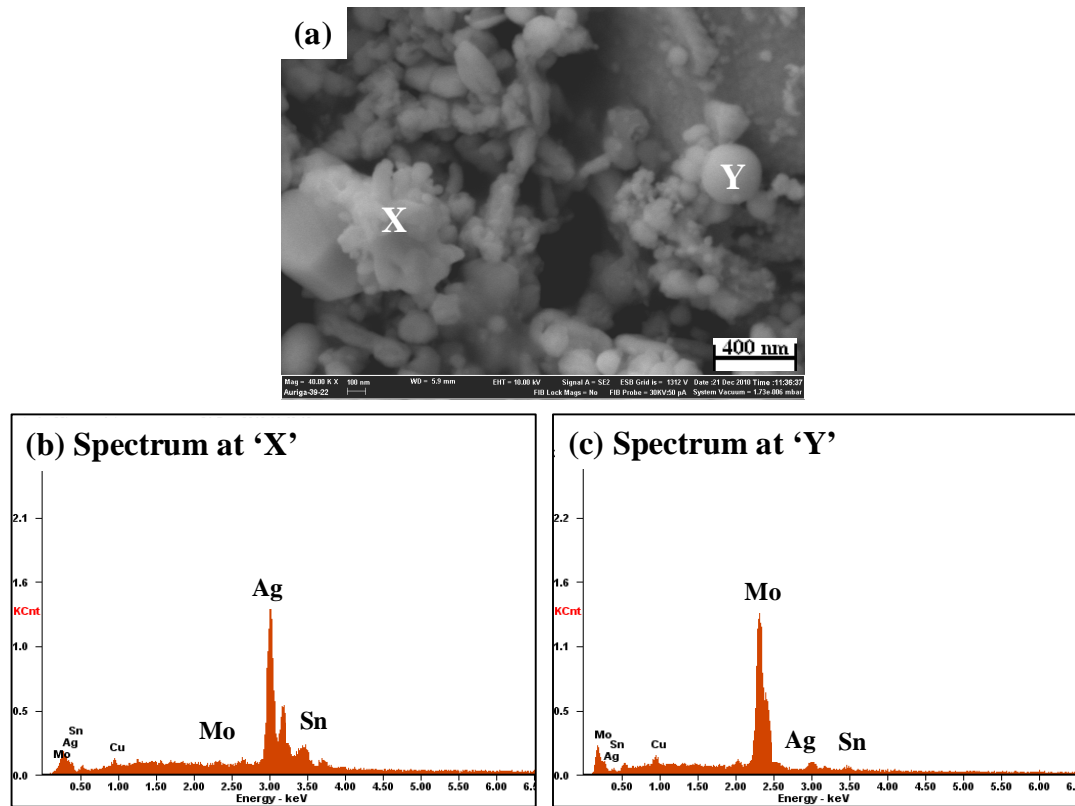


Figure 4. 12: (a) FE-SEM image of (SAC + 0.04 n-Mo) solder after four times reflow (b) EDX spectrum taken on particle 'X' and (c) EDX spectrum on 'Y'.

Figure 4.13 shows a typical elemental map obtained from FE-SEM to show the distribution of Mo nanoparticles on (SAC + 0.10 n-Mo) samples. This sample was reflowed for six times. It is found in Figure 4.13a that the spherical Mo nanoparticles are present on the top surface of IMC scallops and in between the scallop channels. SEM image together with the elemental maps for Mo, Sn and Cu given in Figure 4.13 suggest that spherical Mo nanoparticles are located at the boundaries between IMC scallops. Random EDX area analysis on multiple spots yielded a Mo concentration of about 3-3.5 wt% on the partially etched IMC surface. It may be noted that the average concentration of Mo in the bulk solder for this sample is only 0.1 wt %. It is thus likely that Mo nanoparticles particularly stay at the IMC surface. The reason for the preferential segregation of Mo nanoparticles at the liquid/IMC interface is not clear.

Expulsion of Mo particles as the solidification front of IMC advances into the liquid could be one of the reason. It may be noted that the substrate was placed in a horizontal position during reflow. Thus the density difference between liquid tin (6.99 gm.cm^{-3}) and molybdenum (10.28 gm.cm^{-3}) could also have contributed to this segregation. Through their presence on the IMC surface, Mo nanoparticles are believed to have a retarding effect on the IMC growth.

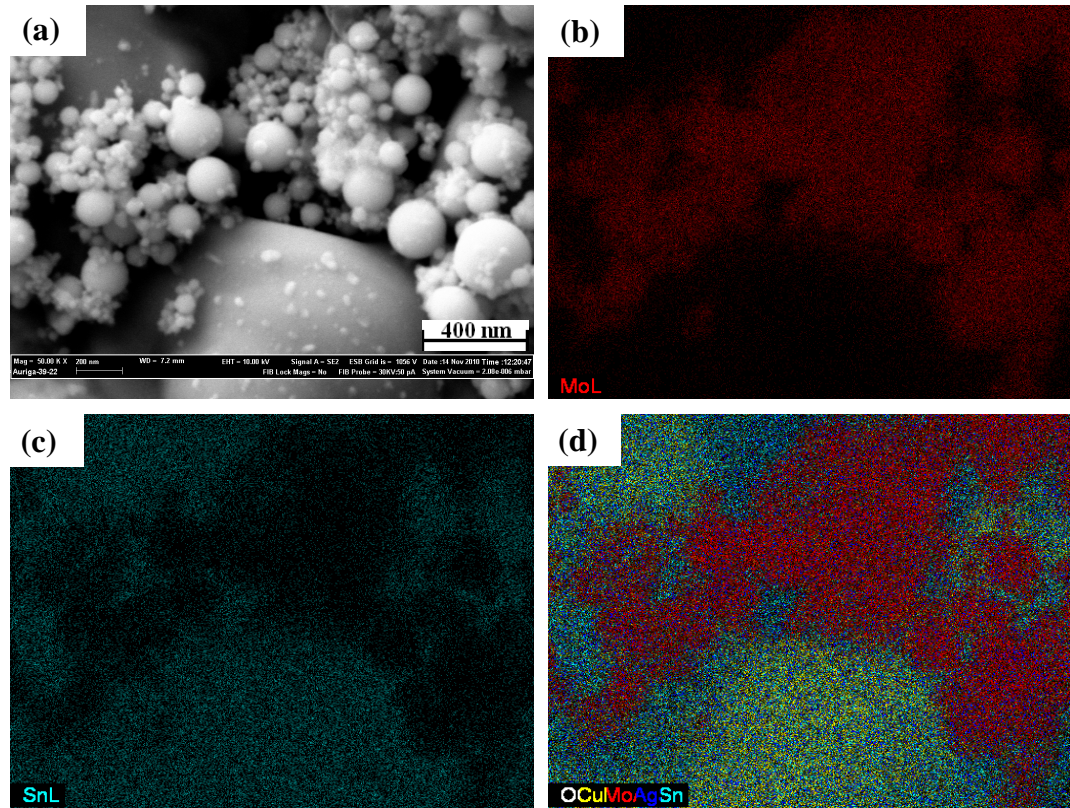


Figure 4. 13: (a) FESEM micrograph of (SAC + 0.10 n-Mo) solder after six times reflow, and elemental distribution of (b) Mo, (c) Sn and (d) overlapping of the elemental distribution of Sn, Ag, Cu, Mo.

4.7 Effect of Mo Nanoparticles on Interfacial IMC

4.7.1 State of Mo Nanoparticles during Reflow

The exact mechanism(s) through which Mo nanoparticles suppresses the growth of interfacial IMC thickness and scallop diameter is not clear. However, several scenarios can be speculated. In one extreme, nanoparticles may remain as discrete, unaltered particles during reflow. On the other extreme, they can be completely consumed in some reaction(s) or through dissolution within the molten solder. Actual alteration that the nanoparticles may undergo will depend on a number of factors, including their melting point and chemical interaction(s) with the solder. Molybdenum has a relatively high melting point (2623°C) compared with the reflow temperature (250°C) used in this study. So, under the present experimental condition, Mo nanoparticles are not expected to physically melt during reflow. Comparing the Figure 4.2 and Figure 4.13, it is found that the original nearly perfect spherical shape of Mo nanoparticles is preserved even after six times reflow. This suggests that the nanoparticles did not undergo any significant physical or chemical changes during multiple reflows. Referring to the Mo-Sn phase diagram, Mo has negligible solubility in Sn. The phase diagram shows that as many as three IMCs e.g., Mo_3Sn , $\text{Mo}_2\text{Sn}_3/\text{Mo}_3\text{Sn}_2$, and MoSn_2 can exist in the Mo-Sn system (Brewer and Lamoreaux, 1980). But no evidence of Mo-Sn compound formation was found on Mo nanoparticles by EDX. For instance, in the elemental map (Figure 4.13), Sn signals does not appear at the places where Mo particles are present. It may be noted that Mo does not form any compound with Cu and Ag at 250°C, and has no solubility in these elements (Baren, 1990, Subramanian and Laughlin, 1990).

4.7.2 Suggested Mechanism for Retardation of IMC Growth by Mo Nanoparticles

When Mo nanoparticles are mixed with SAC solder paste and reflowed at 250°C, they remain as stable solid particles. The nanoparticles do not particularly undergo any kind of chemical reactions or dissolution. So the retardation of IMC growth and scallop diameter are solely due to the particle effect of Mo nanoparticles. There can be three possibilities through which Mo nanoparticles can lower the thickness and reduce the diameter of IMC scallop:

- i) Mo nanoparticles can act as heterogeneous nucleation sites for the formation of Cu_6Sn_5 nucleus. This can increase the density of nucleation of Cu_6Sn_5 grains,
- ii) Mo nanoparticles may have pinning effect on the growing front of Cu_6Sn_5 scallops, and
- iii) Both (i) and (ii).

For a particle to act as a heterogeneous nucleation site, the interfacial energy between the liquid and solid particles should be low. In other words, the wetting angle of the liquid at the solid surface should be low. No data on the interfacial energy and wetting angle between liquid Cu_6Sn_5 and Mo is available in the literature. Available data shown that wetting angle between liquid tin (Lesnik et al., 1970) and molybdenum as well as that between liquid copper (Naidich et al., 1988) and molybdenum is high. So, if the Mo nanoparticles act as heterogeneous nucleation sites, it is likely that the nanoparticles could be formed as inclusions in the Cu_6Sn_5 scallops. Extensive examination of multiple samples on cross-section under high resolution SEM could not identify any such inclusion. These lead on to suggest that Mo nanoparticles are unlikely to act as

heterogeneous nucleation sites. It is therefore believed that the influence of Mo nanoparticles on the Cu_6Sn_5 layer is due to their effect on the growth process.

Experimental results through high resolution FESEM clearly shows that the presence of Mo nanoparticles on the surface of IMC (Figure 4.12) and at channels between the IMC scallops was confirmed (Figure 4.13). In fact higher percentage of Mo was found on the IMC surface (3-3.5 wt %) compared with the average Mo content of the solder. This indicates that the nanoparticles tend to stay on the IMC scallops particularly. Through their presence on the IMC surface, Mo nanoparticles are believed to have a retarding effect on the IMC growth.

The mechanism through which Mo nanoparticles suppress the interfacial IMC thickness and scallop diameter may be explained by referring to Figure 4.14. Kim and Tu (Kim and Tu, 1996), suggested that liquid channels exist between the Cu_6Sn_5 scallops. These channels extend all the way to $\text{Cu}_3\text{Sn}/\text{Cu}$ interface. These channels serve as fast diffusion and dissolution paths for Cu and thus feed the interfacial reaction. Ignoring the presence of Cu_3Sn IMC and all other chemical reactions for convenience, Kim and Tu (Kim and Tu, 1996) considered that two kind of fluxes are responsible for the growth of the scallops. One is flux of ripening (J^R) and the other is flux of interfacial reaction (J^I). At the start of reflow, Cu_6Sn_5 scallops nucleate at the solder/substrate interface and they grow with increasing reflow time due to Cu supply from J^R and J^I . Cu_6Sn_5 scallops grow both in thickness and diameter. J^I feeds the thickness growth, while J^R causes coalescence and increased diameter of the scallops (Figure 4.14a).

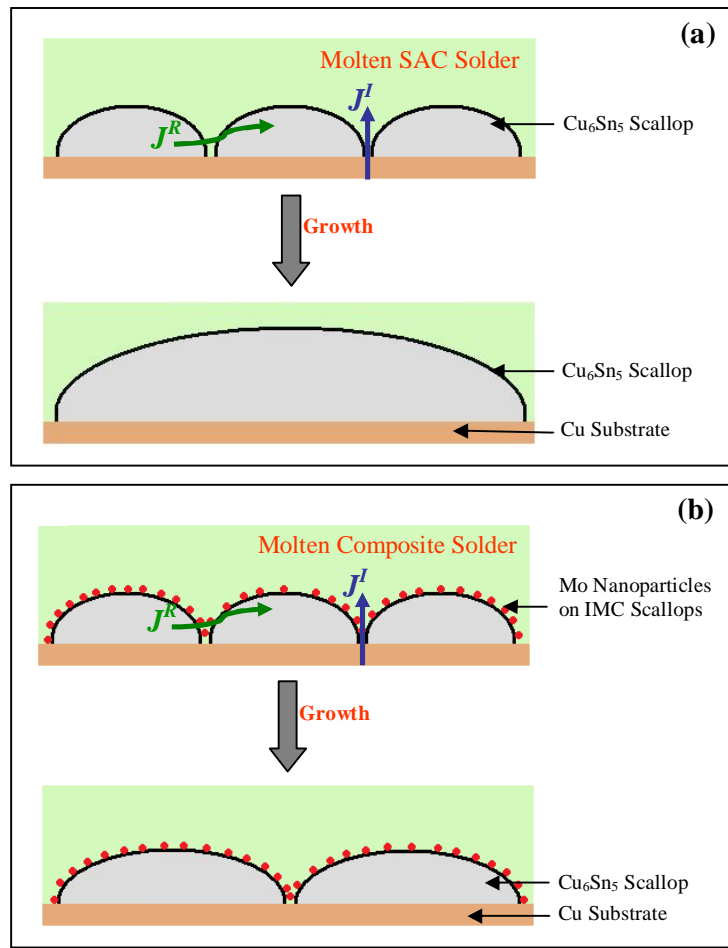


Figure 4. 14: Schematic diagram of scallop growth in (a) SAC solder, (b) Mo nanoparticles added SAC solder preferentially absorbed at the IMC scallops (Figures are not in scale).

When Mo nanoparticles are added to the solder, they block the channels between the IMC scallops and preferentially absorbed at the growth front of IMC scallops (Figure 4.14b). The blocking of the channels obstructs the movement of copper atoms from the substrate to the liquid solder and hence reduces J^I . This helps to reduce the thickness of IMC. The adsorbed Mo nanoparticles on the IMC surface will reduce J^R and act as a barrier to the coalescence of neighboring scallops. This causes a reduction in scallop diameter.

The effect of Mo nanoparticles on the IMC growth could be compared with that of Co nanoparticles as describes in the literature (Haseeb and Leng, 2011). The addition of Co nanoparticles was found to increase the thickness of Cu_6Sn_5 but decrease Cu_3Sn thickness (Haseeb and Leng, 2011). This was very similar to the case when Co is added as alloy addition (Wang et al., 2009). It was therefore suggested (Haseeb and Leng, 2011) that Co nanoparticles dissolve during reflow and exert their influence on IMC through alloying effect. This is in contrast with Mo nanoparticles which remain intact as it is found in this study. Molybdenum being a refractory metal with high melting point and low reactivity remains stable during reflow. These particles do not undergo any detectable alteration during reflow. It is therefore suggested that Mo nanoparticles exert their influence on the interfacial IMC growth as discrete particles.

4.8 High Temperature Aging

4.8.1 Morphology of Interfacial IMC during High Temperature Aging

After first reflow one set of samples were subjected to high temperature aging at the temperature of 100°C, 125°C, 150°C and 175°C for the time period ranging from 24h to 1008h. Figure 4.15(a-l) compares the interfacial IMC in the cross sectional view of solder samples after high temperature aging at 150°C. Both Cu_6Sn_5 and Cu_3Sn IMC layer are clearly visible in the cross sectional view for SAC and nanocomposites. The scallop morphology of the both IMC layers seems to be similar in SAC and nanocomposite solders. Within the resolution of EDX, no molybdenum was found in the Cu_6Sn_5 and Cu_3Sn layer after high temperature aging. Some Ag_3Sn particles were found to be embedded inside and at the growth front of Cu_6Sn_5 IMC during high temperature aging. Formation of Ag_3Sn at the IMC/solder interface also found in the literature for the Sn-based solders (Yu et al., 2005a).

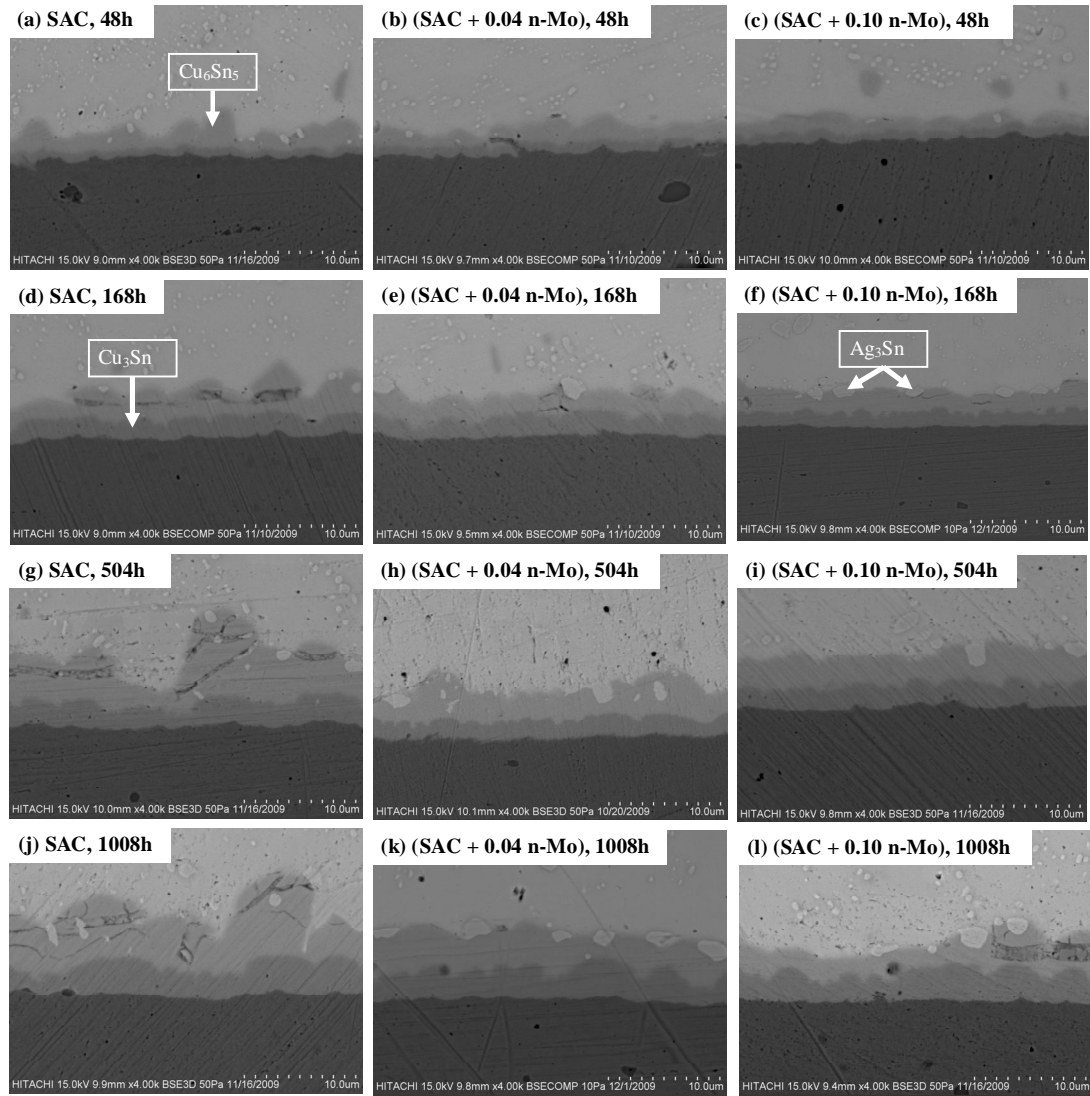


Figure 4. 15: Cross sectional backscattered electron micrographs of solder samples aged at 150°C (a) SAC, 48h; (b) (SAC + 0.04 n-Mo), 48h; (c) (SAC + 0.10 n-Mo), 48h; (d) SAC, 168h; (e) (SAC + 0.04 n-Mo), 168h; (f) (SAC + 0.10 n-Mo), 168h; (g) SAC, 504h; (h) (SAC + 0.04 n-Mo), 504h; (i) (SAC + 0.10 n-Mo), 504h; (j) SAC, 1008h; (k) (SAC + 0.04 n-Mo), 1008h; (l) (SAC + 0.10 n-Mo), 1008h.

With increasing the aging time, the thickness of total IMC layer as well as Cu_3Sn IMC layer is increased as it is seen in Figure 4.16. It is found that the addition of Mo nanoparticles to the SAC solder results in a decrease in the total IMC layer (Figure 4.15 and 4.16a). However, nanoparticles do not have any significant influence on the thickness of the Cu_3Sn IMC layer during high temperature aging (Figure 4.16b). In other words, Mo nanoparticles help to reduce the thickness of Cu_6Sn_5 .

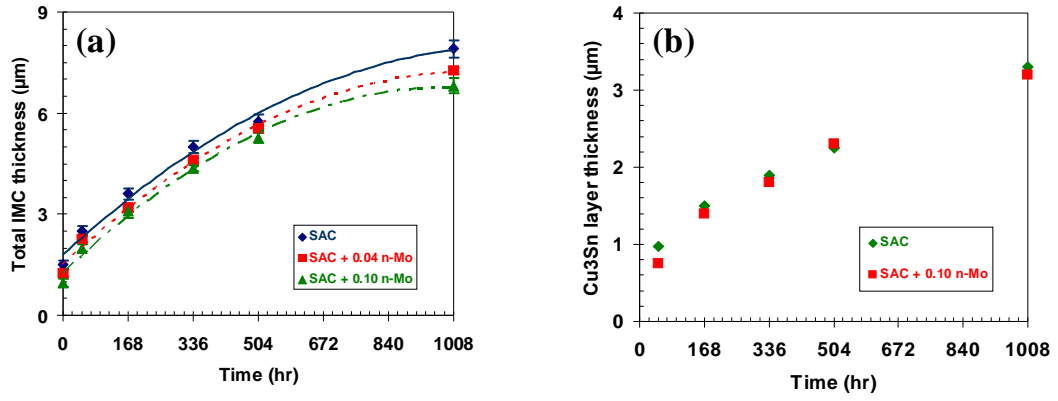


Figure 4. 16: (a) Total IMC thickness, (b) Cu₃Sn layer thickness of the SAC and nanocomposite solder as a function of aging time.

Deep etching was also employed to reveal the top surface of IMC layer in aged samples. Figure 4.17, 4.18, 4.19 and 4.20 shows the secondary electron micrographs of the top surface of IMCs after aging at 100°C, 125°C, 150°C and 175°C for 504 h and 840 h respectively. The ratio of elements in the IMC layer at the top surface by EDX analysis confirms the occurrence of Cu₆Sn₅. In all samples some white particles were found on the top surface of Cu₆Sn₅ IMC. EDX analysis confirms that these white particles are Ag₃Sn. It may be recalled that places undergone complete etching was utilized to observe the top IMC morphology.

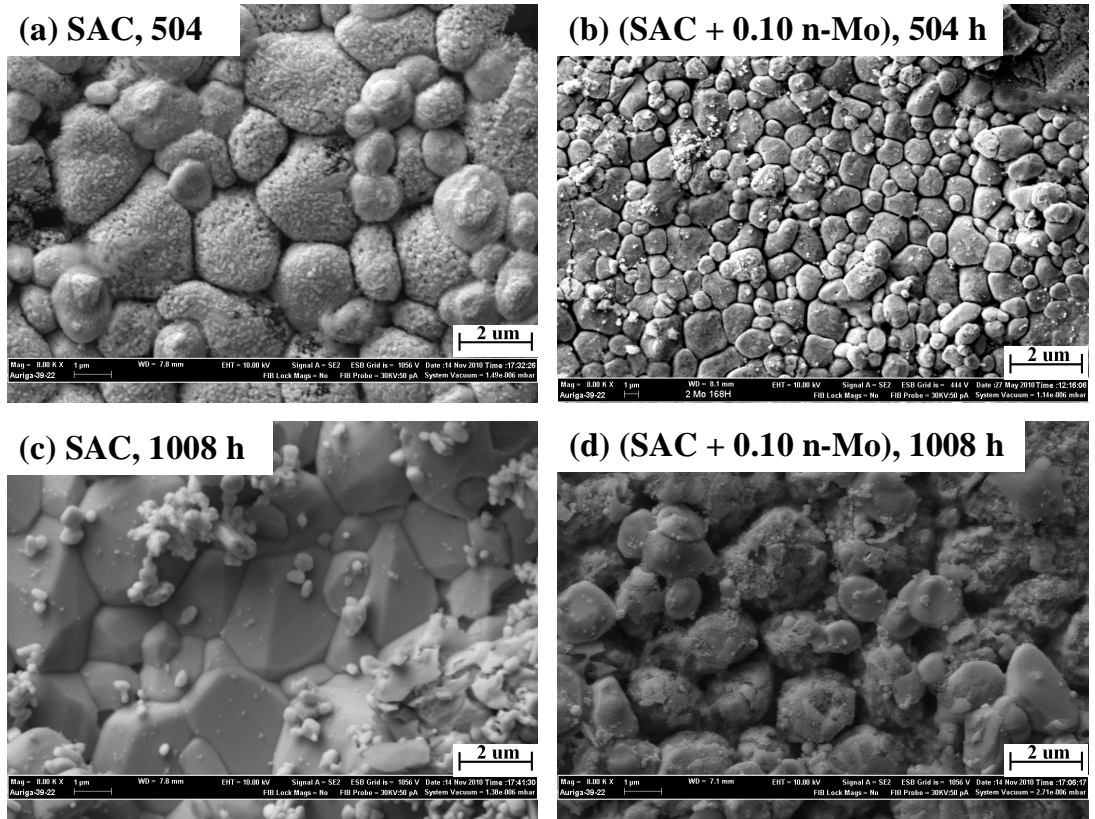


Figure 4. 17: SEM images of the top surface of interfacial IMC of (a) SAC, aged for 504 h, (b) (SAC + 0.10 n-Mo), aged for 504 h, (c) SAC, aged for 840 h, (d) (SAC + 0.10 n-Mo), aged for 840 h at 100°C.

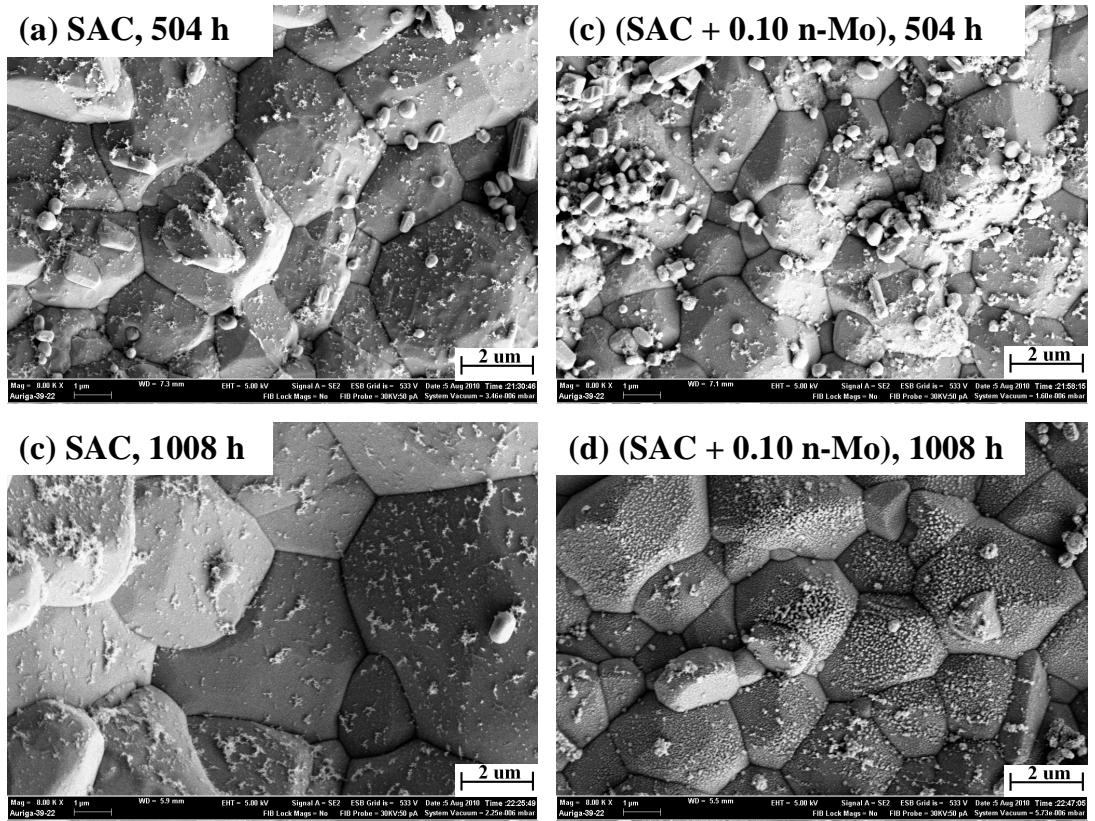


Figure 4. 18: SEM images of the top surface of interfacial IMC of (a) SAC, aged for 504 h, (b) (SAC + 0.10 n-Mo), aged for 504 h, (c) SAC, aged for 840 h, (d) (SAC + 0.10 n-Mo), aged for 840 h at 125°C.

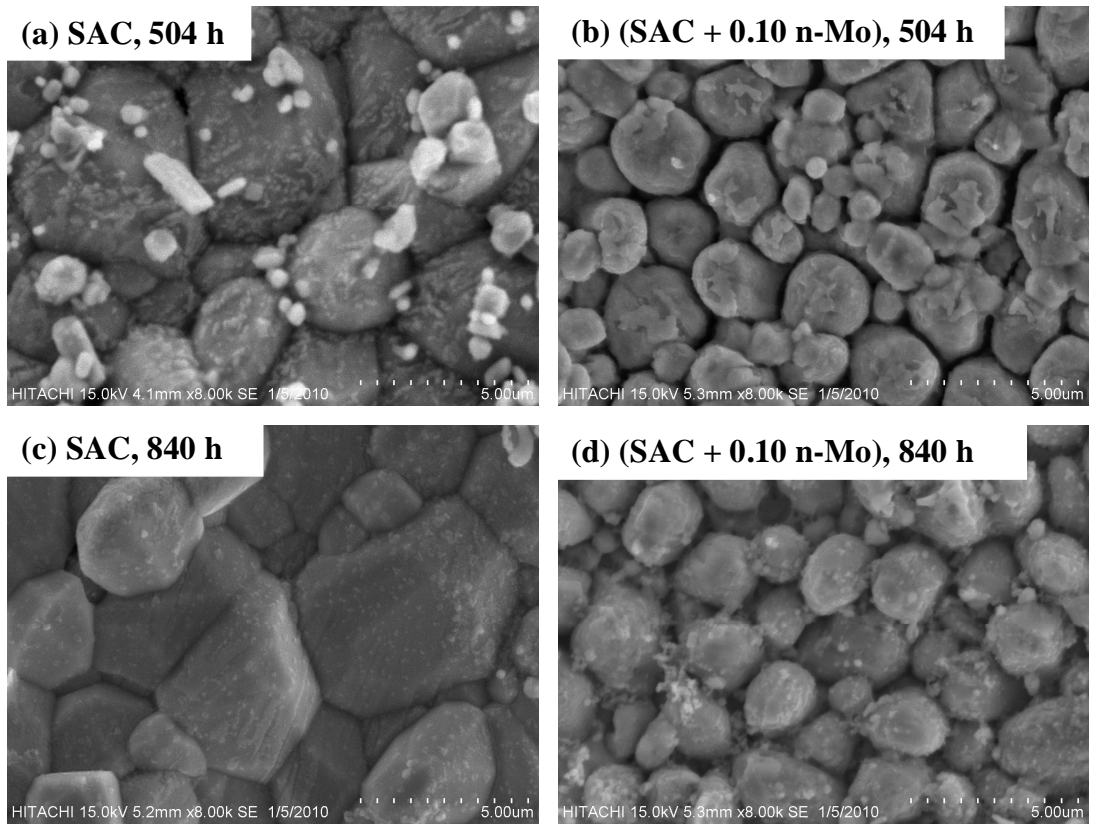


Figure 4. 19: SEM images of the top surface of interfacial IMC of (a) SAC, aged for 504 h, (b) (SAC + 0.10 n-Mo), aged for 504 h, (c) SAC, aged for 840 h, (d) (SAC + 0.10 n-Mo), aged for 840 h at 150°C.

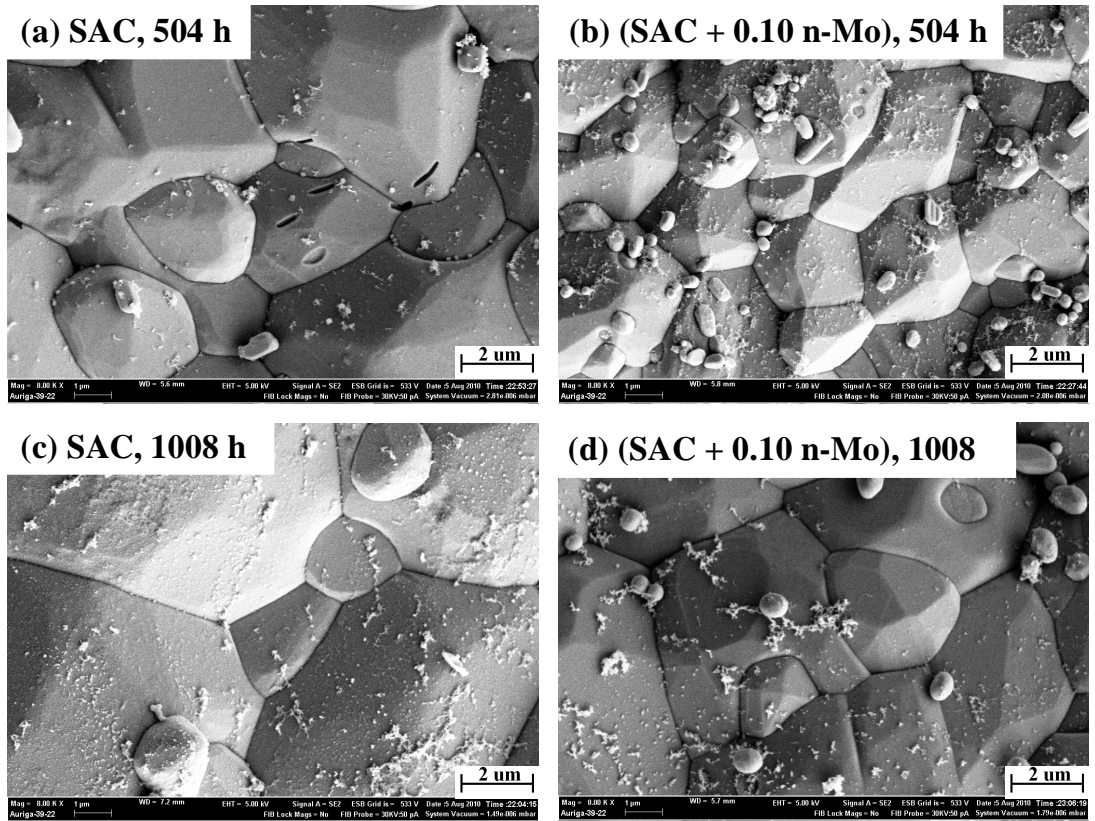


Figure 4.20: SEM images of the top surface of interfacial IMC of (a) SAC, aged for 504 h, (b) (SAC + 0.10 n-Mo), aged for 504 h, (c) SAC, aged for 840 h, (d) (SAC + 0.10 n-Mo), aged for 840 h at 175°C.

It is seen from Figure 4.17-4.20 that with increasing the aging time and temperature, the size of the Cu_6Sn_5 scallops increases for SAC and nanocomposite solder. It is also found that addition of Mo nanoparticles hinders the growth of Cu_6Sn_5 scallops in all aging conditions. Some white particles are found to be dispersed randomly on the top surface of the Cu_6Sn_5 IMC in all samples. The EDX analysis ensures that these white particles are Ag_3Sn . Formation of nanosized Ag_3Sn is frequent during reflow for Sn-based solders (Yu et al., 2005a). It may be noted that the region shown in the Figures 4.17-4.20 underwent complete etching. So, Mo nanoparticles are not likely to be found on these surfaces.

The size of Cu_6Sn_5 scallops is plotted as a function of aging time in the Figure 4.21(a-d) at the aging temperature 100°C , 125°C , 150°C and 175°C respectively. With increasing the aging time it is found that the round scallop shaped Cu_6Sn_5 grains turn to planner type scallops. Evidence of such morphological change of Cu_6Sn_5 during aging is found in the literature for Pb-Sn solder also (Tu, 2007, Yang et al., 2011).

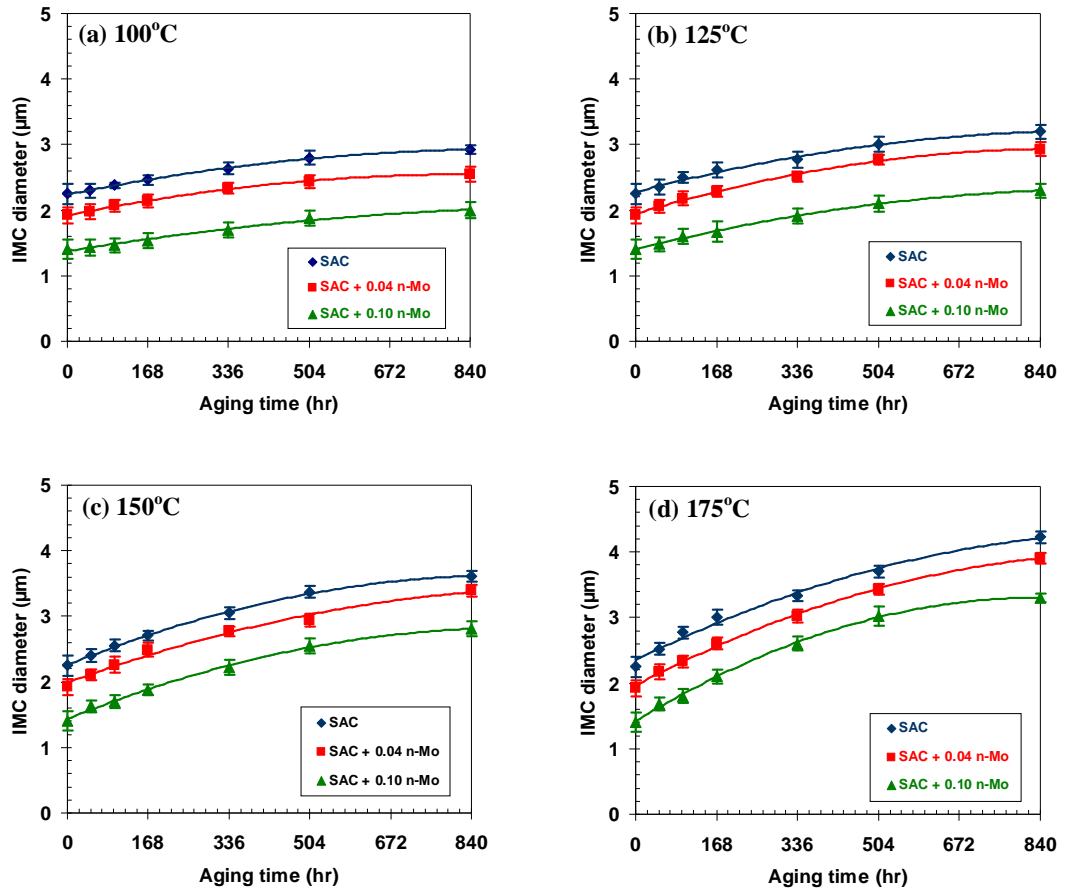


Figure 4. 21: Average IMC diameter of the SAC and nanocomposite solder as a function of aging time at (a) 100°C , (b) 125°C , (c) 150°C and (d) 175°C .

Elemental mapping was carried out on the top surface of the IMC layer of all aged samples at randomly selected positions. In this case also, like in the case of multiple reflow, Mo was found on the top surface of Cu_6Sn_5 IMC in the samples containing nanoparticles. Figure 4.22 shows a typical elemental map obtained on the top surface of the Cu_6Sn_5 of aged nanocomposites. From this figure it can be suggested that Mo

dispersed more or less uniformly on the top of the Cu_6Sn_5 (Figure 4.22e). Analysis on multiple spots showed that the Mo concentration on the top surface of Cu_6Sn_5 was between about 3-3.5%.

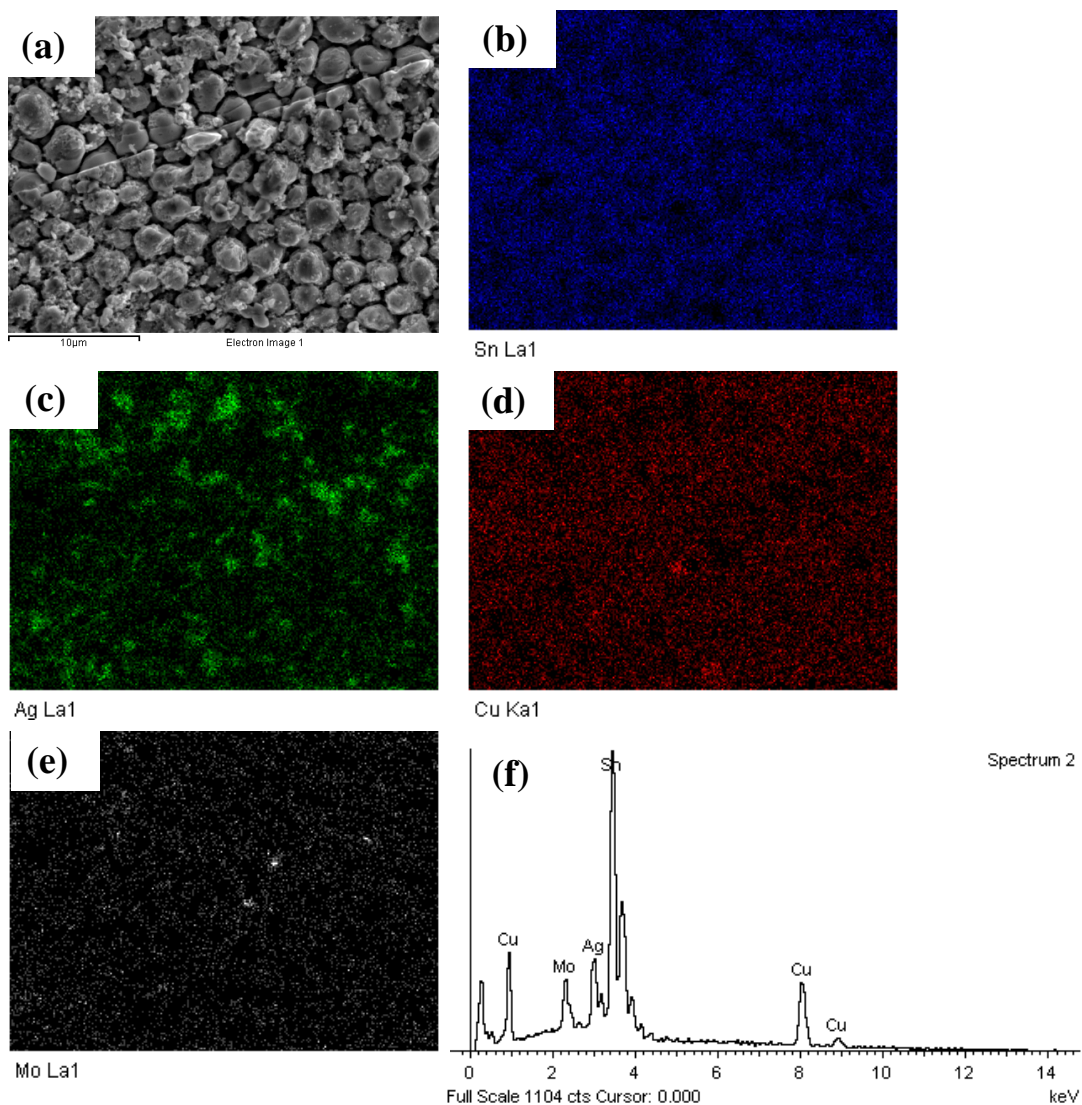


Figure 4. 22: A typical EDX elemental mapping showing the distribution of Sn, Ag, Mo and Cu on the top of Cu_6Sn_5 layer of the (SAC + 0.10 n-Mo) solder age at 150°C for 840h.

4.8.2 Growth Kinetics

4.8.2.1 Mechanism of IMC Growth during Solid State Aging

As presented by Laurila *et al.* (Laurila et al., 2005) for Sn-based solder, Sn is the main diffusion species from Sn-Cu₆Sn₅ interface to Cu₃Sn-Cu₆Sn₅ interface and on the other hand, Cu is the main diffusion species at the Cu-Cu₃Sn interface to Cu₃Sn-Cu₆Sn₅ interface as it is shown in Figure 4.23. According to Laurila *et al.* (Laurila et al., 2005), all reactions occur at the Cu₃Sn-Cu₆Sn₅ interface. The formation of Cu₃Sn or Cu₆Sn₅ depends on the stoichiometric ratio of Sn and Cu diffusion at the Cu₃Sn-Cu₆Sn₅ interface. Therefore, at the Cu₃Sn-Cu₆Sn₅ interface, Cu and Sn react to form either Cu₃Sn or Cu₆Sn₅ depending on the ratio of their diffusion.

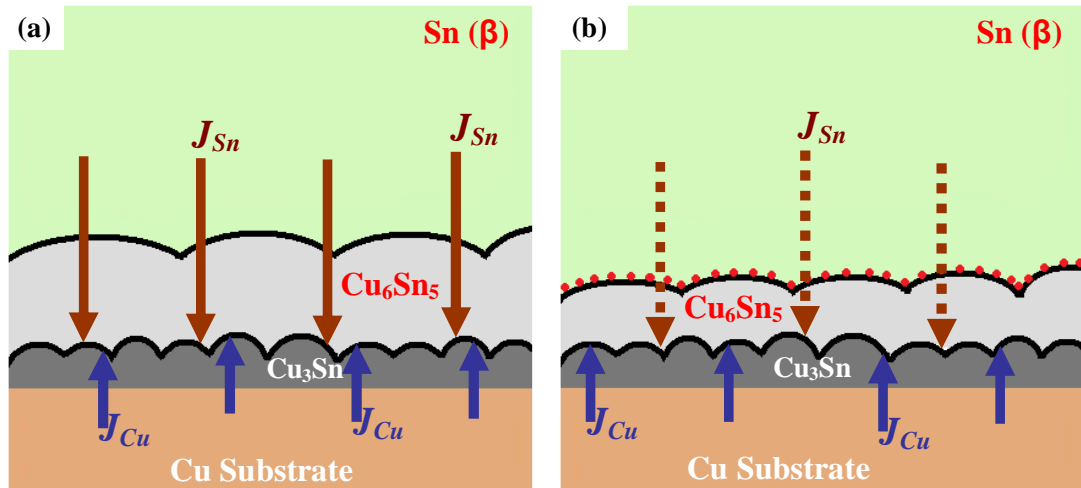


Figure 4. 23: Mechanism of IMC growth during solid state aging (a) SAC solder, (b) Mo nanoparticles added nanocomposite solder (The figure is not in scale).

Due to the diffusion and formation of intermetallics, as the aging time is increased the thickness of Cu₆Sn₅ and Cu₃Sn layers are also increased. But when Mo nanoparticles are added to the solder, it is preferentially absorbed on the Cu₆Sn₅ IMC scallops (Figure 4.22). This means that Mo nanoparticles stay at the solder-Cu₆Sn₅ interface which might hamper the diffusion of Sn to the Cu₃Sn-Cu₆Sn₅ interface. Since the diffusion flux of Sn

is decreased with the addition of Mo nanoparticles the thickness of Cu_6Sn_5 is decreased in the nanocomposite solder compared to the SAC. On the other hand, Mo nanoparticles were not found on the top of Cu_3Sn IMC. So, Cu diffusion flux is not hampered with the addition of Mo nanoparticles. Since the Cu diffusion flux is same for both of SAC and nanocomposite solders there is virtually no effect of Mo nanoparticles on the Cu_3Sn IMC thickness during solid state aging.

4.8.2.2 Calculation of Diffusion Coefficient

In the classical analysis of solid-state interfacial reactions, the kinetics of growth of each IMC layer can be diffusion-controlled or interfacial-reaction-controlled (Tu, 2007). At any particular temperature, the growth kinetics of any reaction layer follow the following empirical power law relationship with time (Alam and Chan, 2005).

$$x_t - x_0 = kt^n \quad (4.1)$$

This equation can also be rewritten in the following logarithmic expression,

$$\log(x - x_0) = \log k + n \log t \quad (4.2)$$

Where x_t is the total IMC thickness at time t , x_0 = thickness of the IMC after reflow, k is the growth rate exponent and n is the time exponent. From the value of n it is possible to deduce the type of solid state growth kinetic at a solder interface and can realized the growth mechanism. The experimental data for total IMC thickness during solid state aging at 150°C from Figure 4.16 is repotted in Figure 4.24(a-c) in the logarithmic scale for the SAC and nanocomposite solders.

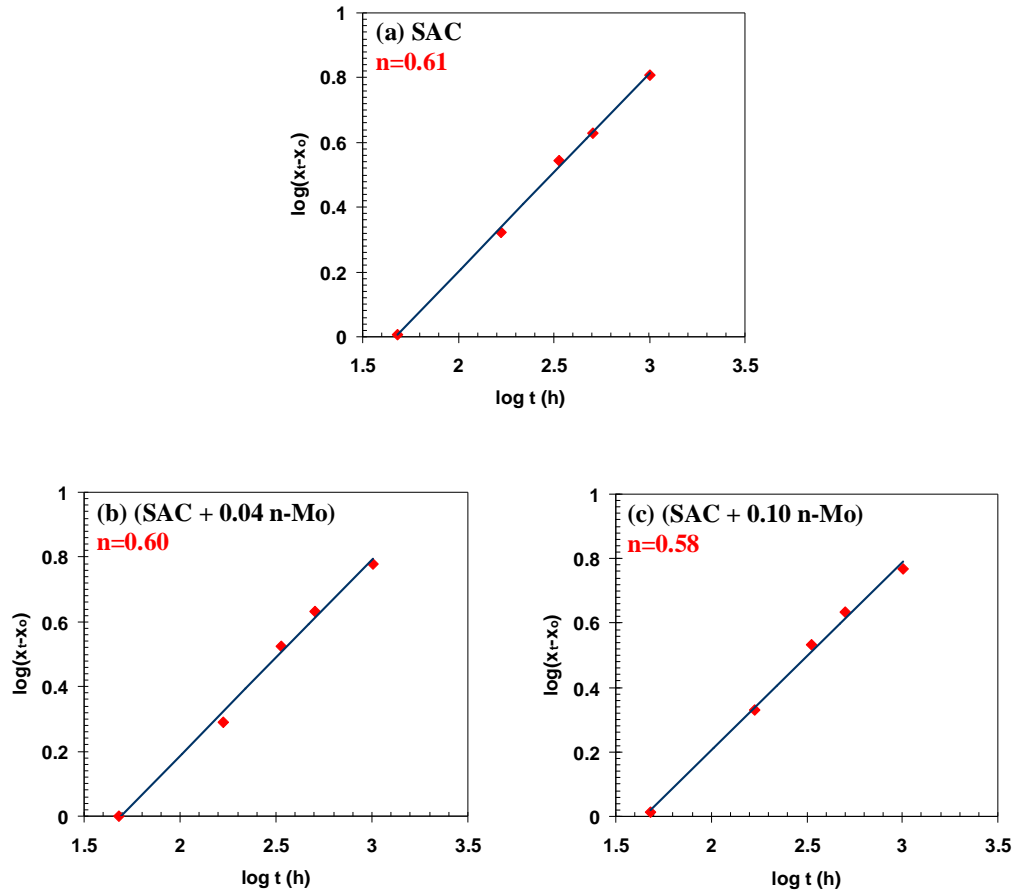


Figure 4. 24: The growth of total IMC layer in logarithmic scale during solid state aging at 150°C of (a) SAC, (b) (SAC + 0.04 n-Mo) and (c) (SAC + 0.10 n-Mo) solder.

From the linear regression analysis the value of n obtained for the SAC, (SAC + 0.04 n-Mo) and (SAC + 0.10 n-Mo) solder with a value of $n = 0.61$, 0.60 and 0.58 respectively. From the values of n , it is considered that the growth kinetics of the total IMC layer is diffusion controlled. Even the addition of Mo nanoparticles did not considerably change the value of n . This indicates that the growth of the IMC still follow the parabolic kinetics. This result confirms that the formation of Cu_6Sn_5 and Cu_3Sn IMC is a diffusion controlled process in both SAC and nanocomposite solders. Addition of Mo nanoparticle did not grossly change the mechanism of growth of the total IMC layer. The addition of nanoparticles, however, suppresses the growth of Cu_6Sn_5 scallops

considerably. The effective inter-diffusion coefficient (D_{eff}) of the total IMC layer can be determined by the following equation (4.3) with conjunction to Figure 4.25.

$$x_t - x_0 = (D_{eff} t)^{\frac{1}{2}} \quad (4.3)$$

The effective inter-diffusion coefficient for the SAC and nanocomposite solders are presented in Table 4.2. In this present study, the inter-diffusion coefficient of interfacial IMC for SAC solder was obtained $1.092 \times 10^{-17} \text{ m}^2\text{s}^{-1}$ at 150°C . Previous studies on inter-diffusion coefficient for the total IMC layer were found 1.96×10^{-17} , 2.96×10^{-17} , and $2.96 \times 10^{-17} \text{ m}^2\text{s}^{-1}$ on (0 0 1), (1 1 1) and (1 2 3) Cu single crystals respectively for Sn solder at 170°C (Zou et al., 2008). These results are close to the present experimental results with same magnitude of order. The reason for the higher inter-diffusion coefficient in the published result may come from the difference of temperature, solder composition and substrate crystallinity.

It is seen from the present experimental results that the effective inter-diffusion coefficient is decreased with the increase of Mo nanoparticles into the solder. With the addition of 0.04 and 0.10 wt% of Mo nanoparticles to the SAC solder the inter-diffusion coefficient is decreased to 9.83×10^{-18} and $9.55 \times 10^{-18} \text{ m}^2\text{s}^{-1}$ respectively. The reason behind the lower inter-diffusion coefficient for the nanocomposite solder may be due to the presence of Mo nanoparticles at the solder/ Cu_6Sn_5 interfaces which hinder the diffusion of Sn towards the $\text{Cu}_6\text{Sn}_5/\text{Cu}_3\text{Sn}$ interface. Moreover, the inter-diffusion coefficient for the Cu_3Sn IMC layer does not change with the addition of Mo nanoparticles to the SAC solder. This is because Mo nanoparticles were not found at the $\text{Cu}_6\text{Sn}_5/\text{Cu}_3\text{Sn}$ interface. So it is expected that the Cu flux during high temperature aging was not affected with the addition of Mo nanoparticles to the SAC solder.

Published results of the inter-diffusion coefficients for the Cu_6Sn_5 and Cu_3Sn IMC layer are shown in Table 2.2. It is found that the inter-diffusion coefficients for the Cu_6Sn_5 and Cu_3Sn IMC layer varies a wide range of order 10^{-17} to 10^{-19} for Sn-based solders (Peng et al., 2007, Yoon et al., 2009, Nishikawa et al., 2007, Flanders et al., 1997, Lee and Chen, 2002). The deviations in the results might come from the experimental conditions, solder alloy compositions, substrate preparation and crystallinity etc.

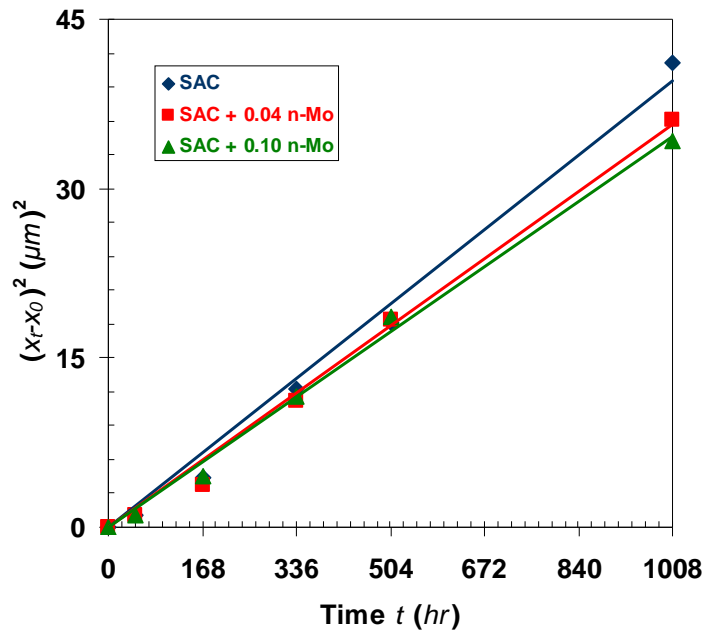


Figure 4. 25: Calculation of diffusion coefficient of SAC and nanocomposite solders.

Table 4. 2: Diffusion Coefficient and n values of SAC and nanocomposite solders.

Solder	Time exponent n	Diffusion coefficient D_{eff} (m^2s^{-1})
SAC	0.61	1.092×10^{-17}
SAC + 0.04 n-Mo	0.60	9.83×10^{-18}
SAC + 0.10 n-Mo	0.58	9.55×10^{-18}

4.8.2.3 Calculation of Activation Energy for the Growth of Scallops Diameter

Figure 4.26(a-c) shows the relationship of the scallop diameter of SAC and nanocomposite solders as a function of aging time at 100°, 125°, 150° and 175°C temperatures. It is seen from these figures that the scallop diameter increases with increasing temperature and time. Moreover the higher the aging temperature, the higher is the scallop diameter growth rate. It is therefore seen, the aging temperature has a significant influence on the grain growth kinetics. For a given aging temperature, the grain growth rate decreases with increasing the aging time.

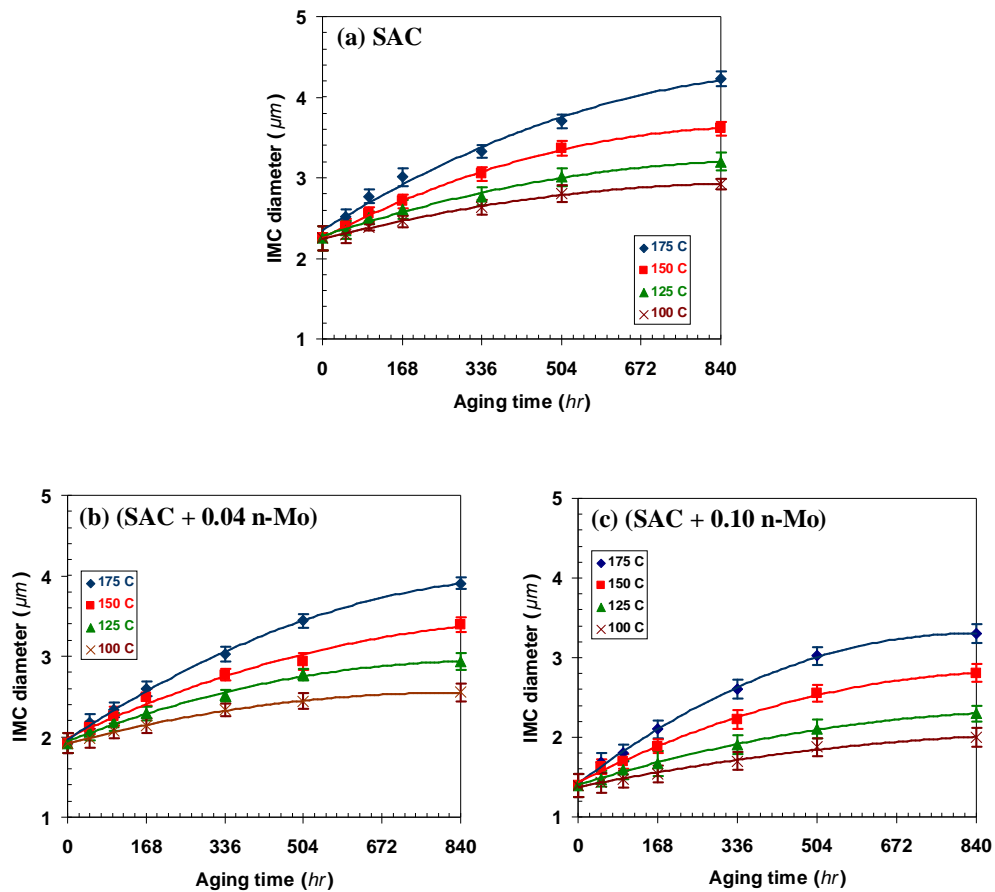


Figure 4. 26: Scallop diameter as a function of aging time for (a) SAC, (b) (SAC + 0.04 n-Mo) and (c) (SAC + 0.10 n-Mo) solder.

Generally, the scallop diameter growth of Cu₆Sn₅ IMC could be well interpreted by the kinetic equation,

$$D_t^n - D_o^n = kt \quad (4.4)$$

In this equation, $k = k_o e^{-\left(\frac{E_g}{RT}\right)}$ (4.5)

Where, D_o and D_t is scallop diameter of the as reflowed and after aging t hr respectively, n is the scallop growth exponent, R is the molar gas constant, T is the aging temperature and E_g is the activation energy of the IMC scallops.

Equation (4.4) can be simplified in the form of straight line as follows:

$$\ln\left(\frac{dD_t}{dt}\right) = (1-n)\ln D + \ln \frac{k}{n} \quad (4.6)$$

Based on the experimental data, $\ln(dD_t/dt)$ is plotted as a function of $\ln D$ for the SAC and nanocomposite solders in the figures from 4.27(a-c). A linear relationship is observed between the logarithm of grain size, $\ln(D)$ and logarithm of grain growth rate, $\ln(dD_t/dt)$. For a specific composition of solder these lines are almost parallel. The value of $(1-n)$ can be obtained from the slope of these straight lines and the scallop growth exponent, n can be calculated from there. The average value of scallop growth exponent, n is 4, 3.2 and 2.7 for the SAC, (SAC + 0.04 n-Mo) and (SAC + 0.10 n-Mo) respectively.

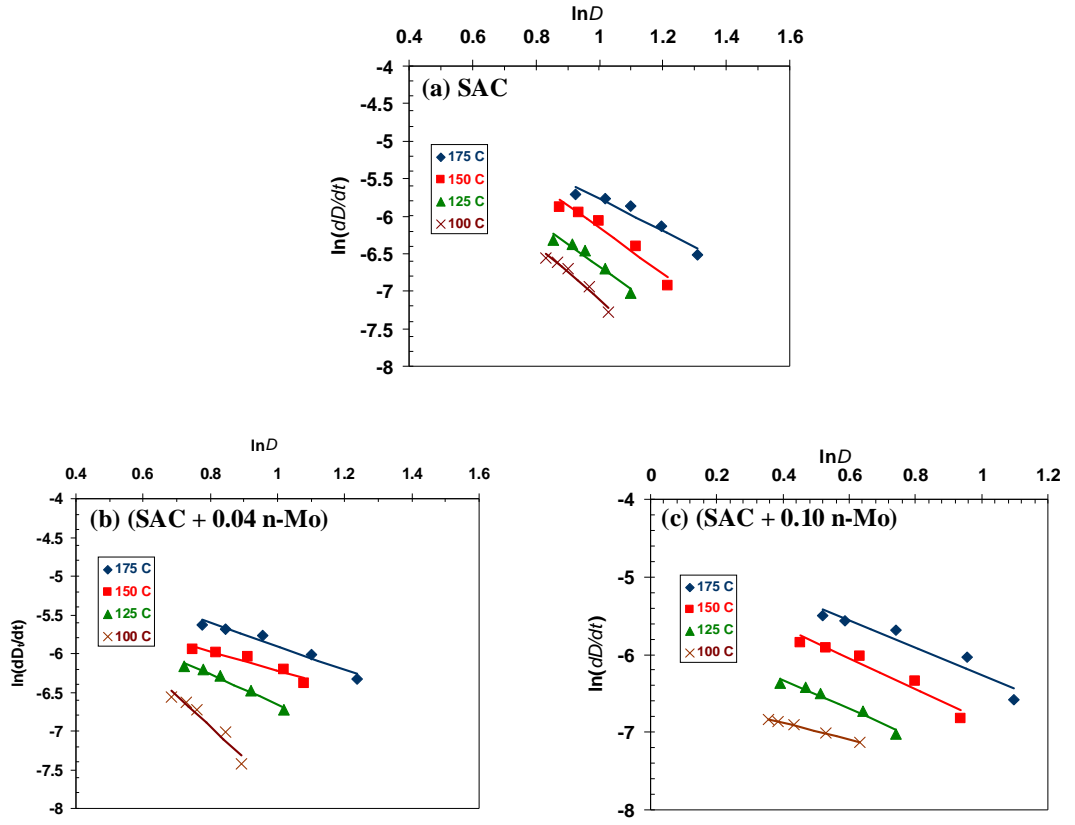


Figure 4. 27: Relationship between logarithm of (dD/dt) vs. logarithm of D for (a) SAC, (b) (SAC + 0.04 n-Mo) and (c) (SAC + 0.10 n-Mo) solder.

By using the data presented in Fig. 4.26(a-c) and referring to the grain growth kinetics in Equation 4.4, it is possible to figure out the relationship between $(D_t^n - D_o^n)$ and aging time for IMC scallops for different solders as it is shown in Figure 4.28(a-c). The value of k can be obtained from the slope of these curves.

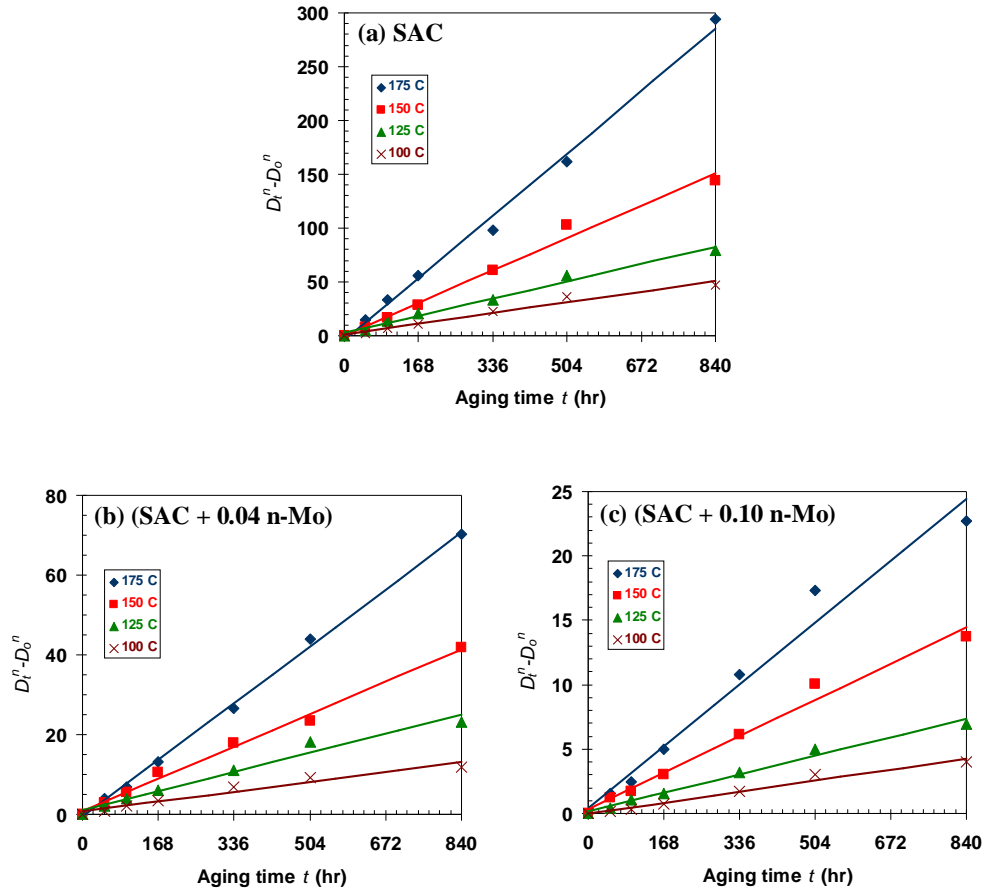


Figure 4. 28: Plot of $(D_t^n - D_o^n)$ vs. aging time for (a) SAC, (b) (SAC + 0.04 n-Mo) and (c) (SAC + 0.10 n-Mo) solder.

The slope of the plots from Fig. 4.28(a-c) provides the value of scallop growth constant, k at different temperature for different solders. The values of k for different solders are listed in Table 4.3. The scallop growth rate constant, k in Equation 4.5 can be simplified in logarithmic form as follows,

$$\ln k = \ln k_o - \frac{E_g}{RT} \quad (4.7)$$

In the Figure 4.29, the values of $\ln k$ for different solders are plotted against $1/T$ to calculate the activation energy of the SAC and nanocomposite. Almost parallel straight lines are obtained for the different composition of the solders. The slope of these

straight lines represents the value of $-(E_a/R)$ of a specific solder. The activation energy, E_a for a specific solder composition is calculated from the values of $-(E_a/R)$ considering $R=8.314 \text{ kg.m}^{-2}.\text{s}^{-2}.\text{K}^{-1}.\text{mole}^{-1}$ and tabulated in Table 4.3.

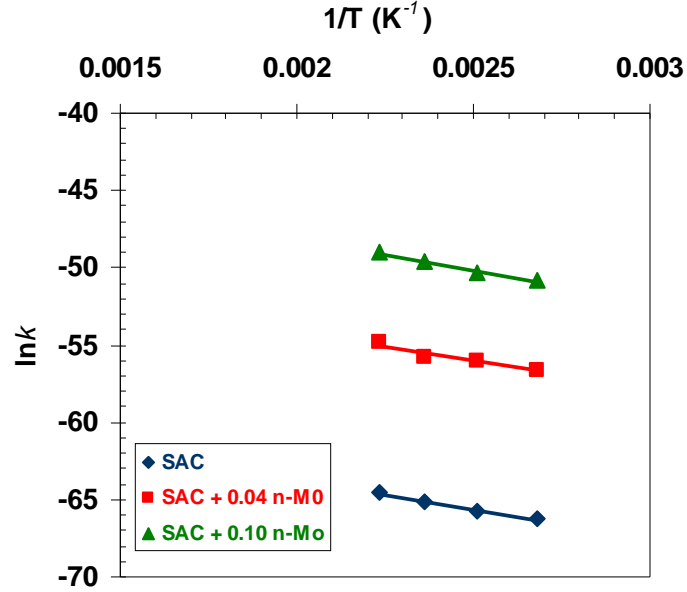


Figure 4. 29: Plot of $\ln(k)$ against $1/T$ for SAC and nanocomposites.

From the values of activation energy, E_a for SAC and nanocomposite solders it is seen that Mo nanoparticles has virtually no effect on the activation energy of IMC scallops growth. But it is found that Mo nanoparticles have a prominent effect on the values of scallop growth exponent, n and scallop growth constant k . Actually, activation energy represents the minimum energy to create a compound. It is found from the reported (Haseeb and Leng, 2011, Amagai, 2008, Lin et al., 2009) results that nanoparticles which have alloying effect such as Co, Ni can influence the activation energy of the IMC formation. However, Mo nanoparticles have no alloying effect, so the formation energy of IMC scallops remain unchanged with the addition of Mo nanoparticles. Only the scallop growth exponent, n and scallop growth constant k of the IMC scallops is changed with the addition of Mo nanoparticles by hindering the diffusion of atoms.

Table 4. 3: Scallop growth exponent, n and scallop growth constant k , activation energy E_a of the SAC and nanocomposite solders.

Solder	Scallop Growth Exponent n	Temperature T ($^{\circ}\text{C}$)	Scallop Growth Constant k (m^4/sec)	$\ln(k)$	Activation Energy of IMC Scallops E_a (KJ/mole)
SAC	4	175	9.5×10^{-29}	64.52	33.5
		150	4.9×10^{-29}	65.17	
		125	2.6×10^{-29}	65.8	
		100	1.6×10^{-29}	66.3	
SAC + 0.04 n-Mo	3.2	175	1.5×10^{-24}	54.8	31
		150	5.83×10^{-25}	55.8	
		125	4.78×10^{-25}	56	
		100	2.6×10^{-25}	56.6	
SAC + 0.10 n-Mo	2.7	175	5.24×10^{-22}	49	33.7
		150	2.88×10^{-22}	49.6	
		125	1.43×10^{-22}	50.3	
		100	8.66×10^{-23}	50.8	

4.9 Effect of Mo Nanoparticles on Interfacial Reaction between Liquid SAC and Cu

During soldering, interfacial reactions between solder and substrate can occur at states: i) reaction between liquid solder and substrate and ii) reaction between solid solder and substrates. The former is encountered mostly during the manufacturing of solder joint, while the latter happens during service. So it is quite important to investigate the interfacial reactions between the solder and substrate in the liquid state. For this reason, Cu wire having a diameter of 250 μm was dipped in the liquid solder for prolonged time. After reaction for a certain time, the solder-Cu wire reaction couple was taken out from the liquid solder and mounted in epoxy followed by standard metallographic polishing. Then the samples were observed under optical microscope, SEM and high resolution FESEM. In this case, effect of Mo nanoparticles on the intermetallic compound (IMC) formation in the liquid solder is the main objective of this experiment.

The results are discussed in terms of dissolution behavior of Cu substrate and IMC formations in presence of Mo nanoparticles.

4.9.1 Effect on Dissolution Behavior of Cu Substrate

Figure 4.30 presents the cross sectional views of Cu wires after dipping in liquid solder maintained at 250°C for different time periods. It is seen that with increasing dipping time, the diameter of the copper decreases in SAC and nanocomposite solders. The diameter of the wire dipped in Mo nanoparticles added nanocomposite solder is large at all dipping periods. The relationship between the dissolved thickness of Cu in the molten solders and dipping time is plotted in Figure 4.31a. This figure reveals that the dissolution of the substrate increases almost linearly with increasing immersion time. Linear relationship between copper dissolution rate and dipping time for different solders was also reported by others (Yen et al., 2008, Yeh et al., 2006). It is also found that the dissolution of the copper substrate is higher in the SAC solder compared with that in the nanocomposite solders.

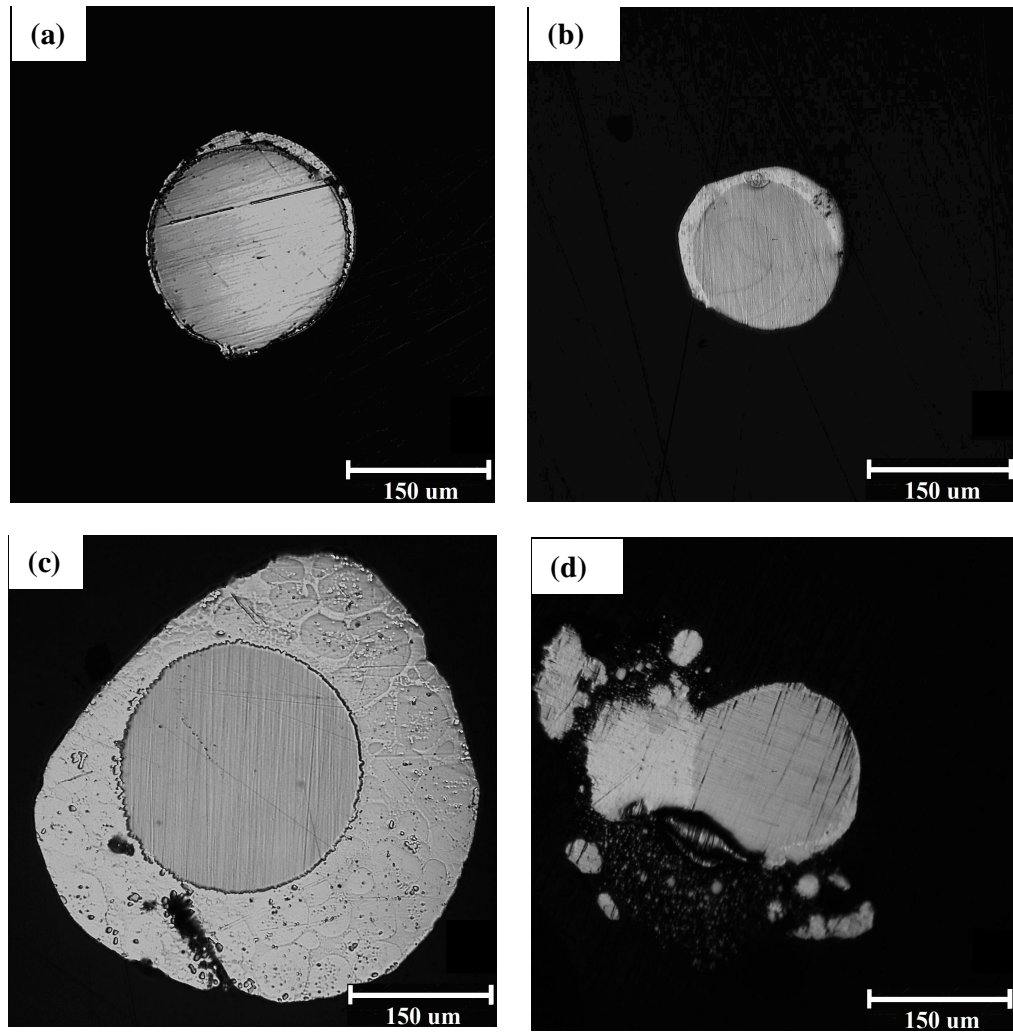


Figure 4. 30: Optical micrographs showing cross-section of copper wire after dipping in molten solder for two different time periods (a) SAC for 5 min, (b) SAC for 15 min, (c) (SAC + 0.30 n-Mo) for 5 min, (d) (SAC + 0.30 n-Mo) for 15 min.

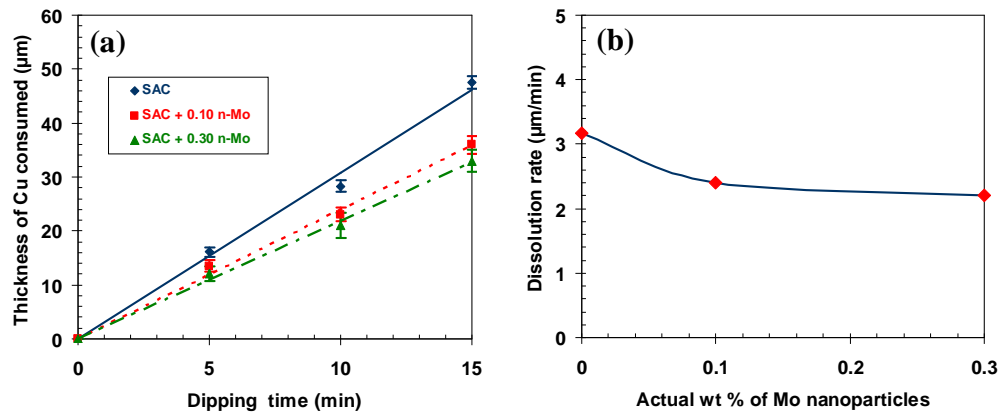


Figure 4. 31: (a) Thickness of consumed Cu in the molten solder and (b) Dissolution rate of Cu substrate at 250°C.

It is thus seen that the presence of Mo nanoparticles in the molten solder decreases the dissolution of Cu wire. Figure 4.31b plots the dissolution rate of Cu calculated from Figure 4.31a for different solder compositions. The dissolution rate of Cu substrate in SAC solder at 250°C is 3.1 $\mu\text{m}/\text{min}$. Yen *et al.* (Yen et al., 2008) found the dissolution rate of Cu in Sn-3.0Ag-0.5Cu solder at 270°C is 2.95 $\mu\text{m}/\text{min}$. This is good agreement with the present study. With the addition of Mo nanoparticles to the liquid solder for actual concentration of 0.30 wt%, the dissolution rate of Cu goes down to 2.2 $\mu\text{m}/\text{min}$.

4.9.2 Interfacial IMC Formation and Growth in Liquid Solder

Figure 4.32 shows backscattered electron image of the solder-copper interface after the dipping of copper in liquid solder under different conditions. It is seen that intermetallic compounds (IMCs) form in all samples. For SAC/Cu interface, the IMC formation is quite pronounced. At shorter dipping time, only Cu_6Sn_5 IMC forms. Cu_3Sn IMC appears after about 10 min of dipping. Cu_6Sn_5 has scallop type morphology. The thickness of the IMC is seen to be much lower for (SAC + 0.30 n-Mo) solder. No Cu_3Sn appears to be present for both dipping periods in (SAC + 0.30 n-Mo) solder.

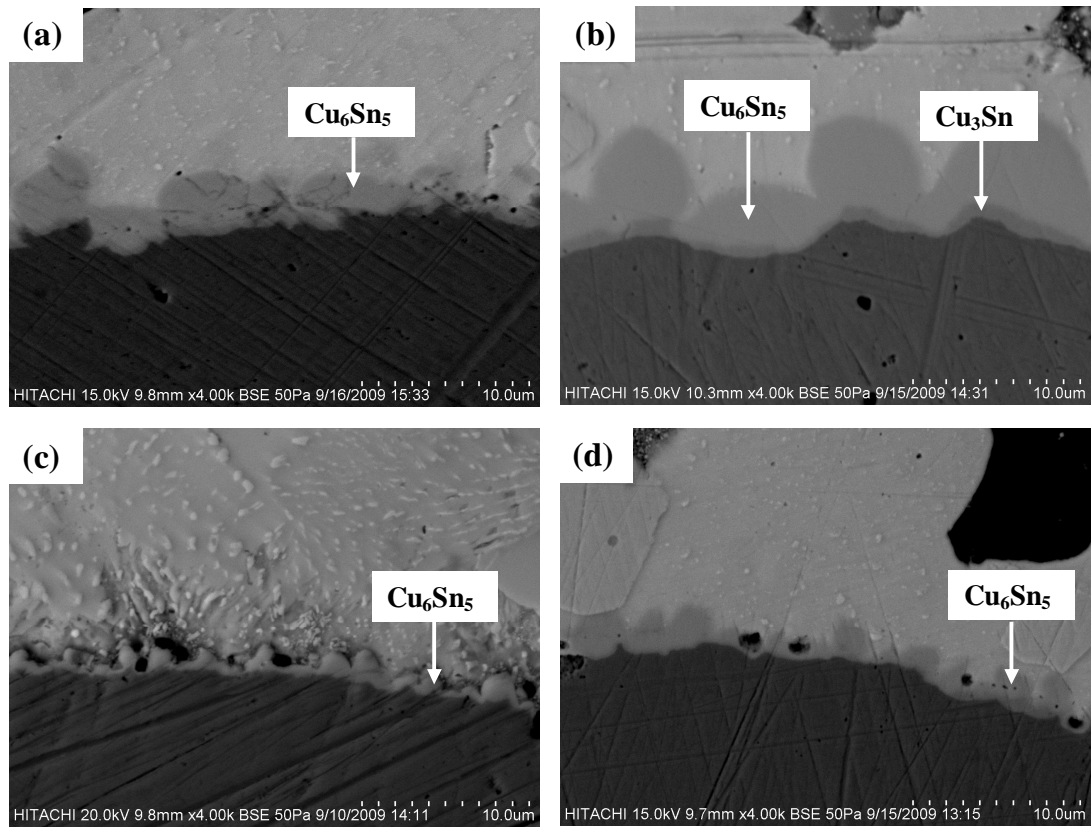


Figure 4.32: Cross sectional SEM micrographs of solder/Cu interface for samples immersed in liquid solder at 250°C (a) SAC for 5 min, (b) SAC for 15 min, (c) (SAC + 0.30 n-Mo) for 5 min, (d) (SAC + 0.30 n-Mo) for 15 min.

Thus the addition of Mo nanoparticles results in thinner IMC layers. The total IMC thickness is plotted as a function of dipping time in Figure 4.33. It is observed that presence of Mo in the liquid solder hinders the growth of IMC layers. For 15 min dipping of Cu wire in the SAC solder, the thickness of IMC layer is around 6 μm . But the presence of 0.30 wt% Mo nanoparticle to the SAC solder, the IMC thickness drops to the value of about 4 μm . It may be noted that the IMC thickness is measured from area analysis by using build-in software in stereoscope (Olympus SZX10) and average value is IMC thickness is taken. At least five figures at randomly selected positions were utilized to calculate the average IMC thickness. It was found that the standard deviation among the values of the IMC thickness is small (~ 0.6).

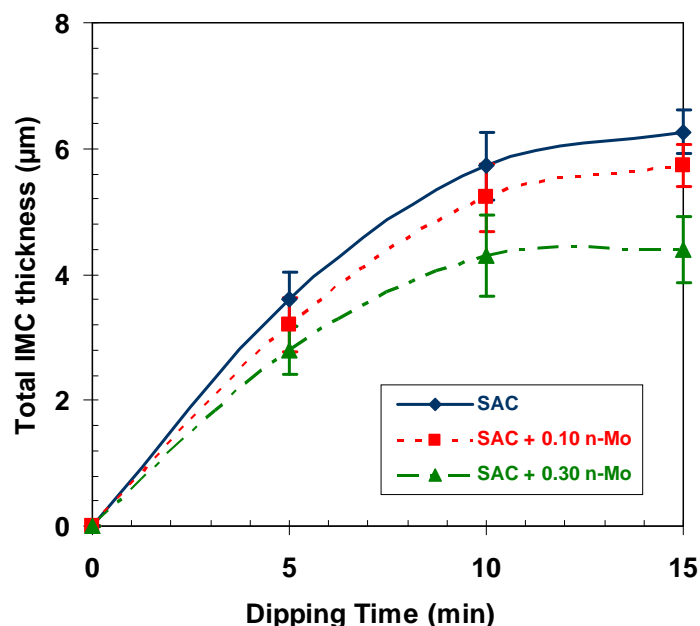


Figure 4. 33: Graphical representation of the total IMC thickness with time in the liquid state reaction.

To find out the distribution of Mo nanoparticles in the liquid state solder sample was reflowed on a Cu sheet with a nominal composition of 5 wt% Mo. In order to investigate the presence of Mo nanoparticles on the IMC, high resolution FESEM was conducted on a few samples. Particularly, locations undergoing incomplete etching were closely examined to identify the presence of Mo nanoparticles. One such location is shown in Figure 4.34. In this case also, on the top surface of Cu_6Sn_5 IMC there is two types of white particles with bright appearance are observed. One type of particles has irregular white shape. The EDX analysis confirms that these irregular shaped particles are Ag_3Sn . These irregular shaped Ag_3Sn form aggregate-type microstructure. On the other hand, another type of white particles, almost perfectly spherical shape, is observed in between the agglomeration of Ag_3Sn . EDX (EDAX-Genesis Utilities) analysis ensures that these spherical shaped particles are Mo nanoparticles. It may be noted that

the shape of Mo nanoparticles on the IMC surface is the same as the starting particles as revealed by TEM (Figure 4.2a).

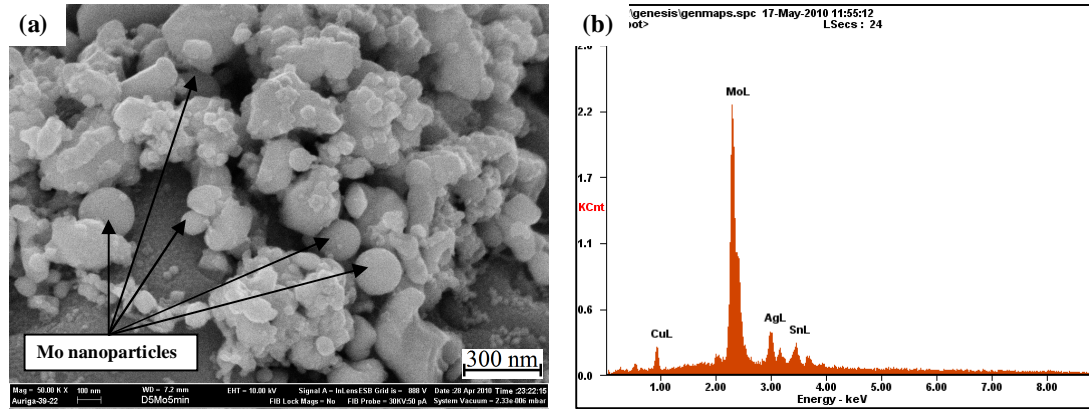


Figure 4. 34: (a) High resolution FESEM image of the top surface of Cu_6Sn_5 IMC for (SAC + 0.30 n-Mo) solder for 5 minute reflow (b) EDX spectrum on Mo particles.

4.9.3 Mechanism for Suppression of Copper Dissolution

It has been mentioned before that Mo has no solubility in tin and it is not likely to have any alloying effects as Co or Ni. Therefore the influence that Mo nanoparticles have shown should be explained through particle effect. The occurrence and distribution of Mo nanoparticles in the IMC and in its neighborhood were investigated both in cross-sections and plan views. Under SEM, in the cross-sectional view of solder/substrate interface no Mo was detected to be embedded in Cu_6Sn_5 . However, extensive observations on the surface of the Cu_6Sn_5 layer at various locations in the plan view samples reveal that Mo nanoparticles are distributed all over the IMC surface. The distribution however is not perfectly uniform. Some places show the presence more particles compared with others.

Reaction between copper and liquid solder takes place through the simultaneous formation of IMC and dissolution of copper (Sharif et al., 2004). It has been suggested

(Gagliano and Fine, 2003) that the growth of Cu_6Sn_5 scallop take place at the Cu_6Sn_5 /solder interface. Copper from the substrate diffuses out particularly through the channels between scallops (Kim and Tu, 1996). The dissolution rate of copper has been expressed by Dybkov (Dybkov, 1998),

$$\frac{dC}{dt} = k \frac{S}{V} (C_s - C) \quad (4.8)$$

Where k is the dissolution rate constant, S is the surface area of the substrate, V is the volume of the molten solder, C_s is the equilibrium concentration of Cu substrate in the solder and C is the concentration of the substrate at the reaction temperature.

Previous result suggested that alloying element has a little effect on the value of dissolution rate constant, k (Barmak et al., 2007). Since Mo does not dissolve into the solder so it can be expected that the addition of nanoparticles such as Mo to the SAC solder would not significantly change the value of k . Again V is also constant in the present case. Therefore the dissolution rate will depend upon the area at the growth front, S , and the concentration of copper in the solder in the immediate vicinity of the Cu_6Sn_5 /solder interface; C . EDX result in the present study suggests a preferential absorption of Mo nanoparticles on the IMC surface (Figure 4.34). Such absorption will block a part of the surface and reduce the effective area available for reaction. Absorption of nanoparticles will also clog the channels between the scallops. This reduction in effective surface area is expected to lead to lower dissolution rate as has been observed in the present study. The surface blockage will also hamper the transfer of Sn atoms to the growth front. This will lead to a lower thickness of IMC which has been found in this study.

CHAPTER 5

CONCLUSIONS AND RECOMMENDATIONS

5.1 Conclusions

In this research work, effects of Mo nanoparticles in Sn-3.8Ag-0.7Cu (SAC) solder on Cu substrate were investigated and compared. Both liquid and solid state reactions of the SAC solder on Cu substrate are examined in presence of Mo nanoparticles. The results obtained from this research work have lead to the following conclusions:

- During reflow only a fraction of Mo nanoparticles is incorporated into the solder. The rest of the nanoparticles stay inside the flux residue. The incorporation of a lower amount of Mo in SAC suggests that Mo nanoparticles experiences rejection by the liquid SAC interface. Poor wetting of SAC on Mo could be a possible reason for this rejection.
- Addition of Mo nanoparticles did not significantly change the melting point of the solders. Slight decrease of the melting point with the addition of Mo is believed for the increased surface instability caused by higher surface energy of nanoparticles.
- The addition of Mo nanoparticles into SAC solder decreases the spreading rate and increases the wetting angle. For the addition of 0.10 wt % of Mo nanoparticles into the SAC solder the spreading rate drops from 79.8 to 76.8% and wetting angle increased from 17.8° to 28.8°.
- Mo nanoparticles do not dissolve or react with the SAC solder and remain stable during multiple reflow at 250°C. The Mo nanoparticles appear to segregate partially and stay on top of the Cu_6Sn_5 and channels between IMC scallops. The

average concentration of Mo on top of Cu_6Sn_5 IMC is 3-3.5 wt% which is higher than the average concentration of Mo inside solder matrix (0.14 wt%).

- The addition of Mo nanoparticles to SAC solder causes a decrease in the thickness and diameter of interfacial Cu_6Sn_5 scallops during multiple reflow. During reflow, Mo nanoparticles exert their influence on the interfacial IMC through discrete particle effect by preferentially absorbing at the grain boundaries of interfacial IMC scallops. This mechanism suppresses the growth of Cu_6Sn_5 IMC and produces smaller scallops during reflow. Mo nanoparticles are suggested to influence IMC growth rather than nucleation.
- During high temperature aging Mo nanoparticles suppress the growth of thickness and scallop diameter of Cu_6Sn_5 IMC layer. But there is virtually no effect of Mo nanoparticles on the growth of Cu_3Sn IMC. It is suggested that presence of Mo nanoparticles on the top surface of Cu_6Sn_5 IMC layer hampers the Sn diffusion from Sn/ Cu_6Sn_5 interface to $\text{Cu}_3\text{Sn}/\text{Cu}_6\text{Sn}_5$ interface. This mechanism results smaller thickness and scallop diameter of Cu_6Sn_5 IMC layer.
- With the addition of 0.10 wt % Mo nanoparticles to the SAC solder, the effective inter-diffusion coefficient of total IMC layer is decreased from $1.092 \times 10^{-17} \text{ m}^2\text{s}^{-1}$ to $9.55 \times 10^{-18} \text{ m}^2\text{s}^{-1}$. There is no effect of Mo nanoparticles on the activation energy of the IMC scallops. Mo has no alloying effect with the SAC solder at 250°C. So the formation energy of the IMC scallops (activation energy) is not changed with the addition of Mo nanoparticles.
- The dissolution of copper substrate is reduced in the liquid state reaction in presence of Mo nanoparticles.

5.2 Recommendation for the Future Works

- In this present experimental work nanocomposite solders were reflowed on copper substrate. It is recommended for the future work to reflow the nanocomposite solders on different substrates such as ball grid array (BGA), flip chip (FC) with different surface finishes such as electroless Ni(P)/Au, electrolytic Ni/Au, Al/Ni(V)/Cu, Zn(Mo)/Cu etc. These processing techniques are more close to industrial practices in the microelectronics industries.
- The strength of interfacial IMC is important to determine the reliability of the solder. Investigation of the solder joint strength by ball pull, ball shear and nanoindentation test is therefore suggested for the future study.
- Thermo-mechanical testing such as accelerated thermal cycling, thermal shear, thermal fatigue and creep test can be investigated.
- Investigations on the mechanism through which nanoparticles influence the interfacial IMC can be carried out by high resolution transmission electron microscopy.
- Various processing routes for the incorporation of different nanoparticles inside the solder matrix can be explored.
- The cost value of the solders in term of long term reliability and performance can be evaluated.

APPENDIX A

PUBLICATIONS

Journal Papers

1. **Arafat, M. M.,** Haseeb, A. S. M. A., Johan, M. R. (2011). Interfacial reaction and dissolution behavior of Cu substrate in molten Sn-3.8Ag-0.7Cu in the presence of Mo nanoparticles. *Soldering and Surface Mount Technology*, 23(3), 140-149.
2. Haseeb, A. S. M. A., **Arafat, M. M.,** & Johan. M. R. (2012). Stability of Molybdenum nanoparticles in Sn-3.8Ag-0.7Cu solder during multiple reflow and their influence on interfacial intermetallic compounds. *Materials Characterization*, 64, 27-35.

Conference Papers

1. **Arafat, M. M., &** Haseeb, A. S. M. A. (2009). Effects of Mo nano particles on lead free Sn-3.8Ag-0.7Cu solder. *International Conferences in Materials and Processing Technologies*, 26-29 October 2009, Kuala Lumpur, Malaysia, Paper ID: 381.
2. **Arafat, M. M., &** Haseeb, A. S. M. A. (2009) Interfacial reaction and dissolution behavior of Cu substrate in molten Sn-3.8Ag-0.7Cu-nano Mo composite solder, *11th Electronics Packaging Technology Conference*, 9-11 December, 2009, Singapore, Paper ID: P0418.

3. Haseeb, A. S. M. A., **Arafat, M. M.**, & Johan. M. R. (2011). Effects of Molybdenum nanoparticles addition on the interface between Sn-3.8Ag-0.7Cu solder and copper substrate during multiple reflow. *Materials Science and Technology Conference and Exhibition*, 16-20 October, 2011, Columbus, Ohio, USA.

REFERENCES

- Abtew, M. & Selvaduray, G. (2000). Lead-free solders in microelectronics. *Materials Science and Engineering: R: Reports*, 27(5-6), 95-141.
- Alam, M. O. & Chan, Y. C. (2005). Solid-state growth kinetics of Ni_3Sn_4 at the Sn-3.5Ag solder/Ni interface. *Journal of Applied Physics*, 98 123527-4.
- Alam, M. O., Chan, Y. C. & Tu, K. N. (2003). Effect of 0.5 wt. % Cu addition in the Sn-3.5%Ag solder on the dissolution rate of Cu metallization. *Journal of Applied physics*, 94, 7904-7909.
- Amagai, M. (2008). A study of nanoparticles in Sn-Ag based lead free solders. *Microelectronics Reliability*, 48(1), 1-16.
- Arafat, M. M., Haseeb, A. S. M. A. & Johan, M. R. (2011). Interfacial reaction and dissolution behavior of Cu substrate in molten Sn-3.8Ag-0.7Cu in the presence of Mo nanoparticles. *Soldering and Surface Mount technology*, 23(3), 140-149.
- Baren, M. (1990). The Ag-Mo (Silver-Molybdenum) system. *Journal of Phase Equilibria*, 11(6), 548-549.
- Barmak, K., Berry, D. C., Khoruzha, V. G., Meleshevich, K. A. & Dybkov, V. I. (2007). Dissolution kinetics of nickel in lead-free Sn-Bi-In-Zn-Sb soldering alloys. *Mater Res Soc Symp Proc*, 2007.
- Barmak, K. & Dybkov, V. I. (2004). Interaction of iron-chromium alloys with liquid aluminium: Part II-formation of intermetallic compounds. *Journal of Materials Science*, 39(13), 4219-4230.
- Bartels, F., Morris, J., Dalke, G. & Gust, W. (1994). Intermetallic phase formation in thin solid-liquid diffusion couples. *Journal of Electronic Materials*, 23(8), 787-790.
- Bath, J. (2007). *Lead-free soldering*, Springer.
- Bath, J., Handwerker, C. A. & Bradley, E. (2000). Research update: lead-free solder alternatives. *Circuit Assembly*, 31-40.
- Boettinger, W. J., Johnson, C. E., Bendersky, L. A., Moon, K. W., Williams, M. E. & Stafford, G. R. (2005). Whisker and hillock formation on Sn, Sn-Cu and Sn-Pb electrodeposits. *Acta Materialia*, 53(19), 5033-5050.
- Brewer, L. & Lamoreaux, R. (1980). The Mo-Sn (Molybdenum-Tin) system. *Journal of Phase Equilibria*, 1(2), 96-97.

- Chen, S., Gao, Y., Liu, J., Zhai, Q., Zhang, L. & Zhang, Y. (2009). Bivalent lead free solder paste for electronic encapsulating in microelectronics, comprises solder paste having lead free solder paste of tin-silver, tin-bismuth, tin-zinc or tin-zinc-bismuth, and nanometer powder of lead free solder pastes. *Chinese Patent*, Patent publication date: 18 Feb 2009, Patent No. CN101367158-A.
- Cheng, F., Gao, F., Nishikawa, H. & Takemoto, T. (2009). Interaction behavior between the additives and Sn in Sn-3.0Ag-0.5Cu-based solder alloys and the relevant joint solderability. *Journal of Alloys and Compounds*, 472(1-2), 530-534.
- Chernyshev, A. P. (2009). Effect of nanoparticle size on the onset temperature of surface melting. *Materials Letters*, 63(17), 1525-1527.
- Chidambaram, V., Hald, J. & Hattel, J. (2010). Development of Au-Ge based candidate alloys as an alternative to high-lead content solders. *Journal of Alloys and Compounds*, 490(1-2), 170-179.
- COM (2000). European Parliament, Proposal for a directive of the european parliament and of the council on waste electrical and electronic equipment and on the restriction of the use of certain hazardous substances in electrical and electronic equipment. 347.
- Das, S. K., Sharif, A., Chan, Y. C., Wong, N. B. & Yung, W. K. C. (2009a). Effect of Ag micro-particles content on the mechanical strength of the interface formed between Sn-Zn binary solder and Au/Ni/Cu bond pads. *Microelectronic Engineering*, 86(10), 2086-2093.
- Das, S. K., Sharif, A., Chan, Y. C., Wong, N. B. & Yung, W. K. C. (2009b). Influence of small amount of Al and Cu on the microstructure, microhardness and tensile properties of Sn-9Zn binary eutectic solder alloy. *Journal of Alloys and Compounds*, 481(1-2), 167-172.
- Deida (2000). Research and development on lead-free soldering. Tokyo: Japan Electronic Industry Development Association.
- Dhindaw, B. (1999). Interfacial energy issues in ceramic particulate reinforced metal matrix composites. *Bulletin of Materials Science*, 22(3), 665-669.
- Dybkov, V. I. (1998). Growth kinetics of chemical compound layers, Cambridge, UK, Cambridge International Science Publishing.
- Flanders, D., Jacobs, E. & Pinizzotto, R. (1997). Activation energies of intermetallic growth of Sn-Ag eutectic solder on copper substrates. *Journal of Electronic Materials*, 26(7), 883-887.
- Frear, D. R. (1991). Solder mechanics-a state of the art assessment, The Minerals, Metals and Materials Society.
- Fujiuchi, S. (2004). Lead-free solder paste and reflow soldering, New York, Marcel Dekker, Inc.

- Gagliano, R. & Fine, M. (2003). Thickening kinetics of interfacial Cu_6Sn_5 and Cu_3Sn layers during reaction of liquid tin with solid copper. *Journal of Electronic Materials*, 32(12), 1441-1447.
- Gain, A. K., Chan, Y. C. & Yung, W. K. C. (2011). Microstructure, thermal analysis and hardness of a Sn-Ag-Cu-1 wt% nano- TiO_2 composite solder on flexible ball grid array substrates. *Microelectronics Reliability*, 51(5), 975-984.
- Gao, Y., Zou, C., Yang, B., Zhai, Q., Liu, J., Zhuravlev, E. & Schick, C. (2009). Nanoparticles of SnAgCu lead-free solder alloy with an equivalent melting temperature of SnPb solder alloy. *Journal of Alloys and Compounds*, 484(1-2), 777-781.
- Glazer, J. (1994). Microstructure and mechanical properties of Pb-free solder alloys for low-cost electronic assembly: A review. *Journal of Electronic Materials*, 23(8), 693-700.
- Goesele, U. & Tu, K. N. (1982). Growth kinetics of planar binary diffusion couples: thin film case versus bulk cases. *Journal of Applied Physics*, 53(4), 3252-3260.
- Gong, J., Liu, C., Conway, P. P. & Silberschmidt, V. V. (2008). Evolution of CuSn intermetallics between molten SnAgCu solder and Cu substrate. *Acta Materialia*, 56(16), 4291-4297.
- Gong, J., Liu, C., Conway, P. P. & Silberschmidt, V. V. (2009). Initial formation of CuSn intermetallic compounds between molten SnAgCu solder and Cu substrate. *Scripta Materialia*, 60(5), 333-335.
- Gusak, A. M. & Tu, K. N. (2002). Kinetic theory of flux-driven ripening. *Physical review B*, 66(115403-115416).
- Harrison, M. R. & Vincent, J. H. (1999). Improved design life and environmentally aware manufacturing of electronics assemblies by lead-free soldering. *12th Microelectronics and Packaging Conference*, 7-9 June 1999, Harrogate, UK. 98-104.
- Haseeb, A. S. M. A. & Leng, T. S. (2011). Effects of Co nanoparticle addition to Sn-3.8Ag-0.7Cu solder on interfacial structure after reflow and ageing. *Intermetallics*, 19(5), 707-712.
- Hwang, S.-Y., Lee, J.-W. & Lee, Z.-H. (2002). Microstructure of a lead-free composite solder produced by an in-situ process. *Journal of Electronic Materials*, 31(11), 1304-1308.
- ITRS. (2001). International technology roadmap for semiconductors. <http://public.itrs.net/> [Online]. San Jose, CA: Semiconductor Industry Association. [Accessed March 2011].
- Kang, S. & Sarkhel, A. (1994). Lead (Pb)-free solders for electronic packaging. *Journal of Electronic Materials*, 23(8), 701-707.

- Kidson, G. V. (1961). Some aspects of the growth of diffusion layers in binary systems. *Journal of Nuclear Materials*, 3(1), 21-29.
- Kim, H. K., Liou, H. K. & Tu, K. N. (1995). Three-dimensional morphology of a very rough interface formed in the soldering reaction between eutectic SnPb and Cu. *Applied Physics Letters*, 66(18), 2337-2339.
- Kim, H. K. & Tu, T. N. (1996). Kinetic analysis of the soldering reaction between eutectic SnPb alloy and Cu accompanied by ripening. *Physical Review B*, 53(23), 16027-16034.
- Kim, K. S., Huh, S. H. & Suganuma, K. (2003). Effects of fourth alloying additive on microstructures and tensile properties of Sn-Ag-Cu alloy and joints with Cu. *Microelectronics Reliability*, 43(2), 259-267.
- Koo, J.-M. & Jung, S.-B. (2005). Effect of substrate metallization on mechanical properties of Sn-3.5Ag BGA solder joints with multiple reflows. *Microelectronic Engineering*, 82(3-4), 569-574.
- Korhonen, T. M. & Kivilahti, J. (1998). Thermodynamics of the Sn-In-Ag solder system. *Journal of Electronic Materials*, 27(3), 149-158.
- Kumar, K. M., Kripesh, V., Shen, L. & Tay, A. A. O. (2006a). Study on the microstructure and mechanical properties of a novel SWCNT-reinforced solder alloy for ultra-fine pitch applications. *Thin Solid Films*, 504(1-2), 371-378.
- Kumar, K. M., Kripesh, V. & Tay, A. A. O. (2006b). Sn-Ag-Cu lead-free composite solders for ultra-fine-pitch wafer-level packaging. *Proceedings of Electronic Components and Technology Conference (ECTE)*, 2006. 237-243.
- Kumar, K. M., Kripesh, V. & Tay, A. A. O. (2008). Single-wall carbon nanotube (SWCNT) functionalized Sn-Ag-Cu lead-free composite solders. *Journal of Alloys and Compounds*, 450(1-2), 229-237.
- Kumar, K. M. & Tay, A. A. O. (2004). Nano-particle reinforced solders for fine pitch applications. *Proceedings of 6th Electronics Packaging Technology Conference (EPTC)*, 2004. 455-461.
- Laurila, T., Vuorinen, V. & Kivilahti, J. K. (2005). Interfacial reactions between lead-free solders and common base materials. *Materials Science and Engineering: R: Reports*, 49(1-2), 1-60.
- Laurila, T., Vuorinen, V. & Paulasto-Kröckel, M. (2010). Impurity and alloying effects on interfacial reaction layers in Pb-free soldering. *Materials Science and Engineering: R: Reports*, 68(1-2), 1-38.
- Lee, C.-B., Yoon, J.-W., Suh, S.-J., Jung, S.-B., Yang, C.-W., Shur, C.-C. & Shin, Y.-E. (2003a). Intermetallic compound layer formation between Sn-3.5 mass %Ag BGA solder ball and (Cu, immersion Au/electroless Ni-P/Cu) substrate. *Journal of Materials Science: Materials in Electronics*, 14(8), 487-493.

- Lee, H.-T. & Chen, M.-H. (2002). Influence of intermetallic compounds on the adhesive strength of solder joints. *Materials Science and Engineering A*, 333(1-2), 24-34.
- Lee, J.-H., Park, D.-J., Heo, J.-N., Lee, Y.-H., Shin, D.-H. & Kim, Y.-S. (2000). Reflow characteristics of Sn-Ag matrix in-situ composite solders. *Scripta Materialia*, 42(8), 827-831.
- Lee, K., Li, M. & Tu, K. (2003b). Growth and Ripening of (Au, Ni) Sn₄ Phase in Pb-Free and Pb-Containing Solders on Ni/Au Metallization. *Journal of materials research*, 18(11), 2562-2570.
- Lee, Y. G. & Duh*, J. G. (1999). Interfacial morphology and concentration profile in the unleaded solder/Cu joint assembly. *Journal of Materials Science: Materials in Electronics*, 10(1), 33-43.
- Lesnik, N. D., Pestun, T. S. & Eremenko, V. N. (1970). Spreading kinetics of liquid metals on solid surfaces. *Powder Metallurgy and Metal Ceramics*, 9(10), 849-853.
- Li, G., Shi, Y., Hao, H., Xia, Z., Lei, Y., Guo, F. & Li, X. (2009). Effect of rare earth addition on shear strength of SnAgCu lead-free solder joints. *Journal of Materials Science: Materials in Electronics*, 20(2), 186-192.
- Li, G. Y., Chen, B. L., Shi, X. Q., Wong, S. C. K. & Wang, Z. F. (2006). Effects of Sb addition on tensile strength of Sn-3.5Ag-0.7Cu solder alloy and joint. *Thin Solid Films*, 504(1-2), 421-425.
- Li, G. Y. & Shi, X. Q. (2006). Effects of bismuth on growth of intermetallic compounds in Sn-Ag-Cu Pb-free solder joints. *Transactions of Nonferrous Metals Society of China*, 16(2), 739-743.
- Lifshitz, I. M. & Slyozov, V. V. (1961). The kinetics of precipitation from supersaturated solid solutions. *Journal of Physics and Chemistry of Solids*, 19(1-2), 35-50.
- Lin, D., Wang, G. X., Srivatsan, T. S., Al-Hajri, M. & Petraroli, M. (2002). The influence of copper nanopowders on microstructure and hardness of lead-tin solder. *Materials Letters*, 53(4-5), 333-338.
- Lin, D. C., Liu, S., Guo, T. M., Wang, G. X., Srivatsan, T. S. & Petraroli, M. (2003a). An investigation of nanoparticles addition on solidification kinetics and microstructure development of tin-lead solder. *Materials Science and Engineering A*, 360(1-2), 285-292.
- Lin, D. C., Wang, G. X., Srivatsan, T. S., Al-Hajri, M. & Petraroli, M. (2003b). Influence of titanium dioxide nanopowder addition on microstructural development and hardness of tin-lead solder. *Materials Letters*, 57(21), 3193-3198.
- Lin, K.-L., Wen, L.-H. & Liu, T.-P. (1998). The microstructures of the Sn-Zn-Al solder alloys. *Journal of Electronic Materials*, 27(3), 97-105.

- Lin, K. S., Huang, H. Y. & Chou, C. P. (2009). Interfacial reaction between Sn1Ag0.5Cu(Co) solder and Cu substrate with Au/Ni surface finish during reflow reaction. *Journal of Alloys and Compounds*, 471(1-2), 291-295.
- Liu, A. A., Kim, H. K., Tu, K. N. & Totta, P. A. (1996). Spalling of Cu₆Sn₅ spheroids in the soldering reaction of eutectic SnPb on Cr/Cu/Au thin films *Journal of Applied Physics*, 80(5), 2774-2780.
- Liu, N.-S. & Lin, K.-L. (2008). Evolution of interfacial morphology of Sn-8.5Zn-0.5Ag-0.1Al-xGa/Cu system during isothermal aging. *Journal of Alloys and Compounds*, 456(1-2), 466-473.
- Liu, P., Yao, P. & Liu, J. (2008a). Effect of SiC nanoparticle additions on microstructure and microhardness of Sn-Ag-Cu solder alloy. *Journal of Electronic Materials*, 37(6), 874-879.
- Liu, Y. C., Teo, J. W. R., Tung, S. K. & Lam, K. H. (2008b). High-temperature creep and hardness of eutectic 80Au/20Sn solder. *Journal of Alloys and Compounds*, 448(1-2), 340-343.
- Liu, Y. C., Wan, J. B. & Gao, Z. M. (2008c). Intermediate decomposition of metastable Cu₅Zn₈ phase in the soldered Sn-Ag-Zn/Cu interface. *Journal of Alloys and Compounds*, 465(1-2), 205-209.
- Lord, R. A. & Umantsev, A. (2005). Early stages of soldering reactions. *Journal of Applied Physics*, 98, 063525.
- Mannan, S. & Clode, M. P. (2004). Dissolution of solids in contact with liquid solder. *Soldering and Surface Mount technology*, 16(3), 31-33.
- Moon, K., Boettinger, W., Kattner, U., Biancaniello, F. & Handwerker, C. (2000). Experimental and thermodynamic assessment of Sn-Ag-Cu solder alloys. *Journal of Electronic Materials*, 29(10), 1122-1136.
- Nai, S. M. L., Wei, J. & Gupta, M. (2006). Influence of ceramic reinforcements on the wettability and mechanical properties of novel lead-free solder composites. *Thin Solid Films*, 504(1-2), 401-404.
- Naidich, Y. V., Perevertailo, V. M. & Zabuga, V. V. (1988). Influence of temperature on the process of spreading of tin on copper and germanium. *Powder Metallurgy and Metal Ceramics*, 27(5), 379-382.
- NCMS (1997). Lead-free solder project final report. Michigan: National Center for Manufacturing Sciences.
- Nishikawa, H., Hamada, Y. & Takemoto, T. (2009). Estimation method for liquidus temperature of lead-free solder using differential scanning calorimetry profiles. *Journal of Electronic Materials*, 38(12), 2610-2616.

- Nishikawa, H., Komatsu, A. & Takemoto, T. (2007). Morphology and pull strength of Sn-Ag(-Co) solder joint with copper pad. *Journal of Electronic Materials*, 36(9), 1137-1143.
- Oh, C.-S., Shim, J.-H., Lee, B.-J. & Dong Nyung, L. (1996). A thermodynamic study on the Ag-Sb-Sn system. *Journal of Alloys and Compounds*, 238(1-2), 155-166.
- Ohnuma, I., Miyashita, M., Anzai, K., Liu, X., Ohtani, H., Kainuma, R. & Ishida, K. (2000). Phase equilibria and the related properties of Sn-Ag-Cu based Pb-free solder alloys. *Journal of Electronic Materials*, 29(10), 1137-1144.
- Pang, J. H. L., Low, T. H., Xiong, B. S., Luhua, X. & Neo, C. C. (2004). Thermal cycling aging effects on Sn-Ag-Cu solder joint microstructure, IMC and strength. *Thin Solid Films*, 462-463, 370-375.
- Park, J.-Y., Kabade, R., Kim, C.-U., Carper, T., Dunford, S. & Puligandla, V. (2003). Influence of Au addition on the phase equilibria of near-eutectic Sn-3.8Ag-0.7Cu Pb-free solder alloy. *Journal of Electronic Materials*, 32(12), 1474-1482.
- Peng, W., Monlevade, E. & Marques, M. E. (2007). Effect of thermal aging on the interfacial structure of SnAgCu solder joints on Cu. *Microelectronics Reliability*, 47(12), 2161-2168.
- Qi, W. H. (2005). Size effect on melting temperature of nanosolids. *Physica B: Condensed Matter*, 368(1-4), 46-50.
- Rao, B. S. S. C., Kumar, K. M., Zeng, K. Y., Tay, A. A. O. & Kripesh, V. Year. (2009) Effect of strain rate and temperature on tensile flow behavior of snagcu nanocomposite solders. *11th Electronic Packaging Technology Conference (EPTC)*, 2009. 272-277.
- Robert, M. & Warren, S. (1993). *Joining of advanced materials*, Stoneham, Massachusetts: Butterworth Hinemann.
- Schaefer, M., Fournelle, R. & Liang, J. (1998). Theory for intermetallic phase growth between cu and liquid Sn-Pb solder based on grain boundary diffusion control. *Journal of Electronic Materials*, 27(11), 1167-1176.
- Shang, P. J., Liu, Z. Q., Pang, X. Y., Li, D. X. & Shang, J. K. (2009). Growth mechanisms of Cu₃Sn on polycrystalline and single crystalline Cu substrates. *Acta Materialia*, 57(16), 4697-4706.
- Sharif, A. & Chan, Y. C. (2004). Dissolution kinetics of BGA Sn-Pb and Sn-Ag solders with Cu substrates during reflow. *Materials Science and Engineering B*, 106(2), 126-131.
- Sharif, A. & Chan, Y. C. (2005). Effect of indium addition in Sn-rich solder on the dissolution of Cu metallization. *Journal of Alloys and Compounds*, 390(1-2), 67-73.

- Sharif, A., Chan, Y. C. & Islam, R. A. (2004). Effect of volume in interfacial reaction between eutectic Sn-Pb solder and Cu metallization in microelectronic packaging. *Materials Science and Engineering B*, 106(2), 120-125.
- Shen, J. & Chan, Y. C. (2009). Research advances in nano-composite solders. *Microelectronics Reliability*, 49(3), 223-234.
- Shen, J., Liu, Y. C., Han, Y. J., Tian, Y. M. & Gao, H. X. (2006). Strengthening effects of ZrO₂ nanoparticles on the microstructure and microhardness of Sn-3.5Ag lead-free solder. *Materials Science and Engineering: A*, 441(1-2), 135-141.
- Sheng, H. W., Lu, K. & Ma, E. (1998). Melting and freezing behavior of embedded nanoparticles in ball-milled Al-10 wt% M (M=In, Sn, Bi, Cd, Pb) mixtures. *Acta Materialia*, 46(14), 5195-5205.
- Shi, Y., Liu, J., Yan, Y., Xia, Z., Lei, Y., Guo, F. & Li, X. (2008). Creep properties of composite solders reinforced with nano and micro-sized particles. *Journal of Electronic Materials*, 37(4), 507-514.
- Sivasubramaniam, V., Bosco, N. S., Janczak-Rusch, J., Cugnoni, J. & Botsis, J. (2008). Interfacial intermetallic growth and strength of composite lead-free solder alloy through isothermal aging. *Journal of Electronic Materials*, 37(10), 1598-1604.
- Su, L. H., Yen, Y. W., Lin, C. C. & Chen, S. W. (1997). Interfacial reactions in molten Sn/Cu and molten In/Cu couples. *Metallurg. Mater. Trans. B*, 28(5), 927-934.
- Subramanian, P. & Laughlin, D. (1990). The Cu-Mo (Copper-Molybdenum) system. *Journal of Phase Equilibria*, 11(2), 169-172.
- Suganuma, K. (2001). Advances in lead-free electronics soldering. *Current Opinion in Solid State and Materials Science*, 5(1), 55-64.
- Suh, J. O., Tu, K. N., Lutsenko, G. V. & Gusak, A. M. (2008). Size distribution and morphology of Cu₆Sn₅ scallops in wetting reaction between molten solder and copper. *Acta Materialia*, 56(5), 1075-1083.
- Suraski, D. & Seelig, K. (2001). The current status of lead-free solder alloys. *IEEE Transactions on Electronics Packaging Manufacturing*, 24(4), 244-248.
- Tai, F., Guo, F., Xia, Z., Lei, Y., Yan, Y., Liu, J. & Shi, Y. (2005). Processing and creep properties of Sn-Cu composite solders with small amounts of nanosized Ag reinforcement additions. *Journal of Electronic Materials*, 34(11), 1357-1362.
- Takaku, Y., Felicia, L., Ohnuma, I., Kainuma, R. & Ishida, K. (2008). Interfacial reaction between Cu substrates and Zn-Al base high-temperature pb-free solders. *Journal of Electronic Materials*, 37(3), 314-323.
- Takemoto, T., Okamoto, I. & Matsumura, J. (1987). Phase diagrams of copper-silver-phosphorus and copper-tin-phosphorus ternary brazing filler metals-copper phosphorus brazing filler metals with low melting temperature (II). *Trans. JWRI*, 16(2), 301-307.

- Tu, K. N. (2007). Solder joint technology materials, properties, and reliability, New York, Springer.
- Tu, K. N. & Zeng, K. (2001). Tin-lead (SnPb) solder reaction in flip chip technology. *Materials Science and Engineering: R: Reports*, 34(1), 1-58.
- Wade, N., Wu, K., Kunii, J., Yamada, S. & Miyahara, K. (2001). Effects of Cu, Ag and Sb on the creep-rupture strength of lead-free solder alloys. *Journal of Electronic Materials*, 30(9), 1228-1231.
- Wang, H., Zhao, H., Sekulic, D. & Qian, Y. (2008). A comparative study of reactive wetting of lead and lead-free solders on Cu and (Cu₆Sn₅/Cu₃Sn)/Cu substrates. *Journal of Electronic Materials*, 37(10), 1640-1647.
- Wang, Y. W., Lin, Y. W., Tu, C. T. & Kao, C. R. (2009). Effects of minor Fe, Co, and Ni additions on the reaction between SnAgCu solder and Cu. *Journal of Alloys and Compounds*, 478(1-2), 121-127.
- Watanabe, H., Hidaka, N., Shohji, I. & Ito, M. (2006). Effect of Ni and Ag on interfacial reaction and microstructure of Sn-Ag-Cu-Ni-Ge lead-free solder. *Materials Science and Technogy*, 1, 135-146.
- Wild, R. W. (1971). Properties of some low melting fusible alloys, Technical Report. New York: IBM Federal Systems Division Laboratory.
- Wilde, G. & Perepezko, J. H. (2000). Experimental study of particle incorporation during dendritic solidification. *Materials Science and Engineering A*, 283(1-2), 25-37.
- Wood, E. & Nimmo, K. (1994). In search of new lead-free electronic solders. *Journal of Electronic Materials*, 23(8), 709-713.
- Wu, C. M. L. & Wong, Y. W. (2007). Rare-earth additions to lead-free electronic solders. *Lead-Free Electronic Solders*. Springer US.
- Wu, C. M. L., Yu, D. Q., Law, C. M. T. & Wang, L. (2004). Properties of lead-free solder alloys with rare earth element additions. *Materials Science and Engineering: R: Reports*, 44(1), 1-44.
- Xiao, W., Shi, Y., Xu, G., Ren, R., Guo, F., Xia, Z. & Lei, Y. (2009). Effect of rare earth on mechanical creep-fatigue property of SnAgCu solder joint. *Journal of Alloys and Compounds*, 472(1-2), 198-202.
- Yang, M., Li, M., Wang, L., Fu, Y., Kim, J. & Weng, L. (2011). Cu₆Sn₅ Morphology transition and its effect on mechanical properties of eutectic Sn-Ag solder joints. *Journal of Electronic Materials*, 40(2), 176-188.
- Yao, J. H., Elder, K. R., Guo, H. & Grant, M. (1993). Theory and simulation of Ostwald ripening. *Physical Review B*, 47(21), 14110-14125.
- Yeh, P.-Y., Song, J.-M. & Lin, K.-L. (2006). Dissolution behavior of Cu and Ag substrates in molten solders. *Journal of Electronic Materials*, 35(5), 978-987.

- Yen, Y.-W., Chou, W.-T., Tseng, Y., Lee, C. & Hsu, C.-L. (2008). Investigation of dissolution behavior of metallic substrates and intermetallic compound in molten lead-free solders. *Journal of Electronic Materials*, 37(1), 73-83.
- Yoon, J.-W., Noh, B.-I., Kim, B.-K., Shur, C.-C. & Jung, S.-B. (2009). Wettability and interfacial reactions of Sn-Ag-Cu/Cu and Sn-Ag-Ni/Cu solder joints. *Journal of Alloys and Compounds*, 486(1-2), 142-147.
- Yoon, J.-W., Noh, B.-I., Lee, Y.-H., Lee, H.-S. & Jung, S.-B. (2008). Effects of isothermal aging and temperature-humidity treatment of substrate on joint reliability of Sn-3.0Ag-0.5Cu/OSP-finished Cu CSP solder joint. *Microelectronics Reliability*, 48(11-12), 1864-1874.
- Yu, C., Lu, H. & Li, S. (2008). Effect of Zn addition on the formation and growth of intermetallic compound at Sn-3.5 wt% Ag/Cu interface. *Journal of Alloys and Compounds*, 460(1-2), 594-598.
- Yu, C. H. & Lin, K. L. (2005). Early dissolution behavior of copper in a molten Sn-Zn-Ag solder. *J. Mater. Res.*, 20, 666-671.
- Yu, D. Q., Wang, L., Wu, C. M. L. & Law, C. M. T. (2005a). The formation of nano-Ag₃Sn particles on the intermetallic compounds during wetting reaction. *Journal of Alloys and Compounds*, 389(1-2), 153-158.
- Yu, D. Q., Wu, C. M. L., Law, C. M. T., Wang, L. & Lai, J. K. L. (2005b). Intermetallic compounds growth between Sn-3.5Ag lead-free solder and Cu substrate by dipping method. *Journal of Alloys and Compounds*, 392(1-2), 192-199.
- Zakel, E., Azdasht, G. & Reichl, H. (1991). Investigations of laser soldered TAB inner lead contacts. *IEEE Transaction on Components, Hybrids, and Manufacturing Technology*, 14(4), 672-679.
- Zeng, G., Xue, S., Zhang, L., Gao, L., Dai, W. & Luo, J. (2010). A review on the interfacial intermetallic compounds between Sn-Ag-Cu based solders and substrates. *Journal of Materials Science: Materials in Electronics*, 21(5), 421-440.
- Zerrer, P., Fix, A., Hutter, M. & Pape, U. (2008). Nano flux-doping of solder pastes. In: 2nd Electronics System-Integration Technology Conference (ESTC), 2008. 923-927.
- Zhai, Q. J., Guan, S. K. & Shang, Q. Y. (1999). Alloy thermo-mechanism: theory and application. *Metallurgy Industry Press*, Beijing.
- Zhong, X. L. & Gupta, M. (2008). Development of lead-free Sn-0.7Cu/Al₂O₃ nanocomposite solders with superior strength. *Journal of Physics D: Applied Physics*, 41, 095403.
- Zhu, Q. S., Zhang, Z. F., Shang, J. K. & Wang, Z. G. (2006). Fatigue damage mechanisms of copper single crystal/Sn-Ag-Cu interfaces. *Materials Science and Engineering: A*, 435-436, 588-594.

Zou, H. F., Yang, H. J. & Zhang, Z. F. (2008). Morphologies, orientation relationships and evolution of Cu_6Sn_5 grains formed between molten Sn and Cu single crystals. *Acta Materialia*, 56(11), 2649-2662.